p-PHENYLENEDIAMINE DERIVED CARBON NANODOTS FOR LUMINESCENCE BASED APPLICATIONS

Thesis Submitted to the
University of Calicut for the Award of

DOCTOR OF PHILOSOPHY
IN
CHEMISTRY

By

NIDHISHA V.

Under the Supervision of

Dr. RENUKA N.K.

DEPARTMENT OF CHEMISTRY
UNIVERSITY OF CALICUT
KERALA-673 635

AUGUST 2024

In loving memory of My Father

Gangadharan V

Dedicated to My Teachers…..

Who have inspired,
guided and supported me throughout my academic journey

DEPARTMENT OF CHEMISTRY
UNIVERSITY OF CALICUT

CERTIFICATE

This is to certify that the thesis entitled "**p-PHENYLENEDIAMINE DERIVED CARBON NANODOTS FOR LUMINESCENCE BASED APPLICATIONS**" is an authentic record of precise research work carried out by **Nidhisha V** under my guidance and supervision for the award of the degree of Doctor of Philosophy in Chemistry under the faculty of Sciences, University of Calicut, Kerala and the same has not been submitted elsewhere for any degree or diploma.

The corrections/suggestions recommended by the adjudicators have been incorporated in the thesis and the content in the thesis and the soft copy are one and the same.

Place:
Date:

Dr. Renuka N.K.
(Supervising Teacher)
Professor
Department of Chemistry
University of Calicut

DECLARATION

I, **Nidhisha V**, hereby declare that the work presented in the thesis entitled "**p-PHENYLENEDIAMINE DERIVED CARBON NANODOTS FOR LUMINESCENCE BASED APPLICATIONS**" is based on the original work done by me under the guidance of Dr. Renuka N.K., Professor, Department of Chemistry, University of Calicut and has not been included in any other thesis submitted previously for the award of any degree. The contents of the thesis are undergone plagiarism check using iThenticate software at C.H.M.K. Library, University of Calicut, and the similarity index found within the permissible limit.

Place: **Nidhisha V**

Date:

ACKNOWLEDGEMENT

This research would not have been possible without the unwavering support, guidance, and encouragement of several individuals. I would like to take this opportunity to express my heartfelt gratitude to those who have contributed significantly to the completion of this research. Pursuing a Ph.D. has been a challenging journey for me, but the support and guidance from these people made it worthwhile.

First, I am deeply indebted to my supervising teacher, Dr. Renuka N.K, for her exceptional guidance and support throughout my research journey. I gratefully acknowledge the countless hours she dedicated to discussing research, providing constructive feedback, and sharing her wealth of knowledge. I am also thankful for her trust in me and her encouragement to explore new ideas. I am grateful for the opportunity to have worked under her supervision.

I extend my gratitude to Dr. Rajeev S. Menon, Head of the Department, Department of Chemistry, University of Calicut, for his support and providing the essential facilities during my Ph.D program. I would also like to express my appreciation to former HODs of the department and the other faculty members for their valuable suggestions and encouragement. I offer special thanks to Dr. Praveen V.K, Senior Scientist, CSIR-NIIST, Thiruvananthapuram, and Dr. Vijisha K. Rajan, Assistant Professor, Department of

Nanoscience and Technology, University of Calicut, and Dr. Sunaja Devi K.R., for their invaluable advice and support. I am forever indebted to all my former teachers for laying the foundation for this achievement. I am also grateful to all the current and former non-teaching staff and the librarian of the department for their care and timely support.

I also acknowledge the financial assistance received from University of Calicut. I would also like to acknowledge CSIF-University of Calicut, CIF –IISER. Thiruvananthapuram, STIC-CUSAT, SAIF–MG University and NIIST Thiruvananthapuram for the analysis facilities used for the completion of this research work. I would like to extend my sincere appreciation to my research group members Dr. Arsha Kusumam T.V., Dr.Ansi V.A. Dr. Akhila A.K., Dr. Varsha Raveendran P.T, Anjali.C, Amrutha T.P, Ritu.G, Arya.P.B and Sudhishna.K.K for their love, care and support during the period. Special thanks to Anjali for her unwavering support during my up and downs. I am grateful to Dr.Jijil.C.P for his valuable suggestions and support. I am forever grateful to Dr. Deepak Joshy, Mr.Lijin Rajan and Mr. Sivakrishna Prakash for always being there for me unconditionally. I also convey my heartfelt gratitude to Ms.Nadira.P.P, Mrs Sreesitha C. S and Ms.Rekha V for their love and care. I wish to thank Mr.Nikhil for the cover page design. I also extend my gratitude to all the research scholars in the Department of Chemistry for their support. I wish to express my heartfelt gratitude to all my friends and well-wishers, who directly or indirectly contributed in this venture.

Throughout this thesis, I am humbled by the unwavering support and limitless love I have received from my family as I navigated through the challenges of academia. I owe an immense depth of gratitude to my parents Mrs. Soudamini K.P and Mr.Balan K for their support and care. I will never be able to adequately thank my husband, Mr. Ajin B, for his steadfast encouragement, love, and care from the beginning. I also want to express my sincere gratitude to my daughter Aadvika K. Ajin for her understanding and patience with me as I pursued my studies. I am deeply greatful for my late father's blessings from heaven and for the outstanding support of my mother Mrs. Santha P.K. throughout this journy. As a source of my strength, I also thank my brothers; Mr. Shanil V. and Mr. Nidhin V.G. for their care and support. I also humbly remember the support from Dr.Bincy, Dr. Hrideshna, Mrs. Aparna, Mr. Sreejesh and other family members.

Above all, I am grateful to ***God Almighty*** *for giving me the discernment, bravery, and tenacity that allowed me to successfully finish my research.*

Nidhisha V

CONTENTS

PREFACE

Carbon nanodots (CNDs) are spherical carbon nanoparticles with diameters typically ranging from 1-10 nm. They are composed of carbon atoms arranged in a crystalline or amorphous structure, often with functional groups attached to their surface. They have gained significant attention in recent years due to their unique properties such as inherent luminescence, small size, tunable excitation/emission, high photostability, chemical inertness, relatively low toxicity, environment friendly nature and good biocompatibility. They constitute a promising class of nanomaterials with a wide range of applications in the field of bioimaging, sensing, optoelectronics, energy storage, catalysis, environmental remediation, and biomedicine and drug delivery.

This thesis explores the luminescence based applications of carbon nanodots derived from p-phenylenediamine. It covers the synthesis, characterization, and applications of p-phenylenediamine-derived carbon nanodots (PD-CNDs), focusing on their luminescence properties. The thesis is structured into six chapters. Chapter 1 provides a brief introduction to luminescent carbon nanomaterials, with a particular emphasis on carbon nanodots. It offers a general overview of the research, including details on the synthesis, properties, and applications of carbon nanodots. Chapter 2 presents the details on the materials and methodologies used in the investigation.

Chapter 3 comprises a detailed discussion on the results of the structural and optical characterization techniques, thereby providing the physicochemical features of the obtained carbon nanodots (PD-CNDs). The characterization techniques adopted here include High Resolution Transmission Electron Microscopy (HR-TEM) Analysis, X-Ray Diffraction (XRD) analysis, X-ray photoelectron spectroscopy (XPS) analysis, Fourier Transform Infrared (FT-IR) spectroscopy, Raman spectroscopy analysis, Zeta potential analysis, UV-visible absorbance spectroscopy and Fluorescence spectroscopy.

One of the most extensively explored applications of carbon nanodots is sensing. Chapter 4 delves into the utility of p-phenylenediamine derived carbon nanodots (PD-CNDs) as sensor. The variation in the luminescence intensity of PD-CNDs in presence of various analytes is monitored for the studies. This chapter is divided into two parts based on the analytes. The first part deals with metal ions. When Cu^{2+} ions were present, the photoluminescence intensity of the carbon nanodots (CNDs) was observed to be quenched. This characteristic was utilized to create a CND-based fluorescence sensor that detects Cu^{2+} ions quantitatively. An investigation into the mechanism underlying in the process of luminescence quenching in the presence of this ion led to the conclusion that these alterations are caused by static quenching. The production of a black precipitate at higher concentrations is attributed to the complex PD-CND@Cu, which allowed further extension of the strategy into visual detection approach. Despite the presence of other metal ions, the system

showed excellent selectivity for Cu^{2+} ions. PD-CND-coated filter paper strips were used to expand this detection capability to solid-state application, that allows naked eye detection of cupric ions. In the second part of the investigation, the photoluminescence intensity of PD-CNDs is monitored in presence of nitroaromatic compounds. It is quite interesting to note that the addition of picric acid caused the luminescence intensity to gradually drop, whereas none of the other chosen nitroaromatic compounds responded in this manner. Detailed research is also done to trace the mechanism underlying in this luminescence quenching. These results are also supported by theoretical investigations.

The solvent relaxation (solvatochromism) based applications of PD-CNDs are the main topics of the last working chapter 5. This work explores the fluorescence solvatochromic behaviour of PD-CNDs, which displayed distinct colours of photoluminescence when dissolved in different solvents. These studies present a novel approach to predict the solvent polarity parameters. The dielectric constant value of binary solvent mixtures, like the methanol-1, 4-dioxane system, is reliably determined by the research. Using the solvatochromic nature, a simple and accurate method is also suggested for quantitatively detecting moisture in 1, 4-dioxane. A summary of the entire research work is provided in Chapter 6, along with an outlook for the future.

LIST OF FIGURES

LIST OF TABLES

LIST OF ABBREVIATIONS

CNDs/ CDs	: Carbon nanodots/Carbon dots
LEDs	: Light emitting diodes
CRTs	: Cathode Ray Tubes
PL	: Photoluminescence
IC	: Internal conversion
ISC	: Inter-system crossing
GQD	: Graphene quantum dots
GO	: Graphene oxide
CNTs	: Carbon nanotubes
NV	: Nitrogen vacancy
ND	: Nanodiamond
SWCNTs	: Single walled carbon nanotubes
HR-TEM	: High resolution Transmission electron microscopy
XRD	: X-Ray diffraction
AFM	: Atomic Force Microscopy
FT-IR	: Fourier Transform Infrared Spectroscopy
XPS	: X-Ray Photoelectron spectroscopy
CQD	: Carbon Quantum dots
CPDs	: Carbonized polymer dots
QCE	: Quantum confinement effect
QY	: Quantum Yield
PEG	: Poly(ethylene glycol)
SH-PEG	: Thiol group containing poly (ethylene glycol)

HTC	: Hydrothermal carbonization
N/S-CDs	: N/S doped carbon dots
DMF	: Dimethyl formamide
NCDs	: Nitrogen doped carbon dots
CVD	: Chemical vapor deposition
PVA	: Poly vinyl alcohol
NIR	: Near infrared
TS-CDs	: Table sugar derived carbon dots
PDT	: Photodynamic Therapy
UPCL	: Up conversion photoluminescence
RTP	: Room temperature phosphorescence
P-CNDs	: Phosphorus doped carbon nanodots
PD	: Phenylenediamine
PD-CNDs	: p-Phenylenediaminederived carbon nanodots
TCSPC	: Time-correlated single photon counting
DI	: Deionized
TNP	: 2,4,6-Trinitrophenol
DFT	: Density functional theory
PA	: Picric acid
DAM	: Donor Acceptor Map
HOMO	: Highest occupied molecular orbital
LUMO	: Lowest unoccupied molecular orbital
FMO	: Frontier molecular orbital
IE	: Ionization energy
EA	: Electron affinity
FRET	: Fluorescence resonance energy transfer

PET	: Photo-induced electron transfer
IFE	: Inner filter effect
NACs	: Nitroaromatic compounds
TNT	: 2,4,6-Trinitrotoluene
DNT	: 2,4-Dinitrophenol
NB	: Nitrobenzene
PCNB	: Pentachloronitrobenzene
USEPA	: United States Environmental Protection Agency
ET	: Energy transfer
LOD	: Limit of detection
NP	: Nitrophenol
NT	: Nitrotoluene
NBZA	: Nitrobenzaldehyde
NBA	: Nitrobenzoic acid
CDNB	: 1-Chloro-2,4-dinitrobenzene
DCM	: Dichloromethane
DMSO	: Dimethylsulphoxide
IPA	: Isopropyl alcohol

CHAPTER 1

INTRODUCTION

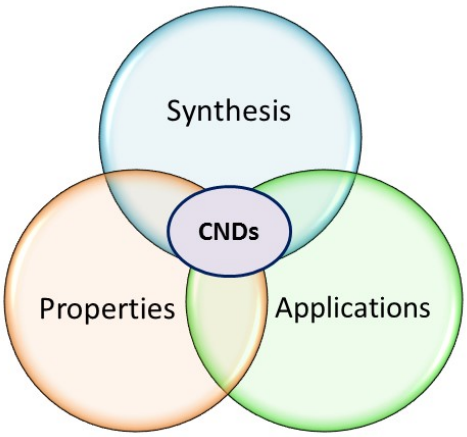

This chapter provides a comprehensive introduction to luminescent carbon nanoparticles, especially on carbon nanodots (CNDs). It covers essential background information, including their history and structural characteristics. Additionally, the chapter summarizes various synthesis methods, physicochemical properties, and applications of carbon nanodots. Finally, it discusses the significance and goals of the current research work.

1.1. Luminescence

Luminescence is the emission of optical radiation by matter. It occurs when electrons in a substance absorb energy and then release that energy as light as they return to their ground state. The term "luminescence" was coined by German physicist Eilhardt Wiedemann in 1888. "Light" is what the Latin word "lumen" signifies. The materials that display this characteristic are termed as "luminescent materials" or "phosphors," which are derived from the Greek word "light bearer,". The wavelength of the light emitted is characteristic of a luminescent substance and not of the incident radiation. This process can happen through various mechanisms, each defined by the energy source that excites the electrons. The main characteristic of luminescence is that the emitted light is an inherent attribute of the object itself, stimulated by some internal or external process. The main types of luminescence include:

1. **Photoluminescence**: Occurs when a substance absorbs photons (light energy) and then re-emits them.

2. **Chemiluminescence**: Light is produced as a result of a chemical reaction. A notable example is bioluminescence, which occurs in living organisms like fireflies and certain marine species that emit light due to chemical reactions.

3. **Electroluminescence**: Light is emitted in response to an electric current or a strong electric field, utilized in devices like light emitting diodes (LEDs).

4. **Cathodoluminescence**: Light is emitted when a material is struck by an electron beam, used in imaging and display technologies such as cathode ray tubes (CRTs).

5. **Thermoluminescence**: Light is emitted when a material that has absorbed energy from prior radiation exposure is heated. This phenomenon is used in dating archaeological artifacts.

6. **Triboluminescence**: Light is generated when a material is mechanically pulled apart, ripped, scratched, crushed, or rubbed. This can be seen when peeling adhesive tape or crushing sugar crystals.

7. **Radioluminescence**: Light is emitted due to exposure to ionizing radiation. This is often observed in glow in the dark materials that use radioactive substances.

Each kind of luminescence has distinct properties and uses, spanning scientific research, medical diagnostics, industrial processes, and consumer products. The fundamental principle behind all these types is the transition of electrons from a higher energy state to a lower energy state, resulting in the emission of light. Luminescence is a ubiquitous phenomenon widely present in nature and living organisms, and it has been applied in diverse research fields including material science, chemistry, environmental science, life sciences, medical research, and more. Research on luminescent materials is continuously advancing in

both fundamental research and industry, due to their significant potential in practical applications such as chemical sensors, data encryption, cellular bioimaging, drug delivery, and light emitting diodes.

Our discussion is centred on photoluminescence (PL). The transitions usually accompanied by absorption of light by materials, are illustrated by the Jablonski diagram (**Figure 1.1**).

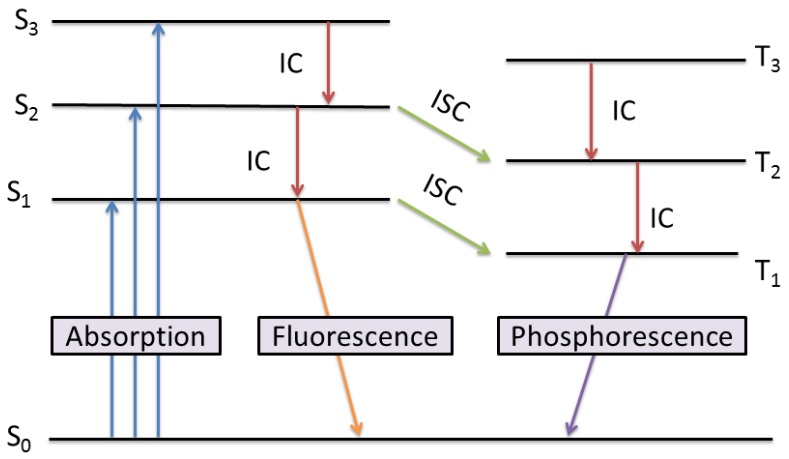

Figure 1.1 Jablonski diagram

As seen in **Figure 1.1**, upon absorption of a light photon, the electron on the absorbing molecule may transition from the ground state S_0 to the singlet excited states S_1, S_2, or S_3. This is dependent upon the energy of the light photon that was absorbed. There is a triplet excited state (T_1, T_2 and T_3) for every singlet excited state. An activated molecule is one that is either in a singlet

or triplet excited state. As a result, the activated molecule dissipates its energy through the following kinds of processes to return to the ground state:

(a) Non-radiative Transitions

The activated molecule returns to a level of same multiplicity, without emitting radiation, and is referred as internal conversion (IC). The energy of activated molecule is released as heat through chemical collisions. This process takes less than 10^{-11} seconds. Inter system crossing (ISC) is another way by which the molecule may lose energy. Transitions between states of different multiplicities are a part of this process. Moreover, these transitions don't emit radiation. Spectroscopically, these transitions are not allowed. They do, however, progress at comparatively slow rates.

(b) Radiative Transitions

The activated molecule returns to the ground state S_0 from the singlet excited state S_1 and triplet excited state T_1, resulting in these transitions. Emissions occur in tandem with these transitions. From a spectroscopic perspective, the shift from the S_1 to S_0 states is permissible and happens in roughly 10^{-8} seconds. Fluorescence is the name given to the radiation released during this transition. Since it is a forbidden transition, the triplet excited state T_1 to the ground state S_0 moves quite slowly. Phosphorescence is the term for the radiation released during this phase. The transition includes spin inversion, which takes time to

occur, and hence phosphorescence has a substantially longer life span of the order of 10^{-3} seconds or more.

(c) Chemical reactions

A chemical reaction may also cause the activated molecule to lose energy. The singlet excited state of the molecule rapidly returns to the ground state, avoiding any chemical reaction. The ground state is attained by the triplet excited state molecule somewhat slowly. This gives the activated molecule plenty of chances to go through a chemical reaction. Therefore, the molecule that undergoes a chemical reaction is the one that was in an excited triplet state before.

1.2. Fluorescent carbon nanostructures

Fluorescent carbon nanostructures are a class of carbon based materials that exhibit fluorescence. They can absorb light at a particular wavelength and emit at another wavelength, typically longer. These nanostructures include various forms, such as:

i. **Carbon Nanodots (CNDs)**: Small, quasi-spherical nanoparticles with sizes typically below 10 nm. They have unique optical properties and are known for their bright fluorescence, biocompatibility, and low toxicity.

ii. **Graphene Oxide Quantum Dots (GQDs)**: Nanometer-sized fragments of graphene with one or a few layers. Graphene oxide quantum dots or graphene quantum dots (GQDs) are

formed by the creation of edge functional groups on graphene oxide (GO) through oxidative cutting and the exfoliation of layers from the starting material under external forces such as refluxing, hydrothermal treatment, or electrochemical methods. GQDs exhibit size-dependent fluorescence and possess excellent photostability, making them useful in bioimaging and optoelectronics.

iii. **Carbon Nanotubes (CNTs)**: Cylindrical nanostructures made up of rolled-up sheets of graphene. Certain single walled carbon nanotubes can emit fluorescence in the near infrared region, which is beneficial for deep tissue imaging in biomedical applications. The first report on the photoluminescence of carbon nanotubes (CNTs) was published in 2000, by Riggs *et al.* [1]. The origins and mechanisms of PL in CNTs are complex, as the wide variety of geometrical and chemical arrangements in nanotubes significantly influence their PL properties.

iv. **Nanodiamonds (NDs)**: Diamond nanoparticles are also reported to be fluorescent due to the presence of various color centers, such as nitrogen vacancy (NV) centers in doped nanodiamond systems [2]. The mechanism of color center related photoluminescence (PL) in nanodiamonds (NDs) is distinct from that of sp^2 hybridized carbon allotropes. In NDs, the particle size does not significantly impact the general optical properties of PL centers, as their

light emission mechanism does not rely on quantum confinement. Due to the high surface-to-volume ratio and polydispersity of nanodiamonds (NDs), their surface chemistry can significantly modulate the emission states of their NV centers, much more than in bulk crystals. As a result, nanosized photoluminescent NDs could be extremely useful in sensors because of their high sensitivity to changes in the nanoenvironment [3, 4].

Among fluorescent carbon nanostructures, carbon nanodots (CNDs) have garnered significant attention due to their inherent fine features including luminescence.

1.3. Carbon Nanodots

Over the past decade, the field of carbon nanodots (CNDs) has opened up a completely new area of research in nanoscience and technology due to their extraordinary optical properties and diverse applications. Carbon nanodots (CNDs) are quasi-spherical carbon nanoparticles with size < 10 nm. As already mentioned, they have inherent luminescence, which makes them different from other carbon nanostructures. The photophysical and chemical properties of CNDs can be significantly altered by adjusting their shapes and sizes and by doping them with heteroatoms such as oxygen, nitrogen, phosphorus, sulfur, and boron. Surface engineering is crucial for CNDs in various applications, including explosive detection, chemical sensing, food safety, bioimaging, drug delivery, energy conversion, and

photocatalysis. Additionally, CNDs offer advantages over other well recognized quantum dots due to their photostability, high quantum yield, biocompatibility, low toxicity, water solubility, good conductivity, and environmental friendliness.

1.3.1. Discovery of Carbon Nanodots

Carbon nanodots (CNDs) were discovered in 2004 during the purification of single walled carbon nanotubes (SWCNTs) by Xu *et al*. [5]. The discovery was accidental, occurring during the synthesis of SWCNTs using laser ablation method. The researchers noticed a strong photoluminescence emission from a sample that was supposed to contain only SWCNTs. Further investigations revealed that the PL emission was coming from tiny, spherical carbon particles with diameters less than 10 nm, which were later, termed carbon nanodots (CNDs). This serendipitous discovery opened up a new field of research, as CNDs were found to possess unique optical, electrical and chemical properties, making them suitable for various applications. The discovery of CNDs has been considered a significant milestone in the field of nanotechnology and material science, and has led to a rapid expansion of research in this area.

Two years later, in 2006, Sun *et al.* [6] synthesized stable photoluminescent carbon nanoparticles of different sizes and named them “carbon quantum dots” (CQDs). Within a year, Cao *et al.* [7] reported water soluble CNDs passivated with poly-(propionylethylenimine)-co-ethylenimine. These as prepared

CNDs exhibited two photon induced luminescence spectra and were used to detect human breast cancer MCF-7 cells. Since the remarkable emergence of this new carbon material, researchers from various fields have shown great interest due to its non-toxicity and excellent photoluminescence properties. The number of publications on carbon nanodots is increasing almost exponentially every day. Significant milestones have been achieved in the development of carbon nanodots till date, focusing on improving their structure and photoluminescence. In 2010, Li *et al.* [8] prepared the first crystalline carbon nanaodots with size dependent photoluminescence from graphite using an electrochemical process. Zhu *et al.* [9] synthesized polymer like amorphous carbon nanodots, which were applied in sensing, bioimaging, and as invisible ink. Chiral nanostructures based on semiconductors are attractive materials for polarization enabled optoelectronic devices. Suzuki *et al.* [10] introduced chirality into graphene quantum dots by functionalizing them with D or L cysteine molecules. Other notable work includes tuning the photoluminescence of carbon nanodots through surface oxidation and nitrogen atom doping. Optically tunable, differently shaped carbon quantum dots with narrow band gaps have also emerged as promising materials. Recently, hexagonal and triangular shaped optically tunable graphene/carbon quantum dots have been reported [11, 12].

1.3.2. Structure of Carbon Nanodots

Exact identification of the chemical structure of carbon nanodots (CNDs) is implausible to determine due to the variety of precursors utilized, techniques employed, and post-chemical treatments. It is generally accepted that the structure of CNDs is made up of a carbogenic core that harbours a number of functional groups, primarily oxygen-bearing groups such as carboxyl, carbonyl, and epoxy functionalities and amine or hydroxyl functionalities. This variability results in completely distinct intrinsic architectures for the CNDs, as the surface and the core structure are extremely sensitive to the synthesis pathways and the reaction settings. Thus, it is nearly hard to compare several CNDs qualitatively. Despite this uncertainty, there have been some intriguing attempts in the literature to systematically classify the most likely basic structures and morphologies of CNDs. In general, the core structure of CND is evaluated using various characterization tools, including High-Resolution Transmission Electron Microscopy (HR-TEM), X-ray Diffraction (XRD) analysis, Atomic Force Microscopy (AFM), and Raman spectroscopy. The attached surface groups are primarily analyzed using Fourier-Transform Infrared (FT-IR) spectroscopy and X-ray Photoelectron Spectroscopy (XPS).

Numerous reports in the literature suggest an extraordinary amorphous core structure for CNDs based on meticulous analysis of their XRD patterns and Raman spectral

profiles. Notably, the peaks around 1350 and 1600 cm^{-1} in the Raman spectra of CNDs indicate the presence of disordered sp^2 carbon and crystalline graphitic carbon. Hu *et al.* assigned a diamond-like orientation to the core structure of CNDs based on the SAED pattern and ring radius ratio. The presence of sp^2 graphitic clusters within the oxygen containing amorphous carbon matrix of CNDs is further confirmed by the HR-TEM images and Raman spectrum in several reports. An arrangement of functionalized graphite layers are envisaged in the system **(Figure 1.2 (a))** and **Figure 1.2 (b)** shows a representative structure for CNDs.

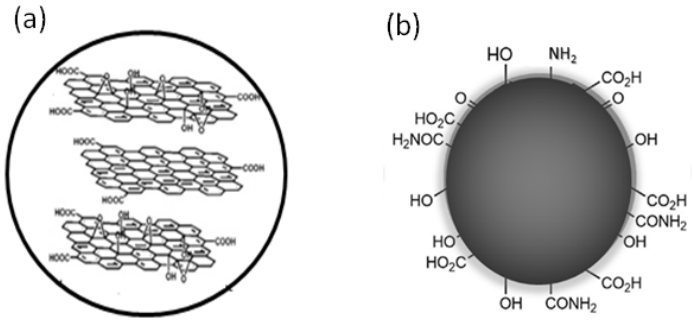

Figure 1.2 (a) Functionalized graphite layers on CNDs, (b) representative structure for CNDs.

Valcárcel *et al.* [13] conducted a rational and systematic classification of carbon nanodots (CNDs) based on their nature, crystalline structure, and quantum confinement. According to their classification, amorphous quasi-spherical nanodots that lack quantum confinement are termed carbon dots/carbon nanodots

(CNDs), while spherical quantum dots with quantum confinement and crystalline structures are referred to as carbon quantum dots (CQDs). The π-conjugated single sheets are known as graphene quantum dots (GQDs). These different types of CNDs are formed depending on the precursors and synthesis methods used during their fabrication. In 2018, the concept of carbonized polymer dots (CPDs) was proposed, emphasizing their formation process, structure, and photoluminescence mechanism. CPDs possessed a unique core–shell nanostructure [14, 15]. All these categories of CNDs exhibit comparable photoluminescence properties. Classification of CNDs based on their core structure is represented in **Figure 1.3.**

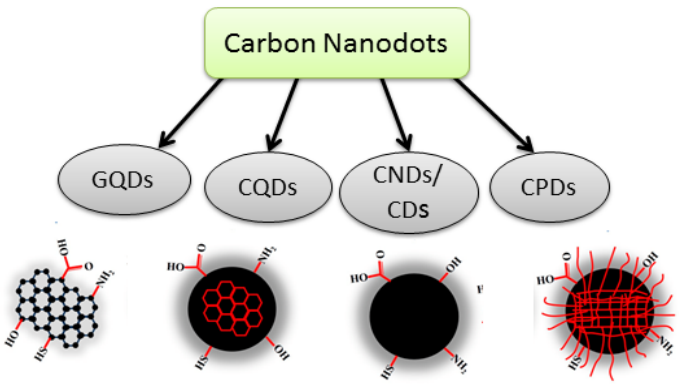

Figure 1.3. Classification of CNDs

1.3.3. Origin of luminescence in Carbon Nanodots

The origin of the luminescence in carbon nanodots has been a perplexing issue ever since CNDs were discovered, and has never had a satisfactory answer. One major issue that the researchers face is the suggestion of a universal mechanism for fluorescence which could be applicable for a broad range of CNDs. The synthesis of CNDs from various precursors using different methods results in complex structures and diverse surface functionalities. The differing optical and structural properties exhibited by various CNDs complicate comparisons and make it challenging to develop a unified theory [16]. Despite the various mechanistic assumptions proposed to explain the fluorescence of CNDs, the actual mechanism still remains a topic of debate among researchers. Currently, the most widely accepted photoluminescence mechanisms include (i) quantum confinement effect/core state emission, (ii) surface state emission, and (iii) molecular fluorescence. In the first one, the fluorescence originates from spherical-like core formed by stacking multiple graphene fragments in an ordered or disordered manner. The second is the luminescence originating from the presence of rich functional groups distributed on the surface of CNDs. The third one, molecular fluorescence mechanism attributes the property to molecules that are associated with CNDs in solution. **Figure 1.4** suggests the major sources of luminescence in CNDs. Details on these three aspects are discussed below.

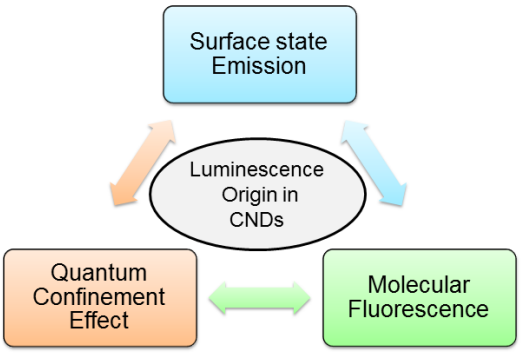

Figure 1.4 Luminescence origins in CNDs

(i) Quantum confinement effect/core state emission

Nanoparticles have potentially useful applications across various fields of science and technology due to their enhanced optical, electrical, and electronic properties compared to their bulk counterparts. This enhancement is largely influenced by their size, which falls within the quantum confinement regime [17, 18]. It has been established that as the size of a particle decreases to dimensions smaller than the exciton Bohr radius, the quasi-continuous electronic levels near the Fermi energy level shift to discrete energy levels. This transition results in the strictly confined motion of carriers, leading to size dependent optical and electronic properties known as the Quantum Confinement Effect (QCE). In the case of CNDs, the quantum confinement effect of conjugated π electrons in the carbon core structure is significant. The carbon core state fluorescence results from the band gap transition of conjugated π electrons within the π domains of the

carbon structure. In the carbon core structure, sp^2 carbon clusters are dispersed within the sp^3 carbon skeleton. Consequently, the optical properties of CNDs are determined by the π-electron state of the sp^2 carbon clusters [19, 20]. As the particle size increases, the size of the conjugated π domains also grows, resulting in a decrease in the band gap. This decrease in band gap causes a red shift in the emission. Therefore, by controlling the size of the carbon core π domains, the fluorescence of CNDs can be tuned.

Numerous studies have evidenced the occurrence of QCE in carbon nanodots. Kim and colleagues investigated the impact of carbon nanodot size on their optical properties by measuring fluorescence and absorbance in CNDs. Their findings revealed that the absorption peak energy of CNDs decreases with increasing size, supporting the presence of QCE [21]. CNDs synthesized from citric acid and urea using various solvents such as water, glycerol, and DMF exhibited emissions ranging from blue to red. The different solvents influence the dehydration and carbonization process during synthesis, resulting in CNDs with varying sizes of π domains [22]. Li and colleagues further elucidated the size-dependent fluorescence emission by conducting optical studies on CNDs of varying sizes (1.2 to 4 nm), separated using column chromatography techniques [8]. Additionally, numerous studies in the literature demonstrate the size dependent absorbance and emission profiles of CNDs [21, 23]. These studies show multi-color emissions from CNDs of different sizes, having identical chemical

composition, suggesting that QCE may be a major contributor to the observed fluorescence characteristics of CNDs.

(ii) Surface state emission

Surface state in CNDs refers to the boundary region or spherical shell distinct from the core structure [23]. Surface state fluorescence encompasses factors such as surface oxidation level, emissive traps, and surface functional groups. Increased surface oxidation primarily induces red-shifted fluorescence in two main ways. Firstly, higher surface oxidation enhances the presence of surface defects, which can act as emissive centers by trapping exciton energy, leading to red-shifted emission. Secondly, elevated oxygen content on the CNDs surface decreases the band gap, also contributing to red-shifted emission.

(a) Surface oxidation: It has been suggested that the surface oxygen content in CNDs plays a crucial role in longer wavelength emissions. Higher degrees of surface oxidation correspond to increased surface defects. Many studies in the literature emphasize that the luminescence characteristics of CNDs are exclusively determined by the degree of surface oxidation [23-25]. Liu *et al.* [25] explained the effect of surface oxidation on the red-shifted emission of CNDs in their work. They prepared CNDs from polyethyleneimine and glutaraldehyde with varying compositions, reporting that changes in the degree of surface oxidation were the primary reason for tunable emission. Ding *et al.* [16] synthesized CNDs with 35% fluorescence quantum yield (QY) from a mixture

of urea and p-phenylenediamine using a hydrothermal method, resulting in reddish-yellow fluorescence. After separating the CNDs by silica column chromatography, the fractions exhibited a gradient of colors from blue to red, all with similar particle size distribution and excitation-independent emission spectra. The key difference was the extent of surface oxidation, leading them to conclude that the red-shifted emission was due to the incorporation of more oxygen species. Some studies have explained that the fluorescence of CNDs is due to the combined effects of surface state and quantum confinement [26]. Bao *et al.* [27] reported that increasing the size of CNDs also enlarged the conjugated π electron system, resulting in red-shifted emission. Additionally, they experimented with different degrees of surface oxidation, which narrowed the energy gap. They proposed that the fluorescence of CND could be due to the synergistic effect of these two phenomena.

(b) Surface functional groups: Different surface functional groups on CNDs are a major reason for their excitation-dependent emission spectra, as they create various energy states. The edge state of CND consists of carbon atoms and surface functional groups attached to the carbon backbone. These edge states can influence the emission centers and thereby tune the fluorescence of CNDs. Zhang *et al.* [28] clearly explained the effect of nitrogen-containing functional groups on tunable fluorescence in their study. Chandra *et al.* [29] developed an easy microwave method to synthesize functionalized CNDs from biodegradable

polysaccharides. Yang *et al.* [30] synthesized intrinsically fluorescent CND from glucose, using monopotassium phosphate as a passivating and functionalizing agent. The surface functionalization occurs through the oxidation of hydroxyl groups during the hydrothermal process.

(iii) Molecular fluorescence

Recent research suggests that molecular fluorescence may play a significant role in determining the luminescent properties of CNDs. This type of fluorescence emission is thought to be due to the presence of organic impurities or by-products formed during the bottom-up synthesis process [31]. Studies on the emission behavior of CNDs derived from citric acid and nitrogen containing precursors indicate that incomplete carbonization or partial decomposition of these precursors results in the formation of inherently fluorescent molecular fragments, such as 2-pyridone derivatives [32, 33] and citrazinic acid [34-36]. These fragments alter the core structure of the CNDs under high temperature conditions [37]. It has been established that luminescent by-products like citrazinic acid typically exhibit blue emission around 420-440 nm [38], which coincides with the emission range of blue-emitting CNDs. Consequently, it is challenging to distinguish the fluorescence emitted by molecular fluorophores from that of the CND structure itself. Rogach *et al.* [38] demonstrated the impact of molecular fluorophores attached to the surface of CNDs on their

emission properties by synthesizing three different types of CNDs from citric acid.

1.3.4. Synthesis of Carbon Nanodots

The synthesis methods for carbon nanodots (CNDs) can be categorized into two: top-down and bottom-up, based on the starting carbon source. Top-down methods involve directly exfoliating a bulk carbon source, such as graphite, graphene, or carbon fiber into nanoscale CNDs, followed by surface treatment. In contrast, bottom-up methods synthesize CNDs from small organic molecules containing carbon, such as glucose or citric acid or natural precursors. To enhance and fine-tune optical characteristics like quantum yield, emission wavelength, and photostability, surface passivation and hetero-atom doping are employed during the synthesis of carbon nanodots.

(i) Top-down Methods

Currently, macroscopic carbonaceous materials like activated carbon, carbon nanotubes (CNTs), and graphite are widely used for producing CNDs through top-down approaches such as the arc discharge, laser ablation, ultrasonic treatment, and electrochemical methods. However, these techniques typically involve high acidity, high potential, and high energy conditions. Due to such harsh conditions, these top-down methods are relatively tedious, in comparison to the bottom-up approaches.

a) Laser ablation

Laser ablation process typically involves irradiating a carbon target with a laser beam in the presence of water vapor and an inert gas as a carrier, all under high temperature and pressure conditions. After a specified irradiation time, the reaction mixture is usually centrifuged, purified, and subjected to surface passivation processes to obtain fluorescent CNDs. The advantages of laser ablation techniques include their rapid production and environmentally friendly nature. However, this method has drawbacks such as requiring skilled personnel, sophisticated equipment, and involving tedious post-synthetic processes. Sun *et al.* [6] produced carbon nanodots through laser ablation by preparing a carbon target from a hot-pressed mixture of graphite powder and cement, followed by baking, curing, and annealing under argon flow. They used a Q-switched Nd laser (1064 nm, 10 Hz) to ablate the carbon target in an argon gas flow with water vapor at 900 °C and 75 KPa. The resulting non-fluorescent nanoparticles were treated with 2.6 M HNO_3 and refluxed for 12 hours. Surface passivation with diamine-terminated poly(ethylene glycol) (PEG_{1500N}) produced fluorescent CNDs with an average size of 3-10 nm. Purification was achieved through dialysis against water and centrifugation, yielding purified carbon nanodots in the supernatant. Hu *et al.* [39] also reported synthesizing CNDs using the laser ablation method, who achieved CNDs with a fluorescence quantum yield (QY) of up to 20% using C^{13} powder as a molecular precursor.

b) Arc discharge

This method was first used by Xu *et al.* [5], who accidentally synthesized fluorescent carbon nanomaterial during purification of single-walled carbon nanotubes (SWCNTs) derived from arc discharge soot. Bottini *et al.* [40] created highly fluorescent CNDs using an arc discharge treatment on both pristine and oxidized single-walled carbon nanotubes (SWCNTs). The CNDs displayed violet-blue emission when derived from pristine SWCNTs and blue to green emission when derived from oxidized SWCNTs.

c) Electrochemical methods

The first description of an electrochemical method to prepare fluorescent carbon nanodots was provided by Zhou *et al*. [41]. They synthesized blue luminescent CNDs from multi-walled CNTs using tetrabutylammonium perchlorate solution as the electrolyte. Crystalline carbon nanodots , which can act as efficient photocatalysts, were prepared by Li and co-workers [8] through the electrochemical treatment of graphite. These CNDs exhibited size-tunable up-conversion luminescence, a remarkable photoluminescence behavior. In 2015, Hou *et al*. [42] fabricated bright blue-emitting carbon nanodots (CNDs) through the electrochemical treatment and carbonization of urea and sodium citrate in de-ionized water.

d) Chemical oxidation

Chemical oxidation involves treating the substrate with oxidative reagents such as HNO_3 and H_2SO_4. This process introduces abundant oxygen-containing functional groups, such as –COOH and –OH, which provide the carbon nanodots with high aqueous solubility and tunable emission properties. Qiao *et al.* [43] reported the synthesis of multicolour-emitting carbon nanodots through the chemical oxidation of activated carbon. The resulting biocompatible CNDs were utilized for bioimaging. Kim *et al.* [44] fabricated promising near infrared emitting CNDs through acidic oxidation treatment of tire soot. These CNDs were found to be efficient tools for both in-vitro and in-vivo bioimaging.

e) Ultrasonication

In this method, low and high pressure ultrasound waves generate small vacuum bubbles that disperse uniformly throughout the solution. This prevents aggregation and induces strong hydrodynamic shear forces. As a result, macroscopic carbon materials like graphite, activated carbon, and carbon nanotubes (CNTs) are fragmented into nanoscale CNDs due to the intense hydrodynamic shear forces created by the cavitation of these bubbles [45, 46]. Wu *et al.* [47] synthesized amine functionalized CNDs using an ultrasonic method for applications in cell imaging, nucleic acid sensing, and detecting metal ions such as cobalt (II) ions. In a study conducted by Huang *et al*. [48], PEG-decorated carbon nanodots with high quantum yield (QY) suitable for cell

imaging applications were synthesized through one-step ultrasonic treatment of cigarette ash and thiol group containing polyethylene glycol (SH-PEG).

(ii) Bottom-up Methods

Bottom-up approaches that achieve CNDs from molecular precursors are currently gaining popularity due to their advantages, including promising practical applicability, use of non-toxic precursor molecules, cost-effectiveness, ease of instrumentation, precise control, and straightforward methodology. More than 70% of the syntheses of CNDs proceed through bottom-up route.

a) Hydrothermal/solvothermal methods

The hydrothermal strategy for preparing CNDs offers advantages such as low cost and non-toxicity. Compared to other synthetic routes, the hydrothermal method is a simple approach for synthesizing CNDs/CQDs. Zhao's group [49] reported a simple and highly efficient route for preparing graphene quantum dots (GQDs) using hydrothermal treatment. Various raw materials, including chitosan, citric acid, glucose, amino acids, proteins etc. can serve as precursors for synthesizing CNDs using the hydrothermal carbonization (HTC) technique [45, 50]. Hydrothermal treatment of several natural precursors also leads to the formation of carbon nanodots (CNDs) [51, 52]. Hasan *et al.* [53] prepared various types of CQDs using microcrystalline

cellulose, furfural, and hydroxymethylfurfural as precursors through hydrothermal carbonization (HTC). In another study, N/S-doped carbon dots (N/S-CDs) were synthesized via hydrothermal methods using methyl blue, ethylenediamine, and citric acid as sources [54]. The resulting N/S-CDs exhibited excitation-independent blue fluorescence emission. Instead of water, other solvents are used in solvothermal synthesis [55]. Zhu *et al.* [56] reported the solvothermal synthesis of green-emissive CNDs using DMF as the solvent.

b) Microwave assisted treatments

Microwave assisted synthesis represents an energy efficient and eco-friendly approach for synthesizing carbon nanodots (CNDs) with short reaction times [57]. Zhu and colleagues [58] first reported the microwave synthesis of CNDs with precise electrochemiluminescence characteristics in 2009, using carbohydrates. Yu *et al.* [59] utilized a one-step microwave-assisted synthesis approach to produce CNDs from two precursor molecules: triethylenediamine hexahydrate and phthalic acid. This method reportedly enabled the synthesis of CNDs with a broader emission wavelength, excellent biocompatibility, and intense green fluorescence in just 1 minute. Wang *et al.* [60] synthesized bright fluorescent CNDs from egg membranes for dual analyte sensing of Cu^{2+} and glutathione. Ghanem and collaborators [61] proposed a microwave assisted synthesis strategy for nitrogen-doped carbon dots (NCDs). In this method, the resulting NCDs exhibited

exceptional fluorescent properties with a higher quantum yield (QY).

c) Pyrolysis/ Carbonization

Thermal decomposition is a highly favored method for synthesizing carbon nanodots (CNDs). It involves the carbonization or pyrolysis of large sized carbonaceous precursors at elevated temperatures. The advantages of this method include mass production of CNDs, cost-effectiveness, shorter reaction times, broader tolerance of precursor materials, solvent-free strategies, and ease of synthesis. Additionally, the fluorescent properties of CNDs can be optimized using this thermal method by controlling parameters such as the pH of the reaction mixture, reflux duration, and reaction temperatures [45, 62]. Shang and co-workers [63] synthesized CNDs by pyrolyzing citric acid as a precursor molecule, achieved by adjusting the degree of carbonization. A significant number of carbon nanodots are synthesized from various natural precursors through carbonization [64-66]. In another study, Ma *et al.* [67] proposed a strategy for large scale synthesis of nitrogen-doped carbon dots (NCDs) through one-step pyrolysis.

d) Chemical vapour deposition

The chemical vapor deposition (CVD) method, a well-known approach for fabricating carbon nanodots (CNDs), has been widely explored in recent years. In the CVD technique, the size of

the final product can be controlled by adjusting parameters such as the carbon source, growth time, hydrogen (H_2) flow rate, and temperature of the substrate. Fan *et al.* [68] first proposed chemical vapor deposition method for the preparation of CQDs, in which methane was used as a precursor.

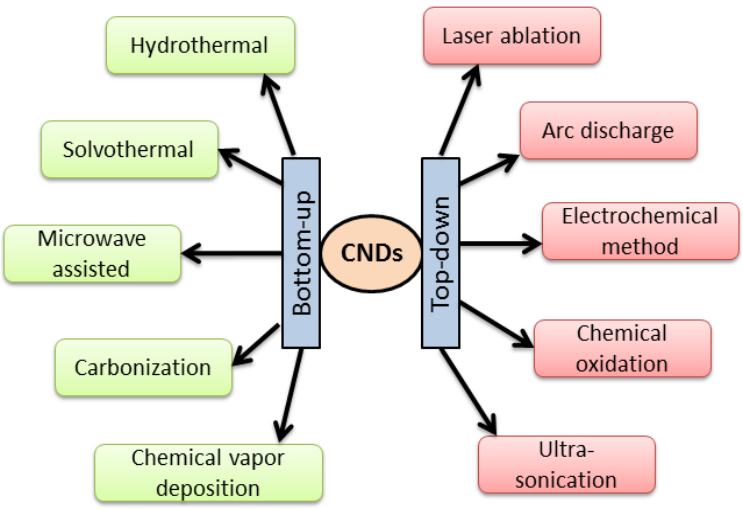

Figure 1.5. Different methods of synthesis of CNDs

1.3.5. Properties of Carbon Nanodots

The starting materials play a crucial role in determining the functionalities of carbon nanodots (CNDs). Consequently, CNDs synthesized from different precursors and reaction procedures exhibit distinct physicochemical properties. Their small size and high aspect ratio, combined with core and surface functionalities, make it challenging to pinpoint the exact origins of these

properties. As we know, the carbon nanodots are commonly classified into graphene quantum dots (GQDs), carbon quantum dots (CQDs), carbon dots/carbon nanodots and carbonized polymer dots (CPDs). These are characterized by a "core-shell" nanostructure, consisting of a nanoscale carbon core and surface functional groups. Their optical, electronic, and catalytic properties are determined by these varying structures. The following sections will discuss some of these properties in detail.

(i) Optical features

a) **Absorption:** Carbon nanodots typically exhibit optical absorption in the UV region, with an extension into the visible region. A common feature among most CNDs is an intense absorption band centered around 250–300 nm, attributed to the π–π* transition of the carbogenic core. Additionally, some CNDs display a weaker absorption peak around 350 nm, which is associated with the n–π* transition of the surface functionalities. The absorbance range of CNDs can vary depending on the type of CND, influenced by the surface functional groups and surface passivation [69, 70].

b) **Fluorescence:** Fluorescence is a distinctive feature of CNDs. Early studies revealed that CNDs exhibit unique excitation-dependent emission behavior, where changing the excitation wavelength results in noticeable shifts in the emission peak position and intensity [71]. The exact cause

of this excitation dependence remains unclear but may involve the optical selection of nanoparticles of different sizes and/or varying emissive traps on the CND surface [72]. Initially, surface passivation was essential to induce fluorescence, though the underlying reasons are only partially understood. Recently, more reports have emerged on CNDs with excitation-independent emission peak positions, likely due to homogeneous size and consistent surface chemical states [73]. The fluorescent properties of carbon nanodots (CNDs) have garnered significant attention from researchers due to their various sensing and analytical applications. Numerous mechanisms have been reported to gain a deeper understanding of the causes of fluorescence in CNDs [72, 74].

c) **Phosphorescence:** Most of the pure CNDs typically do not exhibit phosphorescence, which is usually observed when CNDs are dispersed in a polyvinyl alcohol (PVA) matrix [75]. Preliminary investigations suggest that the triplet states of aromatic carbonyls in CNDs are the source of phosphorescence. In the PVA matrix, PVA molecules form hydrogen bonds with the aromatic carbonyl groups of CNDs, rigidifying them. This reduces the loss of triplet energy through vibrations and rotations. Room-temperature phosphorescence in a carbon nanodot-impregnated polyvinyl alcohol (PVA) matrix was initially

noticed by Zhao's group [75]. After turning off the UV light, this matrix exhibits green phosphorescence.

d) Up-conversion fluorescence: In up-conversion fluorescence, the emission wavelength is shorter than the excitation wavelength, making it highly suitable for in vivo bioimaging in the near-infrared (NIR) region by reducing background fluorescence interference. Cao's research group first observed the up-conversion nature of carbon quantum dots in 2007 and utilized this feature for imaging human breast cancer cells [7]. Later, in 2011, Shen *et al.* [76] reported up-conversion in PEG-passivated graphene quantum dots (GQDs) [68]. Gogoi *et al.* [77] reported the bright up-converted photoluminescence characteristics in citric acid derived CNDs.

e) Photostability: Another notable property of carbon nanodots is their photostability, as many CNDs maintain consistent fluorescence intensity even under continuous UV light illumination. Ju *et al.* [78] emphasised the remarkable photostable properties of green and yellow emissive carbon nanodots, demonstrating a little decrease in intensity even after 8 hours in the presence of 365 nm UV radiation.

(ii) Catalytic properties

Carbon nanodots are utilized as photocatalysts for the degradation of pollutants including organic dyes [79] and others. They are also employed in water splitting [80, 81], CO_2 reduction

[81, 82], and various chemical reactions [83] in the context of solar energy conversion. The advantages of using CNDs for these applications include their broad light absorption range (from UV to NIR), low cost, excellent photostability, and their capability for charge separation and transfer. Due to the excellent photocatalytic activity, CNDs have been widely applied in the photocatalytic field to enhance the activity of catalysts. Prasannan and coworkers [84] synthesized a CND/ZnO composite that exhibits higher photocatalytic activity than the pure ZnO catalyst. Tyagi *et al.* [85] reported CQD/TiO_2 catalyst used for the degradation of methylene blue. Efficient degradation of methyl orange dye by CQDs/TiO_2 composites was prepared by Deg *et al.* [86]

(iii) Reducing properties

In addition to their intrinsic fluorescence, good aqueous solubility, as well as low toxicity, carbon nanodots have recently been recognized for their reducing properties. This reducing capability is primarily utilized in the synthesis of metal nanoparticles through the reduction of noble metals [87, 88]. Lu *et al.* [89] utilized hydroxyl rich carbon nanodots as both reducing and stabilizing agents for the formation of metal nanoparticles. The presence of surface oxygen functionalities enables CNDs to act as electron donors, making them potential candidates as reducing agents. Exploring the use of these CNDs as a novel class of environmentally friendly and cost-effective reducing agents could be valuable, even if their applications are somewhat limited. Ansi

and coworkers demonstrate that table sugar (sucrose)-derived carbon dots (TS-CDs) can serve as an environmentally benign reducing agent for the synthesis of metal nanoparticles, effectively substituting traditional chemicals such as $NaBH_4$ and hydrazine [88]. In 2019, Ghosh and colleagues investigated the synthesis of gold nanoparticles using citric acid derived CND with the addition of sodium hydroxide. They demonstrated the catalytic action of these nanoparticles against 4-nitrophenol [90]. In addition to their reducing action on Ag (I) and Au(III), CNDs have also been proven effective in reducing Fe(III) to Fe(II) [91].

1.3.6. Applications of Carbon Nanodots

Since their discovery, scientists have been eager to explore the applications of carbon nanodots (CNDs). Initially, CNDs were primarily used for sensing and imaging. However, recent research has significantly expanded their applicability to various fields, leading to a growing and ever-expanding list of CND applications. Here we briefly mention some important applications.

a) **Sensing:** Due to their strong fluorescence emission, carbon nanodots can serve as fluorescence based optical sensors for detecting various analytes. The detection method, based on the fluorescence response, may involve either 'fluorescence enhancement' or 'fluorescence quenching.' Most CND-based sensors utilize the fluorescence quenching process. CNDs-based fluorescence sensors have been used to detect a wide variety of analytes, including metal ions

[92-98], anions [99-104], and biologically important molecules [105-107]. CNDs and CND-based composites have proven to be useful for detection purposes. Numerous reports highlight the use of CNDs for the sensitive detection of explosives, demonstrating better efficiency and low-cost technology [108, 109].

b) **Bioimaging/Drug delivery:** CNDs, with their unique properties such as high quantum yield (QY), low toxicity, photostability, and resistance to photobleaching and degradation, are promising for biological applications. Sahu *et al.* [110] synthesized CNDs from orange juice and used them for in-vitro bioimaging of human osteosarcoma (MG-63) cells. CNDs can enable the diagnosis of various types of cancer and other diseases by providing real-time 3D imaging and significant information about the location, size, and type of tumors within the human body. Different cell, tissue structures and shapes exhibit specific responses to substances like CNDs. Ya-Ping Sun *et al.* [6] pioneered the use of carbon nanodots for bioimaging. They initially employed carbon nanodots, synthesized via laser ablation, to label E. coli ATCC 25922 cells. Ray's team achieved successful synthesis of water soluble fluorescent CNDs with diameters ranging from 2 to 6 nm through nitric acid oxidation of carbon soot. These CNDs exhibit green fluorescence when exposed to UV light, demonstrating potential for use in cell imaging due to their ability to

penetrate HepG2 cells without requiring additional functionalization [111]. CNDs offer advantages in visualizing drug accumulation and activities at pathological sites due to their fluorescent properties. These properties are crucial for assessing the therapeutic efficacy of medicines [112-114]. Zheng *et al.* [115] employed carbon nanodots synthesized via thermal pyrolysis of citric acid and polyene polyamine to transfer oxaliplatin, a platinum-based anticancer drug widely utilized in over 50% of clinical chemotherapeutic treatments for cancer due to its high effectiveness. The biocompatibility of functionalized CND is crucial for their use in biological media such as live cells, tissues, and animals. Over the past few years, numerous researchers have systematically evaluated the cytotoxicity of both raw and passivated CNDs [116, 117]. Generally, the carbon cores of CNDs are nontoxic, and any potential toxicity is primarily due to the agents used for surface passivation. It has been demonstrated that CNDs with nontoxic surface passivating agents can be safely used for in vivo imaging, even at very high concentrations [118]. Photodynamic therapy is a recent advancement in biomedical nanotechnology that utilizes energy transfer to destroy damaged cells and tissues. This technique is particularly effective against cancer cells, as it targets and eliminates malignant tissues while sparing healthy ones. The targeted destruction in photodynamic therapy is

achieved using fluorescent CNDs, which possess sufficient photostability [119]. Zhao *et al.* [120] produced N and P co-doped red emissive CNDs as efficient photodynamic therapy (PDT) agents, utilizing o-phenylenediamine and phosphoric acid as the raw materials. Choi *et al.* [119] reported multifunctional CNDs that can act as both bioimaging and targeted photodynamic therapeutic agents in cancer cells. The authors confirmed the in vitro and in vivo potential of folic acid-modified CNDs with zinc phthalocyanine acting as a photosensitizer**.** He *et al.* [121] synthesised diketopyrrolopyrrole-coupled fluorescent CNDs (DPP-CNDs) via hydrothermal method, using chitosan and diketopyrrolopyrrole (DPP) as the precursors and thereafter explored the potential applications of DPP-CNDs in photodynamic treatment. Li and colleagues [122] proposed a carbon nanodots (CNDs)-based drug delivery system for use in both photodynamic therapy and chemotherapy. Kuo *et al.* [123] reported that N-doped CNDs exhibit good biocompatibility and water solubility, making them suitable for in vivo bioimaging.

c) **Photocatalysis:** Numerous researches have investigated the photocatalytic potential of CNDs due to their broad light absorption, PL characteristics, and electron transfer capabilities. CNDs can combine with other materials to form composite catalysts or function as a single photocatalyst in the absence of a co-catalyst. Li *et al.* [124] synthesized CNDs

from graphite rods using an alkali-assisted electrochemical method. These CNDs exhibited both down and up-converted photoluminescence and were effective as near-infrared (NIR) light-driven photocatalysts. They achieved 92% conversion and 100% selectivity in the selective oxidation of benzyl alcohol to benzaldehyde after 12 hours of irradiation in the presence of H_2O_2. Yang *et al.* [125] reported that combining silver nanoparticles with carbon nanodots created an ideal catalyst for the oxidation of cyclohexane. The fabrication of CNDs/ZnO composites and the evaluation of their activity for the photo-degradation of dyes have garnered substantial attention [126-128]. Ming *et al.* [129] successfully produced carbon nanodots (CNDs) using a one-pot electrochemical process. This cost-effective and environmentally friendly synthetic methodology demonstrated great promise, exhibiting high photocatalytic activity of CNDs for the degradation of methyl orange. A two-step hydrothermal process was developed by Song *et al.* [130] to create a CND–WO_2 photocatalyst. Rhodamine B was photocatalytically degraded by the authors using this catalyst. Several other examples can be found for various organic dyes, including methylene blue [131-135], rhodamine B [131, 133, 136, 137], methyl orange [135, 138, 139], crystal violet [140], methyl violet [139], metanil yellow [138] and malachite green [139]. Using CND-based photocatalysts to produce hydrogen fuel from water is the

most promising area of research in recent years. A study by Sun *et al.* [141] revealed the photo-decomposition of CO_2 using doped CNDs containing Au as the photocatalyst. Liu *et al.* [142] reported the successful production of H_2 through water splitting using an inexpensive, ecologically friendly CNDs-gC_3N_4 hybrid catalyst.

d) **Optoelectronics:** Carbon nanodots are promising materials for light emitting diodes (LED) compared to toxic and expensive metal-based phosphors or semiconducting materials, owing to their non-toxic nature, cost-effectiveness, and high luminescence properties. The use of carbon nanodots (CNDs) in optoelectronic devices has garnered significant scientific attention in recent years [143, 144]. In 2010, Wang *et al.* [145] achieved direct white light emission from CNDs, opening the possibility of fabricating CND-based white light emitting devices [12, 146-149]. The tunable fluorescence behavior of carbon nanodots (CNDs) allows them to be used in the creation of different color-emissive or multi-color-emissive LEDs. Lu *et al.* [150] synthesized CNDs with red emission and a high quantum yield (QY) of 33.96%. These particles were incorporated into poly (methylmethacrylate) and utilized in red and white LEDs. CNDs with different emission colors were prepared and embedded into epoxy resin to prevent aggregation while serving as the active layer for white light-emitting diodes (WLEDs) [151]. In a study, it was

demonstrated that the emission of WLEDs could be tuned from cold white to warm white by adjusting the amount of CNDs in the epoxy resin [152].

e) **Anti-counterfeiting**: Anti-counterfeiting technologies are gaining increasing interest for enhancing tracking and preventing fraud in items such as tag labels, banknotes, brands, certificates and more. Recently, researchers have investigated CNDs for anti-counterfeiting applications [153-157]. Jiang *et al.* [153] developed carbon nanodot dispersions within a polyvinyl alcohol (PVA) matrix, creating a comprehensive anti-counterfeit system that integrates photoluminescence, up-conversion photoluminescence (UCPL), and room-temperature phosphorescence (RTP). The carbon nanodots were synthesized by dissolving m-phenylenediamine in ethanol and heating the solution in an autoclave for several hours, followed by purification using a silica column chromatography. PVA is a popular and eco-friendly packaging material. Liu *et al.* [158] proposed that adding CNDs to PVA packaging material can be a convenient route to anti-counterfeiting. The stability of CND-based fluorescent inks and CND-polymer composites, which are employed to generate random fluorescent patterns for anti-counterfeiting, was demonstrated by Zhu *et al.* [9]. Kalytchuk and co-workers synthesized CNDs from citric acid and ethylenediamine, which have applications in anti-

counterfeiting [159]. Yang *et al.* [160] reported the synthesis of phosphorus-doped carbon nanodots (PC-dots) with promising anti-counterfeiting applications. When illuminated at 365 nm, these PC-dots emitted green light at pH 3-7, while at higher pH levels, they emitted a blue/green color. The QR code printed with an aqueous dispersion of PC-dots appeared golden yellow under daylight. Under 365 nm radiation, the emission could be reversibly adjusted from green to cyan by brushing with dilute NaOH solution and back to cyan by brushing with dilute CH_3COOH.

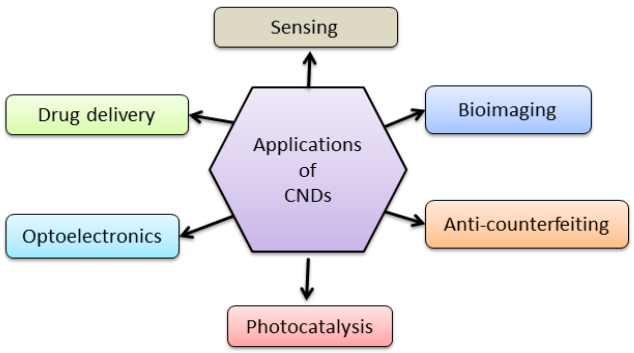

Figure 1.6 Applications of CNDs

1.4. Present Work

The wright selection of the precursor is crucial in CND synthesis for fine-tuning their applications. The simple preparation, excellent performance, low cost, and good biocompatibility of CNDs make them popular in chemistry, optics,

energy and biology. Research on CNDs derived from small organic molecules has significantly advanced, covering preparation strategies, properties, mechanisms, and applications. These findings suggest that CNDs derived from organic molecule precursors offer unique opportunities to explore new phenomena and characteristics across various disciplines, despite some unresolved key issues. In this study, p-phenylenediamine is chosen as the precursor for synthesizing CNDs. Recently, phenylenediamine isomers have been extensively explored as a carbon source for CND preparation.

1.4.1. Phenylenediamine derived carbon nanodots

Phenylenediamine ($C_6H_4(NH_2)_2$, PD) possesses highly active amino groups, allowing it to generate various oxidation products through oxidation and polymerization at high, low, and even room temperatures. These oxidation products can be further cross-linked, carbonized, or polymerized to produce carbon nanodots (CNDs) [161-163]. Three isomers of PD exist (o-PD, m-PD and p-PD) and CNDs made from PD, have distinct characteristics. In 2015, Lin *et al.* utilized three isomers of phenylenediamine (o-PD, m-PD, and p-PD) as precursors to synthesize CNDs that exhibited red, green, and blue photoluminescence emission under a single light excitation. This was the first systematic preparation of multicolor PL materials, and the PL mechanism of these three PD isomers was investigated together. Since then, the preparation of CNDs derived from PD and its derivatives has become a hot

research topic. Compared with other isomers, p-PD is mostly selected as carbon source for the preparation of CNDs with long wavelength emission. **Table 1.1** displays some previous works on p-PD derived carbon nanodots**.** In most of the works researchers often mix PD with other compounds to obtain CNDs. Here, in this work we explore the utility of p-PD as a single carbon source to produce CNDs.

Table 1.1 List of few CNDs derived from p-PD

Carbon source	Method	λ_{em} (nm)	Size (nm)	Reference
p-PD and Oxalic acid	solvothermal	609	2.66	[164]
p-PD and $FeCl_3$	Catalytic oxidation	600	1.2-2.8	[165]
p-PD and folic acid	Hydrothermal	470	2.06	[166]
p-PD, and Cystamine hydrochloride	Solvothermal	550	5	[167]
p-PD, phosphoric acid and $Mn(OAc)_2$	Microwave	600	6.47	[168]
p-PD and amino benzoic acid	Hydrothermal	653	10-12	[169]
p-PD	solvothermal	615	2-6.5	[170]

1.4.2. Objectives of the work

Herein, synthesis, characterization and application of p-PD derived carbon nanodots are provided. The effect of various solvents on the luminescence of CNDs is examined and luminescence based sensors are proposed for species of

environmental/biological significance. The analyte species included moisture, metal ion and nitroaromatics. Specific objectives of the work are:

- Synthesis of CNDs from p-Phenylenediamine through hydrothermal method.
- Thorough characterization of the system using different characterization techniques such as HR-TEM, FT-IR spectroscopy, XRD, XPS, Raman spectroscopy, UV-visible and Fluorescence spectroscopy.
- Study the influence of solvents on the luminescence of CNDs: Solvatochromic nature.
- Developing fluorimetric/ naked eye sensor for analytes of significance:

  (i) Metal ions

  (ii) Picric acid

  (iii) Moisture in organic solvent.

References

1. Riggs, J.E., et al., *Strong luminescence of solubilized carbon nanotubes.* Journal of the American Chemical Society, 2000. **122**(24): p. 5879-5880.

2. Mochalin, V., et al., *The properties and applications of nanodiamonds.* Nano-enabled medical applications, 2020: p. 313-350.

3. Basso, L., et al., *Nanodiamonds: Synthesis and application in sensing, catalysis, and the possible connection with some processes occurring in space.* Applied Sciences, 2020. **10**(12): p. 4094.

4. Schirhagl, R., et al., *Nitrogen-vacancy centers in diamond: nanoscale sensors for physics and biology.* Annual review of physical chemistry, 2014. **65**: p. 83-105.

5. Xu, X., et al., *Electrophoretic analysis and purification of fluorescent single-walled carbon nanotube fragments.* Journal of the American Chemical Society, 2004. **126**(40): p. 12736-12737.

6. Sun, Y.-P., et al., *Quantum-sized carbon dots for bright and colorful photoluminescence.* Journal of the American Chemical Society, 2006. **128**(24): p. 7756-7757.

7. Cao, L., et al., *Carbon dots for multiphoton bioimaging.* Journal of the American Chemical Society, 2007. **129**(37): p. 11318-11319.

8. Li, H., et al., *Water-soluble fluorescent carbon quantum dots and photocatalyst design.* Angewandte Chemie, 2010. **26**(122): p. 4532-4536.

9. Zhu, S., et al., *Highly photoluminescent carbon dots for multicolor patterning, sensors, and bioimaging.* Angewandte Chemie International Edition, 2013. **52**(14).

10. Suzuki, N., et al., *Chiral graphene quantum dots.* ACS nano, 2016. **10**(2): p. 1744-1755.

11. Lee, S.H., et al., *Synthesis of single-crystalline hexagonal graphene quantum dots from solution chemistry.* Nano letters, 2019. **19**(8): p. 5437-5442.

12. Yuan, F., et al., *Engineering triangular carbon quantum dots with unprecedented narrow bandwidth emission for multicolored LEDs.* Nature communications, 2018. **9**(1): p. 2249.

13. Cayuela, A., et al., *Semiconductor and carbon-based fluorescent nanodots: the need for consistency.* Chemical Communications, 2016. **52**(7): p. 1311-1326.

14. Xia, C., et al., *Hydrothermal addition polymerization for ultrahigh-yield carbonized polymer dots with room temperature phosphorescence via nanocomposite.* Chemistry–A European Journal, 2018. **24**(44): p. 11303-11308.

15. Liu, J., et al., *One-step hydrothermal synthesis of nitrogen-doped conjugated carbonized polymer dots with 31% efficient red emission for in vivo imaging.* Small, 2018. **14**(15): p. 1703919.

16. Ding, H., et al., *Full-color light-emitting carbon dots with a surface-state-controlled luminescence mechanism.* ACS nano, 2016. **10**(1): p. 484-491.

17. Yan, X., B. Li, and L.-s. Li, *Colloidal graphene quantum dots with well-defined structures.* Accounts of chemical research, 2013. **46**(10): p. 2254-2262.

18. Li, Q., et al., *Nitrogen-doped colloidal graphene quantum dots and their size-dependent electrocatalytic activity for the oxygen reduction reaction.* Journal of the American Chemical Society, 2012. **134**(46): p. 18932-18935.

19. Sk, M.A., et al., *Revealing the tunable photoluminescence properties of graphene quantum dots.* Journal of Materials Chemistry C, 2014. **2**(34): p. 6954-6960.

20. Kwon, W., et al., *Size-controlled soft-template synthesis of carbon nanodots toward versatile photoactive materials.* Small, 2014. **10**(3): p. 506-513.

21. Kim, S., et al., *Anomalous behaviors of visible luminescence from graphene quantum dots: interplay between size and shape.* ACS nano, 2012. **6**(9): p. 8203-8208.

22. Tian, Z., et al., *Full-color inorganic carbon dot phosphors for white-light-emitting diodes.* Advanced Optical Materials, 2017. **5**(19): p. 1700416.

23. Bao, L., et al., *Electrochemical tuning of luminescent carbon nanodots: from preparation to luminescence mechanism.* Advanced materials (Deerfield Beach, Fla.), 2011. **23**(48): p. 5801-5806.

24. Hu, S., et al., *Tunable photoluminescence across the entire visible spectrum from carbon dots excited by white light.* Angewandte Chemie International Edition, 2015. **54**(10): p. 2970-2974.

25. Liu, H., et al., *Microwave-assisted synthesis of wavelength-tunable photoluminescent carbon nanodots and their potential applications.* ACS Applied Materials & Interfaces, 2015. **7**(8): p. 4913-4920.

26. Zhu, S., et al., *Photoluminescence mechanism in graphene quantum dots: Quantum confinement effect and surface/edge state.* Nano Today, 2017. **13**: p. 10-14.

27. Bao, L., et al., *Photoluminescence-tunable carbon nanodots: surface-state energy-gap tuning.* Advanced Materials, 2015. **27**(10): p. 1663-1667.

28. Zhang, Y., et al., *Multicolour nitrogen-doped carbon dots: tunable photoluminescence and sandwich fluorescent glass-based light-emitting diodes.* Nanoscale, 2017. **9**(45): p. 17849-17858.

29. Chandra, S., et al., *Tuning of photoluminescence on different surface functionalized carbon quantum dots.* RSC advances, 2012. **2**(9): p. 3602-3606.

30. Song, Y., S. Zhu, and B. Yang, *Bioimaging based on fluorescent carbon dots.* Rsc Advances, 2014. **4**(52): p. 27184-27200.

31. Essner, J.B., et al., *Artifacts and errors associated with the ubiquitous presence of fluorescent impurities in carbon nanodots.* Chemistry of Materials, 2018. **30**(6): p. 1878-1887.

32. Shi, L., et al., *Carbon dots with high fluorescence quantum yield: the fluorescence originates from organic fluorophores.* Nanoscale, 2016. **8**(30): p. 14374-14378.

33. Das, A., et al., *On the molecular origin of photoluminescence of nonblinking carbon dot.* The Journal of Physical Chemistry C, 2017. **121**(17): p. 9634-9641.

34. Reckmeier, C.J., et al., *Aggregated molecular fluorophores in the ammonothermal synthesis of carbon dots.* Chemistry of Materials, 2017. **29**(24): p. 10352-10361.

35. Sharma, A., et al., *Molecular origin and self-assembly of fluorescent carbon nanodots in polar solvents.* The journal of physical chemistry letters, 2017. **8**(5): p. 1044-1052.

36. Wang, W., et al., *Shedding light on the effective fluorophore structure of high fluorescence quantum yield carbon nanodots.* RSC advances, 2017. **7**(40): p. 24771-24780.

37. Liu, X., et al., *Structure and photoluminescence evolution of nanodots during pyrolysis of citric acid: from molecular nanoclusters to carbogenic nanoparticles.* Journal of Materials Chemistry C, 2017. **5**(39): p. 10302-10312.

38. Schneider, J., et al., *Molecular fluorescence in citric acid-based carbon dots.* The Journal of Physical Chemistry C, 2017. **121**(3): p. 2014-2022.

39. Hu, S.-L., et al., *One-step synthesis of fluorescent carbon nanoparticles by laser irradiation.* Journal of Materials Chemistry, 2009. **19**(4): p. 484-488.

40. Bottini, M., et al., *Isolation and characterization of fluorescent nanoparticles from pristine and oxidized electric arc-produced single-walled carbon nanotubes.* The Journal of Physical Chemistry B, 2006. **110**(2): p. 831-836.

41. Zhou, J., et al., *An electrochemical avenue to blue luminescent nanocrystals from multiwalled carbon nanotubes (MWCNTs).* Journal of the American Chemical Society, 2007. **129**(4): p. 744-745.

42. Hou, Y., et al., *One-pot electrochemical synthesis of functionalized fluorescent carbon dots and their selective sensing for mercury ion.* Analytica Chimica Acta, 2015. **866**: p. 69-74.

43. Qiao, Z.-A., et al., *Commercially activated carbon as the source for producing multicolor photoluminescent carbon dots by chemical oxidation.* Chemical Communications, 2010. **46**(46): p. 8812-8814.

44. Ko, H.Y., et al., *In vivo imaging of tumour bearing near-infrared fluorescence-emitting carbon nanodots derived from tire soot.* Chemical Communications, 2013. **49**(87): p. 10290-10292.

45. Tajik, S., et al., *Carbon and graphene quantum dots: a review on syntheses, characterization, biological and sensing applications for neurotransmitter determination.* RSC advances, 2020. **10**(26): p. 15406-15429.

46. Tsai, I.-H., J.-T. Li, and C.-W. Chang, *Effects of sonication and hydrothermal treatments on the optical and chemical properties of carbon dots.* ACS omega, 2021. **6**(22): p. 14174-14181.

47. Wu, Y., et al., *Facile ultrasonic synthesized NH2-carbon quantum dots for ultrasensitive Co2+ ion detection and cell imaging.* Talanta, 2019. **205**: p. 120121.

48. Huang, H., et al., *A one-step ultrasonic irradiation assisted strategy for the preparation of polymer-functionalized carbon quantum dots and their biological imaging.* Journal of colloid and interface science, 2018. **532**: p. 767-773.

49. Zhao, Y., et al., *A facile and high-efficient approach to yellow emissive graphene quantum dots from graphene oxide.* Carbon, 2017. **124**: p. 342-347.

50. Wang, S., et al., *Synthesis of non-doped and non-modified carbon dots with high quantum yield and crystallinity by one-pot hydrothermal method using a single carbon source and used for ClO– detection.* Dyes and Pigments, 2019. **164**: p. 7-13.

51. Bandi, R., et al., *Facile and green synthesis of fluorescent carbon dots from onion waste and their potential applications as sensor and multicolour imaging agents.* RSC advances, 2016. **6**(34): p. 28633-28639.

52. Wang, N., et al., *Green preparation of carbon dots with papaya as carbon source for effective fluorescent sensing of Iron (III) and Escherichia coli.* Biosensors and Bioelectronics, 2016. **85**: p. 68-75.

53. Hasan, M.R., et al., *Formation of carbon quantum dots via hydrothermal carbonization: Investigate the effect of precursors.* Energies, 2021. **14**(4): p. 986.

54. Lee, H., et al., *One-pot hydrothermal synthesis of carbon dots as fluorescent probes for the determination of mercuric and hypochlorite ions.* Nanomaterials, 2021. **11**(7): p. 1831.

55. Yang, X., et al., *Novel and green synthesis of high-fluorescent carbon dots originated from honey for sensing and imaging.* Biosensors and Bioelectronics, 2014. **60**: p. 292-298.

56. Zhu, S., et al., *Strongly green-photoluminescent graphene quantum dots for bioimaging applications.* Chemical communications, 2011. **47**(24): p. 6858-6860.

57. Gul, U., et al., *Microwave-assisted synthesis of carbon dots as reductant and stabilizer for silver nanoparticles with enhanced-peroxidase like activity for colorimetric determination of hydrogen peroxide and glucose.* Microchimica Acta, 2020. **187**: p. 1-8.

58. Zhu, H., et al., *Microwave synthesis of fluorescent carbon nanoparticles with electrochemiluminescence properties.* Chemical Communications, 2009(34): p. 5118-5120.

59. Yu, T., et al., *A rapid microwave synthesis of green-emissive carbon dots with solid-state fluorescence and pH-sensitive properties.* Royal Society open science, 2018. **5**(7): p. 180245.

60. Wang, Q., et al., *Microwave-assisted synthesis of carbon nanodots through an eggshell membrane and their fluorescent application.* Analyst, 2012. **137**(22): p. 5392-5397.

61. Ghanem, A., R.A.-Q.B. Al-Marjeh, and Y. Atassi, *Novel nitrogen-doped carbon dots prepared under microwave-irradiation for highly sensitive detection of mercury ions.* Heliyon, 2020. **6**(4).

62. Ludmerczki, R., et al., *Carbon dots from citric acid and its intermediates formed by thermal decomposition.* Chemistry–A European Journal, 2019. **25**(51): p. 11963-11974.

63. Shang, W., et al., *Facile one pot pyrolysis synthesis of carbon quantum dots and graphene oxide nanomaterials: All carbon hybrids as eco-environmental lubricants for low friction and remarkable wear-resistance.* Tribology International, 2018. **118**: p. 373-380.

64. Zhou, J., et al., *Facile synthesis of fluorescent carbon dots using watermelon peel as a carbon source.* Materials Letters, 2012. **66**(1): p. 222-224.

65. Xue, M., et al., *Green synthesis of stable and biocompatible fluorescent carbon dots from peanut shells for multicolor living cell imaging.* New Journal of Chemistry, 2016. **40**(2): p. 1698-1703.

66. Praneerad, J., et al., *Environmentally friendly supercapacitor based on carbon dots from durian peel as an electrode.* Key Engineering Materials, 2019. **803**: p. 115-119.

67. Ma, C.a., et al., *Highly efficient synthesis of N-doped carbon dots with excellent stability through pyrolysis method.* Journal of Materials Science, 2019. **54**(13): p. 9372-9384.

68. Fan, L., et al., *Direct synthesis of graphene quantum dots by chemical vapor deposition.* Particle & Particle Systems Characterization, 2013. **30**(9): p. 764-769.

69. Bhartiya, P., et al., *Carbon dots: Chemistry, properties and applications.* Journal of the Indian Chemical Society, 2016. **93**(7): p. 759-766.

70. Liu, M., *Optical properties of carbon dots: a review.* Nanoarchitectonics, 2020: p. 1-12.

71. Hsu, P.-C., et al., *Synthesis and analytical applications of photoluminescent carbon nanodots.* Green Chemistry, 2012. **14**(4): p. 917-920.

72. Baker, S.N. and G.A. Baker, *Luminescent carbon nanodots: emergent nanolights.* Angewandte Chemie International Edition, 2010. **49**(38): p. 6726-6744.

73. Wang, H., et al., *Excitation wavelength independent visible color emission of carbon dots.* Nanoscale, 2017. **9**(5): p. 1909-1915.

74. Demchenko, A.P. and M.O. Dekaliuk, *Novel fluorescent carbonic nanomaterials for sensing and imaging.* Methods and applications in fluorescence, 2013. **1**(4): p. 042001.

75. Deng, Y., et al., *Long lifetime pure organic phosphorescence based on water soluble carbon dots.* Chemical communications, 2013. **49**(51): p. 5751-5753.

76. Shen, J., et al., *Facile preparation and upconversion luminescence of graphene quantum dots.* Chemical communications, 2011. **47**(9): p. 2580-2582.

77. Gogoi, S. and R. Khan, *NIR upconversion characteristics of carbon dots for selective detection of glutathione.* New Journal of Chemistry, 2018. **42**(8): p. 6399-6407.

78. Ju, B., et al., *Photostable and low-toxic yellow-green carbon dots for highly selective detection of explosive 2, 4, 6-trinitrophenol based on the dual electron transfer mechanism.* ACS applied materials & interfaces, 2018. **10**(15): p. 13040-13047.

79. Han, M., et al., *Carbon dots–implanted graphitic carbon nitride nanosheets for photocatalysis: simultaneously manipulating carrier transport in inter-and intralayers.* Solar RRL, 2020. **4**(4): p. 1900517.

80. Luo, H., et al., *Pt single-atoms supported on nitrogen-doped carbon dots for highly efficient photocatalytic hydrogen generation.* Journal of Materials Chemistry A, 2020. **8**(29): p. 14690-14696.

81. Yan, Y., et al., *Systematic bandgap engineering of graphene quantum dots and applications for photocatalytic water splitting and CO_2 reduction.* ACS nano, 2018. **12**(4): p. 3523-3532.

82. Li, M., et al., *Facile microwave assisted synthesis of N-rich carbon quantum dots/dual-phase TiO_2 heterostructured nanocomposites with high activity in CO_2 photoreduction.* Applied Catalysis B: Environmental, 2018. **231**: p. 269-276.

83. Sarma, D., B. Majumdar, and T.K. Sarma, *Visible-light induced enhancement in the multi-catalytic activity of sulfated carbon dots for aerobic carbon–carbon bond formation.* Green Chemistry, 2019. **21**(24): p. 6717-6726.

84. Prasannan, A. and T. Imae, *One-pot synthesis of fluorescent carbon dots from orange waste peels.* Industrial & Engineering Chemistry Research, 2013. **52**(44): p. 15673-15678.

85. Tyagi, A., et al., *Green synthesis of carbon quantum dots from lemon peel waste: applications in sensing and photocatalysis.* RSC advances, 2016. **6**(76): p. 72423-72432.

86. Deng, Y., et al., *Visible–ultraviolet upconversion carbon quantum dots for enhancement of the photocatalytic activity of titanium dioxide.* ACS omega, 2021. **6**(6): p. 4247-4254.

87. Raveendran, V. and R.N. Kizhakayil, *Fluorescent carbon dots as biosensor, green reductant, and biomarker.* ACS omega, 2021. **6**(36): p. 23475-23484.

88. Ansi, V., et al., *Table sugar derived carbon dot—A promising green reducing agent.* Materials Research Bulletin, 2021. **139**: p. 111284.

89. Lu, Q., et al., *Hydroxyl-rich C-dots synthesized by a one-pot method and their application in the preparation of noble metal nanoparticles.* Chemical Communications, 2015. **51**(33): p. 7164-7167.

90. Ghosh, S., et al., *Carbon Dots Assisted Synthesis of Gold Nanoparticles and Their Catalytic Activity in 4-Nitrophenol Reduction.* ChemistrySelect, 2019. **4**(12): p. 3416-3422.

91. Shariati-Rad, M., T. Mohseninasab, and F. Parno, *Application of response surface methodology and green carbon dots as reducing agents in speciation of iron.* RSC advances, 2018. **8**(4): p. 2173-2180.

92. Mohammed, L.J. and K.M. Omer, *Dual functional highly luminescence B, N Co-doped carbon nanodots as nanothermometer and Fe^{3+}/Fe^{2+} sensor.* Scientific reports, 2020. **10**(1): p. 3028.

93. Sun, S., et al., *Highly luminescence manganese doped carbon dots.* Chinese Chemical Letters, 2019. **30**(5): p. 1051-1054.

94. Singaravelu, C.M., et al., *Solid-state fluorescent carbon dots for fluorimetric sensing of Hg^{2+}.* ACS Applied Nano Materials, 2021. **4**(6): p. 6386-6397.

95. Xu, Q., et al., *Preparation of highly photoluminescent sulfur-doped carbon dots for Fe (III) detection.* Journal of Materials Chemistry A, 2015. **3**(2): p. 542-546.

96. Liu, R., et al., *Ultra-sensitive and selective Hg^{2+} detection based on fluorescent carbon dots.* Materials Research Bulletin, 2013. **48**(7): p. 2529-2534.

97. Jiang, Y., et al., *N-doped carbon dots synthesized by rapid microwave irradiation as highly fluorescent probes for Pb^{2+} detection.* New Journal of Chemistry, 2015. **39**(5): p. 3357-3360.

98. Yoo, D., et al., *Carbon dots as an effective fluorescent sensing platform for metal ion detection.* Nanoscale research letters, 2019. **14**: p. 1-13.

99. Xiang-Jun, X., et al., *Fluorescent carbon dots for sensing metal ions and small molecules.* Chinese Journal of Analytical Chemistry, 2022. **50**(2): p. 103-111.

100. Xu, J., et al., *Carbon dots as a luminescence sensor for ultrasensitive detection of phosphate and their bioimaging properties.* Luminescence, 2015. **30**(4): p. 411-415.

101. Sun, X.-Y., et al., *Highly selective and sensitive sensing for Al^{3+} and F^- based on green photoluminescent carbon dots.* RSC advances, 2016. **6**(99): p. 97346-97351.

102. Li, Z., et al., *Highly luminescent nitrogen-doped carbon quantum dots as effective fluorescent probes for mercuric and iodide ions.* Journal of Materials Chemistry C, 2015. **3**(9): p. 1922-1928.

103. Yin, B., et al., *Green synthesis of carbon dots with down-and up-conversion fluorescent properties for sensitive detection of hypochlorite with a dual-readout assay.* Analyst, 2013. **138**(21): p. 6551-6557.

104. Jin, H., et al., *Carrot-derived carbon dots modified with polyethyleneimine and nile blue for ratiometric two-photon fluorescence turn-on sensing of sulfide anion in biological fluids.* Talanta, 2017. **169**: p. 141-148.

105. Li, X., et al., *Microwave synthesis of nitrogen and sulfur co-doped carbon dots for the selective detection of Hg^{2+} and glutathione.* Optical Materials, 2020. **99**: p. 109559.

106. Wang, L., et al., *Glutathione modified N-doped carbon dots for sensitive and selective dopamine detection.* Dyes and Pigments, 2021. **186**: p. 109028.

107. Jiang, Y., et al., *Microwave-assisted preparation of N-doped carbon dots as a biosensor for electrochemical dopamine detection.* Journal of colloid and interface science, 2015. **452**: p. 199-202.

108. Zhang, L., et al., *Simple and sensitive fluorescent and electrochemical trinitrotoluene sensors based on aqueous carbon dots.* Analytical chemistry, 2015. **87**(4): p. 2033-2036.

109. Chen, B.B., et al., *Highly selective detection of 2, 4, 6-trinitrophenol by using newly developed terbium-doped blue carbon dots.* Analyst, 2016. **141**(9): p. 2676-2681.

110. Sahu, S., et al., *Simple one-step synthesis of highly luminescent carbon dots from orange juice: application as excellent bio-imaging agents.* Chemical communications, 2012. **48**(70): p. 8835-8837.

111. Ray, S., et al., *Fluorescent carbon nanoparticles: synthesis, characterization, and bioimaging application.* The Journal of Physical Chemistry C, 2009. **113**(43): p. 18546-18551.

112. Li, S., et al., *Targeted tumour theranostics in mice via carbon quantum dots structurally mimicking large amino acids.* Nature biomedical engineering, 2020. **4**(7): p. 704-716.

113. Scialabba, C., et al., *Highly homogeneous biotinylated carbon nanodots: red-emitting nanoheaters as theranostic agents toward precision cancer medicine.* ACS applied materials & interfaces, 2019. **11**(22): p. 19854-19866.

114. Li, J., et al., *Emancipating target-functionalized carbon dots from autophagy vesicles for a novel visualized tumor therapy.* Advanced Functional Materials, 2018. **28**(30): p. 1800881.

115. Zheng, M., et al., *Integrating oxaliplatin with highly luminescent carbon dots: an unprecedented theranostic agent for personalized medicine.* Advanced materials (Deerfield Beach, Fla.), 2014. **26**(21): p. 3554-3560.

116. Chan, M.-H., et al., *Natural carbon nanodots: Toxicity assessment and theranostic biological application.* Pharmaceutics, 2021. **13**(11): p. 1874.

117. Khan, W.U., et al., *Water-soluble green-emitting carbon nanodots with enhanced thermal stability for biological applications.* Nanoscale, 2021. **13**(7): p. 4301-4307.

118. Kasouni, A., T. Chatzimitakos, and C. Stalikas, *Bioimaging applications of carbon nanodots: A review.* C, 2019. **5**(2): p. 19.

119. Choi, Y., et al., *Highly biocompatible carbon nanodots for simultaneous bioimaging and targeted photodynamic therapy in vitro and in vivo.* Advanced Functional Materials, 2014. **24**(37): p. 5781-5789.

120. Zhao, J., et al., *Preparation of N-doped yellow carbon dots and N, P co-doped red carbon dots for bioimaging and photodynamic therapy of tumors.* New Journal of Chemistry, 2019. **43**(16): p. 6332-6342.

121. He, H., et al., *Diketopyrrolopyrrole-based carbon dots for photodynamic therapy.* Nanoscale, 2018. **10**(23): p. 10991-10998.

122. Li, X., et al., *Combined photodynamic-chemotherapy investigation of cancer cells using carbon quantum dot-based drug carrier system.* Drug delivery, 2020. **27**(1): p. 791-804.

123. Kuo, T.-R., et al., *One-pot green hydrothermal synthesis of fluorescent nitrogen-doped carbon nanodots for in vivo bioimaging.* Analytical and bioanalytical chemistry, 2016. **408**: p. 77-82.

124. Li, H., et al., *Near-infrared light controlled photocatalytic activity of carbon quantum dots for highly selective oxidation reaction.* Nanoscale, 2013. **5**(8): p. 3289-3297.

125. Yang, Y., et al., *Silver modified carbon quantum dots for solvent-free selective oxidation of cyclohexane.* New Journal of Chemistry, 2015. **39**(4): p. 2815-2821.

126. Zhang, X., et al., *The visible light catalytic properties of carbon quantum dots/ZnO nanoflowers composites.* Journal of Materials Science: Materials in Electronics, 2015. **26**: p. 2861-2866.

127. Ding, D., et al., *A simple method for preparing ZnO foam/carbon quantum dots nanocomposite and their photocatalytic applications.* Materials Science in Semiconductor Processing, 2016. **47**: p. 25-31.

128. FENG, C., et al., *Fabrication of carbon dots modified porous ZnO nanorods with enhanced photocatalytic activity.* Acta Physico-Chimica Sinica, 2015. **31**(12): p. 2349-2357.

129. Ming, H., et al., *Large scale electrochemical synthesis of high quality carbon nanodots and their photocatalytic property.* Dalton transactions, 2012. **41**(31): p. 9526-9531.

130. Song, B., et al., *Two-step hydrothermally synthesized carbon nanodots/WO_3 photocatalysts with enhanced photocatalytic performance.* Dalton Transactions, 2017. **46**(45): p. 15769-15777.

131. Bhunia, S., et al., *Unraveling the Carrier Dynamics and Photocatalytic Pathway in Carbon Dots and Pollutants of Wastewater System.* The Journal of Physical Chemistry C, 2021. **125**(49): p. 27252-27259.

132. Zhou, Y., et al., *Size-dependent photocatalytic activity of carbon dots with surface-state determined photoluminescence.* Applied Catalysis B: Environmental, 2019. **248**: p. 157-166.

133. Peng, Z., et al., *Facile synthesis of "boron-doped" carbon dots and their application in visible-light-driven photocatalytic degradation of organic dyes.* Nanomaterials, 2020. **10**(8): p. 1560.

134. Aghamali, A., et al., *Synthesis and characterization of high efficient photoluminescent sunlight driven photocatalyst of N-Carbon Quantum Dots.* Journal of Luminescence, 2018. **201**: p. 265-274.

135. Ma, Z., et al., *One-step ultrasonic synthesis of fluorescent N-doped carbon dots from glucose and their visible-light sensitive photocatalytic ability.* New Journal of Chemistry, 2012. **36**(4): p. 861-864.

136. Zhu, Z., et al., *Green preparation of palm powder-derived carbon dots co-doped with sulfur/chlorine and their application in visible-light photocatalysis.* Spectrochimica Acta Part A: Molecular and Biomolecular Spectroscopy, 2020. **227**: p. 117659.

137. Ibarbia, A., H.J. Grande, and V. Ruiz, *On the factors behind the photocatalytic activity of graphene quantum dots for organic dye degradation.* Particle & Particle Systems Characterization, 2020. **37**(5): p. 2000061.

138. Saini, D., et al., *Photodegradation of azo dyes in sunlight promoted by nitrogen–sulfur–phosphorus codoped carbon dots.* ACS Applied Nano Materials, 2021. **4**(9): p. 9303-9312.

139. Wang, C., et al., *Facile and low-energy-consumption synthesis of dual-functional carbon dots from Cornus walteri leaves for detection of p-nitrophenol and photocatalytic degradation of dyes.* Colloids and Surfaces A: Physicochemical and Engineering Aspects, 2022. **640**: p. 128351.

140. Aggarwal, R., et al., *Bitter apple peel derived photoactive carbon dots for the sunlight induced photocatalytic degradation of crystal violet dye.* Solar Energy, 2020. **197**: p. 326-331.

141. Cao, L., et al., *Carbon nanoparticles as visible-light photocatalysts for efficient CO_2 conversion and beyond.* Journal of the American Chemical Society, 2011. **133**(13): p. 4754-4757.

142. Liu, J., et al., *Metal-free efficient photocatalyst for stable visible water splitting via a two-electron pathway.* Science, 2015. **347**(6225): p. 970-974.

143. Li, X., et al., *Carbon and graphene quantum dots for optoelectronic and energy devices: a review.* Advanced Functional Materials, 2015. **25**(31): p. 4929-4947.

144. Yuan, F., et al., *Shining carbon dots: Synthesis and biomedical and optoelectronic applications.* Nano Today, 2016. **11**(5): p. 565-586.

145. Wang, F., et al., *Synthesis of direct white-light emitting carbogenic quantum dots.* Chemical Communications, 2010. **46**(19): p. 3309-3311.

146. Luo, Z., et al., *Microwave-assisted preparation of white fluorescent graphene quantum dots as a novel phosphor for enhanced white-light-emitting diodes.* Advanced Functional Materials, 2016. **26**(16): p. 2739-2744.

147. Zhou, Z., et al., *Hydrogen peroxide-treated carbon dot phosphor with a bathochromic-shifted, aggregation-enhanced emission for light-emitting devices and visible light communication.* Advanced Science, 2018. **5**(8): p. 1800369.

148. Wang, F., et al., *White light-emitting devices based on carbon dots' electroluminescence.* Chemical Communications, 2011. **47**(12): p. 3502-3504.

149. Zhang, X., et al., *Color-switchable electroluminescence of carbon dot light-emitting diodes.* ACS nano, 2013. **7**(12): p. 11234-11241.

150. Wang, B., et al., *Near-infrared emissive carbon dots with 33.96% emission in aqueous solution for cellular sensing and light-emitting diodes.* Science Bulletin, 2019. **64**(17): p. 1285-1292.

151. Yan, F., et al., *Multicolor carbon dots with concentration-tunable fluorescence and solvent-affected aggregation states for white light-emitting diodes.* Nano Research, 2020. **13**: p. 52-60.

152. Feng, X., et al., *A facile approach to solid-state white emissive carbon dots and their application in UV-excitable and single-component-based white LEDs.* Nanomaterials, 2019. **9**(5): p. 725.

153. Jiang, K., et al., *Triple-mode emission of carbon dots: applications for advanced anti-counterfeiting.* Angewandte Chemie International Edition, 2016. **55**(25): p. 7231-7235.

154. Yuan, K., et al., *Great enhancement of red emitting carbon dots with B/Al/Ga doping for dual mode anti-counterfeiting.* Chemical Engineering Journal, 2020. **397**: p. 125487.

155. Yang, H., et al., *Hydrophobic carbon dots with blue dispersed emission and red aggregation-induced emission.* Nature Communications, 2019. **10**(1): p. 1789.

156. Cheng, K., et al., *Tunable excitation-dependent-fluorescence of carbon dots: Fingerprint curves for super anti-counterfeiting.* Dyes and Pigments, 2020. **174**: p. 108106.

157. Guo, J., et al., *Green synthesis of carbon dots toward anti-counterfeiting.* ACS Sustainable Chemistry & Engineering, 2019. **8**(3): p. 1566-1572.

158. Liu, Y., et al., *Highly fluorescent nitrogen-doped carbon dots with excellent thermal and photo stability applied as invisible ink for loading important information and anti-counterfeiting.* Nanoscale, 2017. **9**(2): p. 491-496.

159. Kalytchuk, S., et al., *Carbon dot fluorescence-lifetime-encoded anti-counterfeiting.* ACS applied materials & interfaces, 2018. **10**(35): p. 29902-29908.

160. Yang, P., et al., *Facile synthesis and photoluminescence mechanism of green emitting xylose-derived carbon dots for anti-counterfeit printing.* Carbon, 2019. **146**: p. 636-649.

161. Li, T., et al., *Regulating the photoluminescence of carbon dots via a green fluorine-doping-derived surface-state-controlling strategy.* Journal of Materials Chemistry C, 2021. **9**(48): p. 17357-17364.

162. Qu, D. and Z. Sun, *The formation mechanism and fluorophores of carbon dots synthesized via a bottom-up route.* Materials Chemistry Frontiers, 2020. **4**(2): p. 400-420.

163. Kanwa, N. and A. Chakraborty, *Discriminatory Interaction Behavior of Lipid Vesicles toward Diversely Emissive Carbon Dots Synthesized from Ortho, Meta, and Para Isomeric Carbon Precursors.* Langmuir, 2020. **36**(35): p. 10628-10637.

164. Bai, J., et al., *Solvent-controlled and solvent-dependent strategies for the synthesis of multicolor carbon dots for pH sensing and cell imaging.* Journal of Materials Chemistry C, 2019. **7**(31): p. 9709-9718.

165. Xia, J., et al., *Synthesis of highly stable red-emissive carbon polymer dots by modulated polymerization: from the mechanism to application in intracellular pH imaging.* Nanoscale, 2018. **10**(47): p. 22484-22492.

166. Shi, L., et al., *Lysosome targeting, Cr (vi) and l-AA sensing, and cell imaging based on N-doped blue-fluorescence carbon dots.* Analytical Methods, 2021. **13**(32): p. 3561-3568.

167. Zhang, Z., et al., *A nanosensor made of sulfur–nitrogen co-doped carbon dots for "off–on" sensing of hypochlorous acid and Zn (II) and its bioimaging properties.* New Journal of Chemistry, 2018. **42**(19): p. 15895-15904.

168. Lin, J.-S., et al., *A carbon dot based theranostic platform for dual-modal imaging and free radical scavenging.* Nanoscale, 2019. **11**(43): p. 20917-20931.

169. Pawar, S., S. Kaja, and A. Nag, *Red-emitting carbon dots as a dual sensor for In3+ and Pd2+ in water.* ACS omega, 2020. **5**(14): p. 8362-8372.

170. Zhao, Y., et al., *A fluorescence-switchable carbon dot for the reversible turn-on sensing of molecular oxygen.* Journal of Materials Chemistry C, 2021. **9**(12): p. 4300-4306

CHAPTER 2

MATERIALS AND METHODS

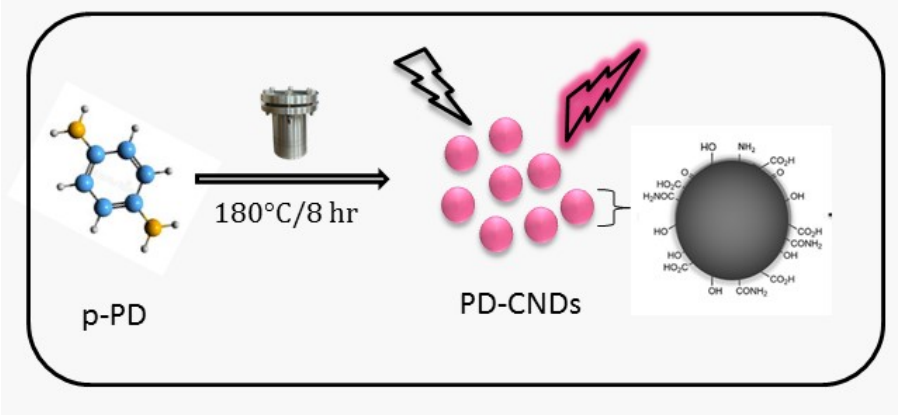

This chapter provides a concise overview of the materials and methodologies adopted for the present study. It consolidates the various chemicals used and offers a brief description of the experimental procedures involved in the synthesis and application studies of the prepared carbon nanodots (CNDs). It also provides a brief description of the material characterization techniques used for the analysis.

2. Materials and Methods

Selecting the appropriate materials and experimental procedure is one of the most important steps in addressing a research problem. This chapter details the experimental methods used for the synthesis of p-phenylenediamine derived carbon nanodots (PD-CNDs) and their luminescence based application studies. It also provides a brief overview of the characterization techniques employed in this research.

2.1. Materials

The list of chemicals used throughout this research is provided in **Table 2.1**.

Table 2.1. List of chemicals used

Materials	Supplied by
p-Phenylenediamine	TCI Chemicals (India)
Chloride salts of iron, magnesium, barium, calcium, strontium, chromium, potassium and lead nitrate.	SISCO Research Laboratories
Cupric nitrate	Fischer scientific
Zinc nitrate hexahydrate, Manganese chloride, Cadmium nitrate.	Alfa Aesar
Nickel nitrate, Mercuric chloride	Hi-Media Laboratories
Sodium chloride	Qualigens
o-Nitrotoluene, m-Nitrotoluene, p-Nitrotoluene, m-Nitrobenzaldehyde, p-Nitrobenzaldehyde, Nitrobenzene, p-Nitrophenol, p-Nitrobenzoic acid, Picric acid and 1-Chloro-2,4-Dinitrobenzene.	Hi-Media Laboratories
Xylene, Toluene, Chloroform, Dichloromethane, 1, 4-Dioxane, Acetone	SISCO Research Laboratories
Methanol, Ethanol	Qualigens
Benzene, Aniline, 1-Butanol, 2-Propanol, DMSO, DMF	Merk life Science

2.2 . Synthesis of p-Phenylenediamine derived carbon nanodots

Typically, 0.05 g of p-phenylenediamine (p-PD) was dissolved in 60 mL of deionized (DI) water. This aqueous solution was then sonicated for 10 minutes before being transferred into a Teflon-lined autoclave for hydrothermal treatment at 180 °C for 8 hours. After cooling to room temperature, the solution was filtered and centrifuged at 3000 rpm for 20 minutes. The resulting filtrate was dialyzed against DI water using a dialysis tube with 1 kDa molecular weight cut-off for 24 hours, with stirring at 80 rpm. The fraction exhibiting orange-red luminescence under UV exposure, PD-CNDs was obtained as the final product and was subsequently vacuum dried to yield a black powder represented in **Figure 2.1**.

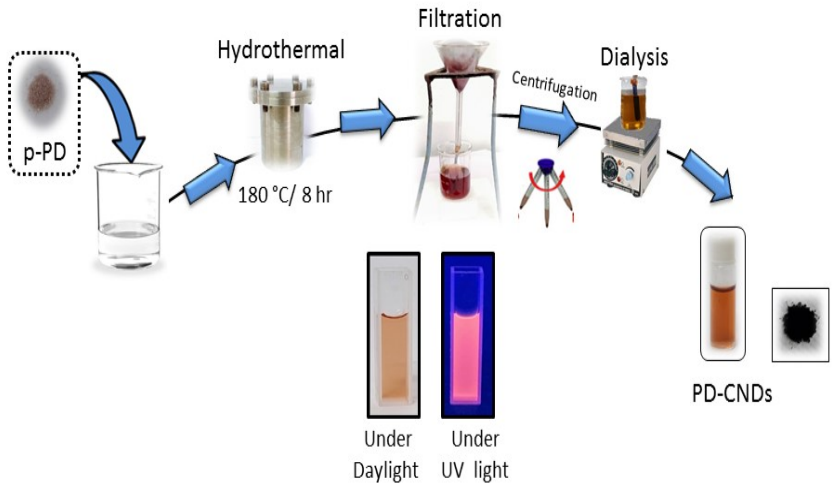

Figure 2.1 Schematic representation of the synthesis of PD-CNDs

2.3. Characterization of carbon nanodots

The synthesized p-phenylenediamine derived carbon nanodots (PD-CNDs) were thoroughly characterized using a variety of analytical techniques, including high-resolution transmission electron microscopy technique (HR-TEM), Fourier Transform infrared (FT-IR) spectral studies, X-ray diffraction (XRD) analysis, X-ray photoelectron spectroscopy (XPS), Raman spectroscopy, zeta potential analysis, UV-visible absorbance spectroscopy, fluorescence spectroscopy and time-correlated single photon counting (TCSPC) technique. The fluorescence color of the samples was visually monitored using an LZC-4X photo-reactor, enabling direct observation of their emission properties.

2.3.1. High-Resolution Transmission Electron Microscopy

This technique was employed to determine the morphology and size of the PD-CNDs at the nanometer scale, providing detailed structural features of the carbon nanodots (CNDs). The basic principle behind Transmission Electron Microscopy (TEM) analysis involves passing a high energy electron beam through the material to be analyzed. An electron source often referred to as the "gun," produces a stream of electrons that is accelerated towards the specimen using a positive electrical potential. This stream is focused into a thin, monochromatic beam by metal apertures and magnetic lenses known as "condenser lenses." When the beam strikes the specimen, part of it is transmitted through the material. This transmitted portion is then focused by a set of lenses called

"objective lenses" to form an image. The image is subsequently directed down the column through "intermediate and projector lenses," which magnify the image according to the set magnification and resolved using an imaging device such as a fluorescent screen, a layer of photographic film, or a high quality sensor device. These micrographs are used to analyze morphology and particle size distribution of the materials.

Here, the morphology of the PD-CNDs was determined using a JEOL JEM 2100 transmission electron microscopy (TEM) instrument, operating at an accelerating voltage of 200 kV. Samples for TEM analysis were prepared by drop-casting an aqueous solution of carbon nanodots onto a carbon-coated copper grid .The particle size distribution, based on the TEM images, was analyzed using Image *J* software.

2.3.2. Fourier-Transform infrared (FT-IR) spectroscopy

FT-IR spectroscopy is often used as the initial step in the material analysis process. The FT-IR instrument sends infrared radiation, ranging from about 10,000 to 100 cm^{-1}, through a sample. Some of this radiation is absorbed by the sample, while the rest passes through. The absorbed radiation is converted into rotational and/or vibrational energy within the sample molecules. The resulting signal at the detector is presented as a spectrum, typically ranging from 4000 cm^{-1} to 400 cm^{-1}. This spectrum represents a molecular fingerprint of the sample, as each molecule or chemical structure produces a unique spectral pattern. This

makes FT-IR analysis an excellent tool for chemical identification. Fourier-transmission infrared (FT-IR) spectrum of PD-CND was recorded using JASCO FTIR-4100 spectrometer using KBr pellet method. Information about the surface functional groups present in the synthesized CNDs was obtained from FT–IR spectral studies.

2.3.3. X-ray Photoelectron Spectroscopy

X-ray Photoelectron Spectroscopy (XPS) is a surface sensitive, quantitative spectroscopic technique capable of measuring all elements except hydrogen and helium. This capability makes XPS a unique and valuable tool for understanding surface chemistry. XPS spectra are obtained by measuring the photoelectrons emitted from surface atoms when materials are exposed to X-ray irradiation. Since the energy of the X-ray with a certain wavelength is fixed (for Al Kα X-ray, E_{photon} = 1486.7 eV, for Mg Kα X-ray, E_{photon} = 1253 eV), measuring the kinetic energy of the emitted electrons allows the determination of the binding energy of each emitted electron. The binding energy is characteristic of specific elements, enabling the identification of elemental compositions and quantities within 1–10 nm of the sample surface. The peak position and shape in the XPS spectrum provide information on chemical composition, oxidation state, and binding structure, while the peak intensity provides information on element content and concentration. Surface element composition of PD-CND was determined with Omicron spectrometer utilizing 1253 eV Mg Kα radiation.

2.3.4. X-ray Diffraction Analysis

X-ray Diffraction (XRD) analysis provides detailed information about the crystallographic structure, chemical composition, and physical properties of the material. It is based on the constructive interference of monochromatic X-rays and a crystalline sample. X-rays, which are shorter wavelength electromagnetic radiation, are generated when electrically charged particles with sufficient energy are decelerated. In X-ray scattering, the produced X-rays are collimated and directed towards a sample of nanomaterial. The sample and incoming rays interact to form a diffracted beam, which is then detected, processed, and tallied. A diffraction pattern is displayed by plotting the intensity of the diffracted rays dispersed at various angles of the material. The interpretation of the obtained diffraction pattern is facilitated by Bragg's law.

$$n\lambda = 2d \sin\theta \qquad (1)$$

Where, 'd' stands for the interplanar spacing, 'θ' represents the angle of incidence, 'n' is an integer and 'λ' denotes the wavelength of the X-ray utilized. Here, the crystallinity or amorphous nature of the carbon nanodots was determined using X-ray Diffraction (XRD) analysis. A Rigaku MiniFlex diffractometer with a Cu Kα radiation source (λ = 0.154 nm) was used for the XRD analysis of PD- CNDs, covering a range from 5° to 90° at a scanning speed of 0.1453°/s.

2.3.5. Raman Spectroscopy

Raman spectroscopy is an analytical technique that measures the vibrational energy modes of a sample using scattered light. Further insights into the core structure of the CNDs were obtained using Raman spectral analysis. It provides both chemical and structural information and can identify substances through their characteristic Raman "fingerprint." This information is extracted by detecting Raman scattering from the sample. When a sample is irradiated with a laser source typically in the UV-visible and near-infrared range, the scattered light is collected by a lens system and then directed through a spectrophotometer to obtain the Raman Spectrum. Raman scattering occurs when the frequency of emitted light is either higher or lower than the incident radiation. Stokes shift occurs when the frequency of emitted light is higher than the incident radiation, while anti-stokes shift occurs when it is lower. The signals provide information regarding the rotational, vibrational, and other low energy transitions of a sample. The Raman spectrum of PD-CND was captured using WI Tec alpha300RRA (WITec GmbH, Ulm, Germany) equipped with a 532 nm DPSS laser.

2.3.6. Zeta potential Analysis

The Zeta (ζ) potential, also known as electrokinetic potential, of the synthesized fluorescent CNDs was measured using zetasizer to obtain the surface charge. It is utilized to determine the surface charge of nanoparticles in solution. This value is

valuable for comprehending and forecasting interactions among particles in suspension. The zeta potential serves as an indicator of dispersion stability, with larger zeta potentials indicating a more stable dispersion. Zeta potential analysis was conducted using the Zetasizer Nano S from Malvern Instruments at a temperature of 25°C and an average of three measurements taken.

2.3.7. UV-visible Absorbance Spectroscopy

UV-visible absorbance spectroscopy, a quantitative technique in analytical chemistry, determines the quantity of light absorbed by a substance. When light interacts with a substance, it absorbs and reflects a specific amount of radiation. As the light traverses the sample, the difference between the incident radiation (I_0) and the transmitted radiation (I) denotes the amount of radiation absorbed by the substance, referred to as absorbance (A). Transmittance (T), expressed as a fraction (I/I_0), indicates the proportion of light that has passed through the sample. Beer-Lambert's Law states that the absorbance of a solution containing the sample is directly proportional to both the concentration of the absorbing species (the sample) and the path length.

$$\text{Absorbance, } A = \log_{10}(I_0/I) = \log_{10}(1/T) = -\log_{10}(T) \qquad (2)$$

$$\mathbf{A = \varepsilon cl} \qquad (3)$$

Where, ε = molar absorptivity (molar extinction coefficient),

c = molar concentration of the absorber (solute),

l = path length (length of the sample cell or cuvette; in cm). It allows direct measurement of the concentration of the absorber in a solution from absorbance for a fixed path length.

The absorbance spectrum of PD-CND solution was recorded using a JASCO V-550 spectrophotometer. The measurement is done by placing the sample in the cuvette made up of quartz. The cuvette is positioned in the path of the radiation as the beam from the monochromator travels through the sample to the detector. The spectrophotometer assesses the light intensity of the incident radiation (I_0) prior to passing through the sample and the intensity of the transmitted radiation (I) that has passed through the sample, then calculates and presents the absorbance spectrum.

2.3.8. Fluorescence Spectroscopy

Fluorescence spectroscopy is an analytical technique that explores the fluorescence properties exhibited by the sample under investigation. The fundamental principle of fluorescence spectroscopy involves the excitation of a sample by a light source, causing it to transition from the ground state to an excited state. Upon returning to the ground state, the sample emits photons with lower energy or longer wavelengths than the absorbed energy. The photoluminescence spectra of CNDs were captured using the Agilent Cary Eclipse Spectrophotometer.

2.3.9. Quantum Yield Measurements

The fluorescence quantum yield of PD-CND was evaluated from UV-visible absorbance and photoluminescence spectrum of reference and CNDs sample solutions, where the reference fluorophore used was Rhodamine 6G (QY= 95%) in DI water. The optical density of all the solutions was maintained below 0.1 units. The following equation was used to calculate the quantum yield (QY) of CNDs, and the value obtained was 0.61.

$$QY = QY_{Ref}\,(I_{CNDs}/\,I_{Ref})(A_{\,Ref}/\,A_{\,CNDs})\,(\eta_{CNDs}/\,\eta_{Ref})^2 \qquad (4)$$

Where, QY = Quantum yield,

I = Integrated fluorescence intensity,

A = Absorbance value,

η = Refractive index.

2.3.10. Fluorescence lifetime measurements

Time-Correlated Single Photon Counting (TCSPC) is a widely used technique for determining the photoluminescence (PL) lifetime of carbon nanodots. Carbon nanodots typically exhibit PL decay values in the nanosecond range, making them promising candidates for various applications in biological and optoelectronic fields. The fluorescence lifetime studies of PD-CNDs were monitored using Horiba-Fluorolog fluorescence spectrometer with TCSPC with a 370 nm nanoLED as the excitation source.

Luminescence based applications of p-phenylenediamine derived carbon nanodots

2.4. p-Phenylenediamine derived carbon nanodots as sensor

PART I

2.4.1. Carbon nanodots based sensor for Cu (II) ions

A stock solution of fifteen selected metal ions (1mM) was prepared in deionized (DI) water. For the fluorescence measurements, 300 μL of the PD-CND solution was mixed with 2 mL of DI water in a cuvette. Analyte solutions at specified concentrations were then added to the cuvette, and the fluorescence response was monitored at an excitation wavelength of 440 nm.

2.4.2. Visual detection of Cu (II) ions with p-phenylenediamine derived carbon nanodots

All the measurements for the naked eye detection of Cu (II) ion were performed against a reference (blank) solution, prepared by adding 1 mL of DI water to 1 mL of PD-CND solution and gently shaking the mixture for 15 seconds. For the typical experiment involving selected metal ions, 1 mL of a specific metal ion salt solution in DI water at a prescribed concentration (1 mM) was added to 1 mL of PD-CND solution and gently shaken for 15 seconds.

PART II

2.4.3. Detection of picric acid with p-phenylenediamine derived carbon nanodots

1 mM solutions of the selected analytes (nitroaromatic compounds) were prepared. The detection of picric acid (2, 4, 6-Trinitrophenol, TNP) was conducted at room temperature using a fluorescence quenching technique. For this, a stock solution of PD-CNDs was prepared by adding 300 µL of PD-CNDs to 2 mL of DI water. Subsequently, 10 µL of a 1 mM picric acid solution was added to the stock solution. The emission intensity of PD-CNDs at 440 nm was measured before and after the addition of picric acid. To further examine the quenching effect, a constant volume of picric acid (10 µL) was gradually added to the same solution. For comparison, other nitroaromatic compounds and aromatic compounds were added to the PD-CND stock solution, and the emission intensity at 440 nm was recorded.

2.4.4. Theoretical investigation of luminescence quenching Computational methodology

The use of computational studies has been increased to a great extent as it gives a clear-cut idea at the molecular level. Density Functional Theory (DFT) is an important computational method which has been used now a day as it has high degree of predicting power and accuracy. Here in the present case, DFT based the computational studies have been employed not only to

explore the preferential sensing of picric acid (PA) by carbon nanodots (CNDs) but also to correlate with the experimental results [1-5]. The global reactive descriptors were computed to plot the Donor Acceptor Map (DAM), which gives an idea about the nature and comparison of reactivity of different nitroaromatics. Then the highest occupied molecular orbitals (HOMOs) and lowest unoccupied molecular orbitals (LUMOs) were analyzed using Gaussian software to draw the mechanism of preferential sensing [1, 2]. The following tools were employed mainly to describe the sensing of CNDs by nitroaromatics in the theoretical point of view.

2.4.4.1. Frontier molecular orbital analysis

The Frontier Molecular Orbitals (FMOs), including the highest occupied molecular orbital (HOMO) and the lowest unoccupied molecular orbital (LUMO) have been obtained from the Gaussian output file and were analyzed to predict the pathway of electron transfer in the studied system. These are of particular relevance in the study of charge transfer complex formation reactions. The FMO theory of chemical reactivity says that the formation of transition state in chemical reactions is due to the interaction between the HOMO and LUMO orbitals of the reacting species. As per FMO theory, a low lying LUMO makes the system a good electron acceptor and a high lying HOMO makes it a good electron donor.

The electron/charge transfer can be regarded as one of the primary processes in nitroaromatics quenching. In this, the

intensity of fluorescence given by CNDs was quenched by nitroaromatics. The process can follow either an oxidative pathway or a reductive pathway depending upon the energies of HOMO and LUMO of both CNDs and quencher. If the LUMO of quencher is less energetic than that of CNDs, transfer carried out through an oxidative pathway in which the electron excited from HOMO to LUMO of CNDs was de-excited to the LUMO of quencher resulting in the fluorescence quenching. On the other hand, if the LUMO of quencher is highly energetic than that of CNDs, then the electron transfer may happen through a reductive pathway in which electrons excited from HOMO to LUMO of CNDs with an electron transfer from HOMO of quencher to HOMO of CNDs. Here the HOMOs of both the quencher and CNDs must be of small energy difference as otherwise no electron transfer occurs [2].

2.4.4.2. Global descriptive parameters and Donor Acceptor Map

The utility of global descriptive parameters of a molecule open up a way to get the relation between the chemical reactivity of a molecule and its sensitiveness to structural perturbations and responses to the changes in external conditions. The global descriptive parameters include the chemical potential, electronegativity, hardness, softness, electrophilicity index, etc. These quantities are corresponding to the linear responses of the electron density with respect to the changes in the external potential and number of electrons. The

chemical hardness fundamentally signifies the reluctance towards the deformation or polarization of the electron cloud of the atoms, ions or molecules under small perturbation encountered during chemical processes. Chemical Softness is the measure of capacity of a molecule to receive electrons; more precisely it is related with the groups or atoms present in that molecule and inversely proportional to chemical hardness. The chemical potential in DFT, measures escaping tendency of an electron from equilibrium, is accounted by the first derivative of energy with respect to the number of electrons and is also the negative of electronegativity, which is a measure of the tendency to attract electrons in a chemical bond. The electrophilic index tells us about the strength of electrophilicity of the species. Global reactive descriptors have been calculated using the following equations [6]:

Ionization Potenial (IP) = E_{cation} - $E_{neutral}$ (5)

Electron Affinity (EA) = $E_{neutral}$ − E_{anion} (6)

Hardness (η) ≈ $\frac{IP-EA}{2}$ (7)

Electronegativity (χ) ≈$\frac{IP+EA}{2}$ (8)

Softness(S) ≈$\frac{1}{2\eta}$ (9)

Chemical potential (μ) ≈ -χ (10)

Electrophilicity index (ω) ≈ $\frac{\mu^2}{2\eta}$ (11)

The fractional charge transfer takes place from one molecule to another can be demonstrated using Donor Acceptor Map (DAM) (See **Figure 2.2**). The necessary parameters called Electron accepting power (ω+) and Electron donating power (ω-) can be computed as:

$$\omega^{-} = (3IE + EA)^2 / 16(IE - EA) \quad (12)$$

$$\omega^{+} = (IE + 3EA)^2 / 16(IE - EA) \quad (13)$$

The tendency of a compound to accept or donate charge is expressed by using ω+ and ω-. As ω- decreases the compound will have a strong tendency to donate electrons, while large value of ω+ implies a strong tendency to accept electrons. Even though ionization energy (IE) and electron affinity (EA) are also related to the electron donating and accepting capacity of a compound, ω+ and ω- are more suitable for explaining the charge transfer mechanisms. It is because of that sometimes there is only a fractional charge transfer taking place. DAM is a plot which simultaneously shows the electron acceptance and electron donating power of studied molecules. Electron accepting index with respect to reference (Ra) and Electron donating index with respect to reference (Rd) are the respective parameters for DAM and are calculated as: [7-9]

$$R_a = \omega^{+}_L / \omega^{+}_R \quad (14)$$

$$R_d = \omega^{-}_L / \omega^{-}_R \quad (15)$$

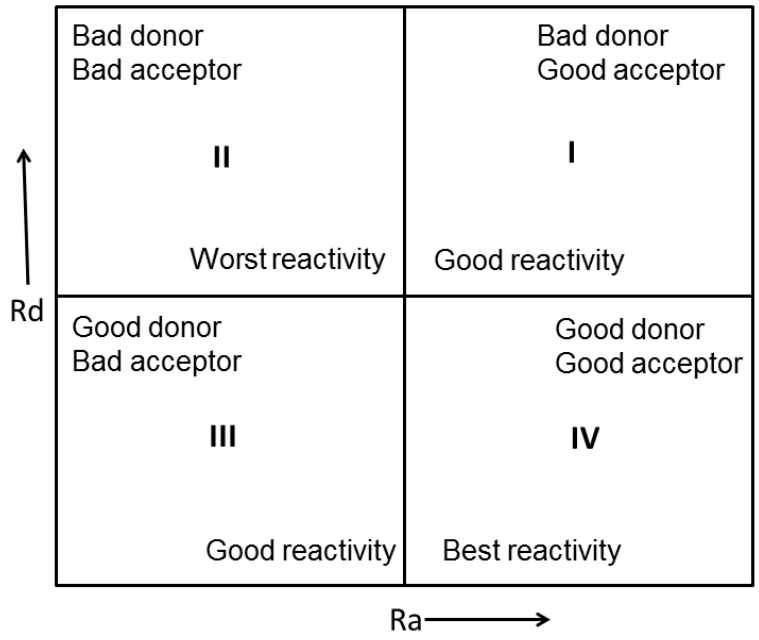

Figure 2.2 Reference DAM

2.5. Solvent relaxation and associated applications of p-phenylenediamine derived carbon nanodots

2.5.1. Assessment of solvatochromic properties of p-phenylenediamine derived carbon nanodots

To study the solvatochromic properties in solvents of varying polarities, PD-CNDs dispersions were prepared at a concentration of 0.1 mg/mL by sonication for 10 minutes. The color changes under daylight and UV light (365 nm) were observed. Subsequently, the absorbance and fluorescence spectra of each solution were measured and analyzed.

2.5.2. Determination of dielectric constant of alcohol–1,4 Dioxane mixture

Primary alcohols and mixtures of alcohol and 1, 4-Dioxane in varying ratios (0.05 to 100%, v/v, with increments of 10%) were prepared. To these mixtures, 0.05 mg/mL of powdered PD-CNDs was added and dispersed by sonication. The shift in the emission peak maximum of the PD-CNDs in the different alcohols and alcohol–1,4-dioxane mixtures was monitored using fluorescence spectroscopy.

2.5.3. Determination of moisture content in 1, 4-Dioxane

For this purpose, various compositions of 1, 4-Dioxane–water mixtures were prepared, ranging from 0.05–8% v/v with intervals of 2%, and 10–100% v/v with intervals of 10%. To each 10 mL mixture, 0.05 mg/mL of PD-CNDs was added and sonicated for 10 minutes. The fluorescence spectra of these samples were then recorded.

References

1. Hemalatha, V. and V. Vijayakumar, *Indole-imidazole hybrid Schiff base for the selective detection of the explosive picric acid via fluorescence "turn-off" process: Experimental and theoretical DFT-D3 study.* Journal of Molecular Structure, 2024. **1311**: p. 138322.

2. Mahto, M.K., et al., *Blue-emissive nitrogen-doped carbon dots for picric acid detection: molecular fluorescence quenching mechanism.* ACS Applied Nano Materials, 2023. **6**(9): p. 8059-8070.

3. Sharma, P., M. Yusuf, and A.K. Malik, *Pyrazoline-based fluorescent probe: Synthesis, Characterization, Theoretical Simulation, and Detection of picric acid.* Journal of Fluorescence, 2023: p. 1-14.

4. Wei, X., et al., *Facile synthesis of red-emissive carbon dots with theoretical understanding for cellular imaging.* Colloids and Surfaces B: Biointerfaces, 2022. **220**: p. 112869.

5. Ju, B., et al., *Photostable and low-toxic yellow-green carbon dots for highly selective detection of explosive 2, 4, 6-trinitrophenol based on the dual electron transfer mechanism.* ACS applied materials & interfaces, 2018. **10**(15): p. 13040-13047.

6. Rajan, V.K. and K. Muraleedharan, *A computational investigation on the structure, global parameters and antioxidant capacity of a polyphenol, Gallic acid.* Food Chemistry, 2017. **220**: p. 93-99.

7. Sandoval-Yañez, C., C. Mascayano, and J.I. Martínez-Araya, *A theoretical assessment of antioxidant capacity of flavonoids by means of local hyper–softness.* Arabian journal of chemistry, 2018. **11**(4): p. 554-563.

8. Martinez, A., *Donator acceptor map of psittacofulvins and anthocyanins: are they good antioxidant substances?* The Journal of Physical Chemistry B, 2009. **113**(14): p. 4915-4921.

9. Martinez, A., R. Vargas, and A. Galano, *What is important to prevent oxidative stress? A theoretical study on electron-transfer reactions between carotenoids and free radicals.* The Journal of Physical Chemistry B, 2009. **113**(35): p. 12113-12120.

CHAPTER 3

CHARACTERIZATIONS OF p-PHENYLENEDIAMINE DERIVED CARBON NANODOTS

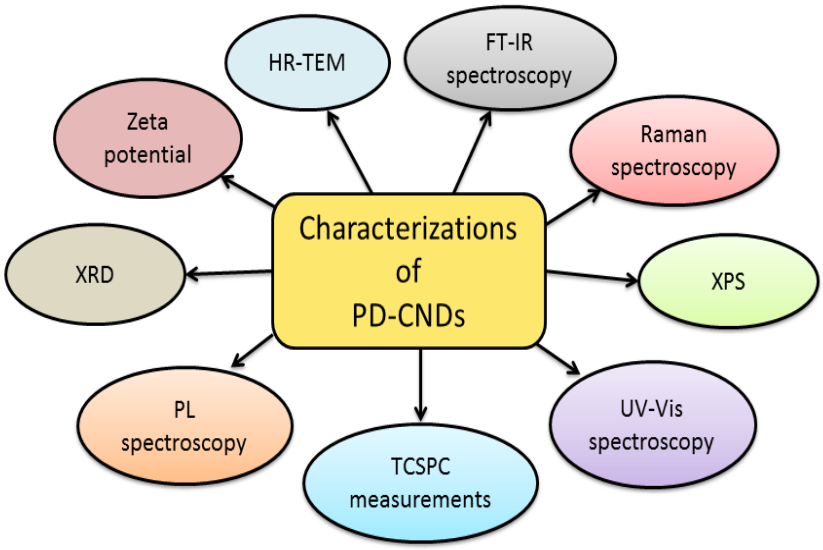

This chapter provides an in-depth analysis of the results obtained from various characterizations of PD-CNDs. These analyses confirm the formation of carbon nanodots from the hydrothermal treatment of p-Phenylenediamine.

3. Characterization of p-phenylenediamine derived carbon nanodots

Hydrothermal carbonization of p-phenylenediamine (p-PD) at 180°C for 8 hours resulted in the formation of p-phenylenediamine derived carbon nanodots (PD-CNDs). The detailed procedure is provided in the previous chapter. As mentioned earlier, the PD-CND solution appeared reddish-brown in color. The as-synthesized carbon nanodots (PD-CNDs) were subjected to various characterization techniques. The results of these analyses are discussed in detail in this chapter.

Structural characterization of p-phenylenediamine derived carbon nanodots

3.1. High-resolution transmission electron microscopy analysis

The High-resolution transmission electron microscopy (HR-TEM) image confirms the spherical morphology of the synthesized carbon nanodots. **Figure 3.1(a)** and **(b)** show TEM images of PD-CNDs, in which the particles are less than 10 nm in size. The higher magnification TEM image validated the presence of lattice fringes with a *d*-spacing value of 0.19 nm (**Figure 3.1(b) inset**), corresponding to the (102) lattice fringes of graphite. This indicates that the crystalline core of the PD-CND has a graphite structure [1]. Additionally, the average particle size was

determined to be 2.8 nm from the TEM image, as shown in the histogram (**Figure 3.1(c)**).

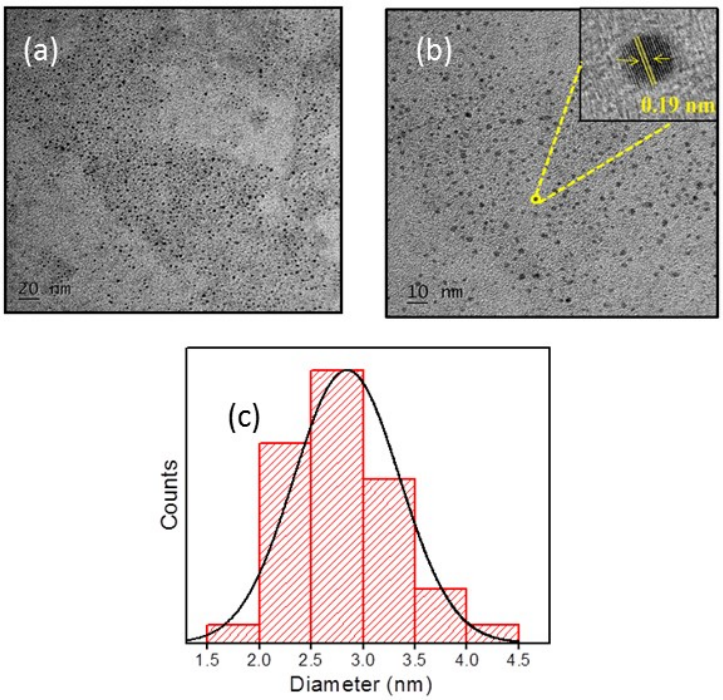

Figure 3.1 (a) and (b) HR-TEM images of PD-CNDs at different magnification, inset shows the lattice fringes with *d*-spacing value of 0.19 nm, (c) Particle size distribution of PD-CNDs, derived from TEM images

3.2. Fourier-Transform infrared (FT-IR) spectroscopy analysis

The functional groups present in PD-CNDs were identified using FT-IR spectral analysis. **Figure 3.2** shows the FT-IR spectrum of PD-CNDs. The broad band at 3427 cm^{-1} indicates -O-H and/or -N-H stretching. The bands at 2923 and 2848 cm^{-1} are attributed to the asymmetric and symmetric stretching vibrations

of -C-H. The bands at 1637 cm^{-1} and 1021 cm^{-1} correspond to -C=O/-C=N and -C-O stretching, respectively. Additionally, the FT-IR bands at 1510 cm^{-1} and 1425 cm^{-1} are assigned to aromatic ring skeleton vibrations and the presence of -C-N moieties [2-5]. Consolidating these data, PD-CNDs are visualized to have carbon cores functionalized with amino (-NH, $-NH_2$), carbonyl, carboxyl (-C=O/-COOH), and hydroxyl (-OH) groups. These functional groups confirm excellent water solubility and long-term stability to the synthesized carbon nanodots.

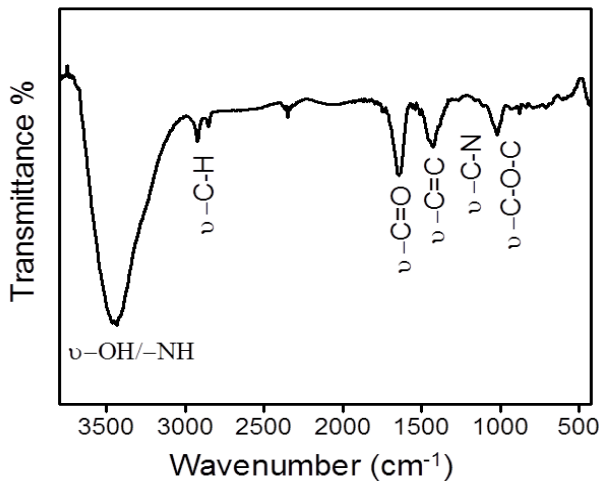

Figure 3.2 FT-IR spectrum of PD-CNDs

3.3. X-ray Photoelectron Spectroscopy analysis

More precise structural information was obtained from the X-ray photoelectron spectroscopy **(**XPS) results. Three major peaks were identified in PD-CNDs at 288.75, 402.51 and 534.75 eV, corresponding to C 1s, N 1s, and O 1s, respectively (**Figure 3.3 (a)**), with atomic percentages 71.88% for C 1s, 11.41% for N 1s,

and 14.71% for O 1s. In **Figure 3.3 (b)**, the C 1s peak was further analyzed to identify the moieties C–C/C=C (284.35 eV), C–N/C–O (285.31 eV), and C=N/C=O (286.36 eV) [4]. Further detailed analysis aids in understanding the nitrogen linkage, facilitated by curve fitting of the N 1s spectral peak. The N 1s peak consists of three distinct peaks: pyridinic, pyrrolic, and amino N's, located at 398.39, 400.18, and 399.21 eV, respectively (**Figure 3.3 (c)**) [6, 7]. These findings clearly indicate the presence of nitrogen in the framework and the presence of amino functionality. Upon curve fitting, the O 1s peak indicates the presence of functionalities: C=O, C–O/C–OH, and O–C=O, characterized by peaks at 531.37, 532.47,

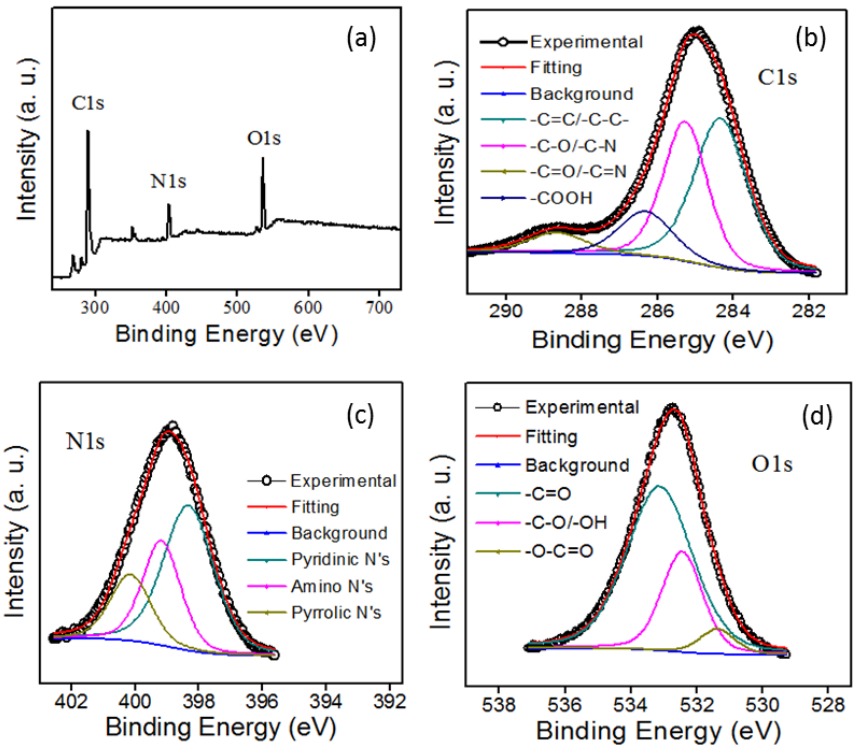

Figure 3.3 (a) XPS survey scan of PD-CNDs, (b)-(d) XPS fitting curves of C 1s, N 1s and O 1s of PD-CNDs.

and 533.14 eV, respectively **(Figure3.3(d))** [8]. XPS results also reveal that the carbon core is rich with amine groups, carboxyl/carbonyl moieties and hydroxyl groups.

3.4. X-Ray Diffraction Analysis

The powder X-ray diffraction (XRD) pattern aids in identifying the extent of crystallinity of PD-CNDs. The broad peak observed in the XRD pattern (**Figure 3.4**) signifies the considerable amorphous nature of the material. The peak at 2θ = 23.4° corresponds to the (002) plane of graphitic carbon [9, 10]. Another diffraction peak corresponding to the (100) plane, observed at 2θ around 42.4°, provides insight into the longitudinal dimension of the structural elements [11]. Additionally, the peak at 2θ = 60° corresponds to the (103) plane of carbon in the hexagonal graphitic lattice [12].

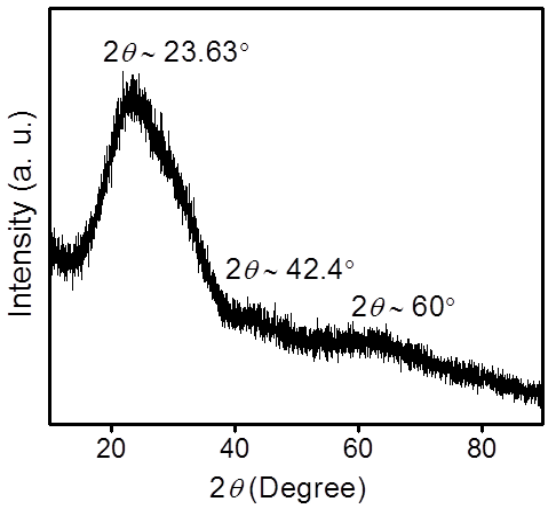

Figure 3.4 XRD patterns of PD-CNDs

3.5. Raman Spectra analysis

The nature of the carbon core was further elucidated using Raman spectroscopy. The Raman spectrum in **Figure 3.5** shows both the D and G bands, which correspond to the sp^2 and sp^3 hybrid character of carbon atoms. The G band, observed at 1545 cm^{-1}, arises from the in-plane vibrations of sp^2-bonded carbon atoms, while the D band at 1368 cm^{-1} indicates structural flaws in the graphite structure caused by substituted framework carbons, corresponding to out-of-plane C–C vibrations [13, 14]. The intensity ratio (I_D/I_G) value of 0.88 indicates significant functionalization of the carbon framework in PD-CNDs.

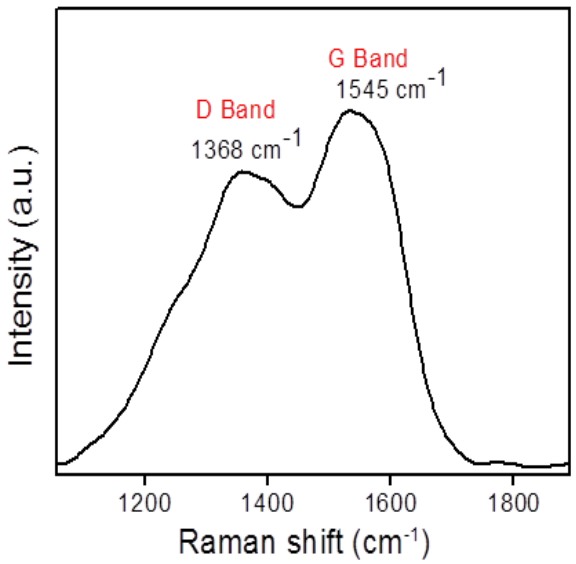

Figure 3.5 Raman spectrum of PD-CNDs

3.6. Zeta potential analysis

The surface charge of the carbon nanodots (CNDs) was determined through zeta potential analysis. The value of zeta (ζ) potential may be positive or negative. The negative zeta potential of the CND is attributed to the dense electron cloud on their surface. The zeta potential value indicates the stability of CND particles over time. CNDs with high zeta potential, whether negative or positive, are considered electrostatically stable, while those with low zeta potential are prone to coagulation or aggregation within a short period, leading to weak physical stability. Scientifically, a high zeta potential signifies that repulsive forces outweigh attractive forces, resulting in a relatively stable system. Highly dispersed nanoparticles like CNDs typically exhibit zeta potential values greater than +30 mV or less than -30 mV. Conversely, nanoparticles with zeta potential values between -10 mV and +10 mV are regarded as neutral [15]. Here the zeta potential of PD-CND (**Figure 3.6**) was found to be positive (55 mV), indicating good dispersion stability of the nanomaterial.

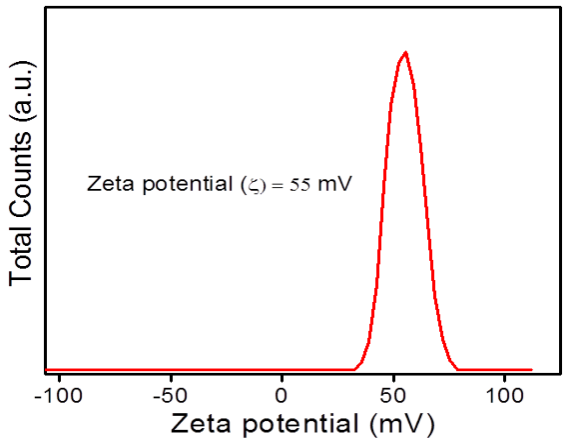

Figure 3.6 Zeta potential curve of PD-CNDs at pH=7

Optical characterization of p-phenylenediamine derived carbon nanodots

3.7. UV-Visible Absorbance Spectrum Analysis

p-PD derived carbon nanodots usually show strong absorption in the ultraviolet region (200-300 nm). **Figure 3.7** represents the UV-visible absorption spectrum of PD-CNDs. The peak observed in 240-280 nm region is assigned to the π-π* transitions of C=O or C=C/ -C=N moieties [16, 17]. In addition, PD-CNDs exhibit an n-π* transition of the C=O/C=N bonds [18], resulting in an absorption peak at 365 nm. It also exhibits broad absorptions in 400-600 nm range, forming a set of low energy absorption tail bands. This broad absorption is attributed to the presence of conjugated groups attached to the edges of the CNDs [19].

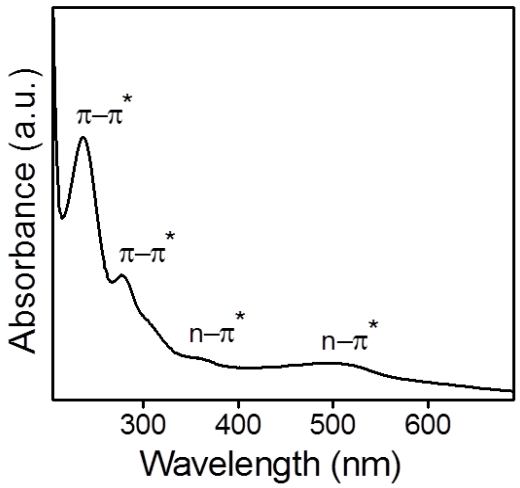

Figure 3.7 UV-Visible absorption spectrum of PD-CNDs

3.8. Photoluminescnce emission spectrum of p-phenylenediamine derived carbon nanodots

One of the most attractive features of CNDs is their photoluminescence emission. The photoluminescence spectrum of p-phenylenediamine derived carbon nanodots (PD-CNDs) is shown in **Figure 3.8(a).** The spectrum clearly indicates that the system is dual emissive, with two emission maxima at 504 nm and 618 nm. Dual emission CNDs are highly popular because their dual-channel emission can effectively mitigate the effects of environmental fluctuations and changes in probe concentration [20, 21].

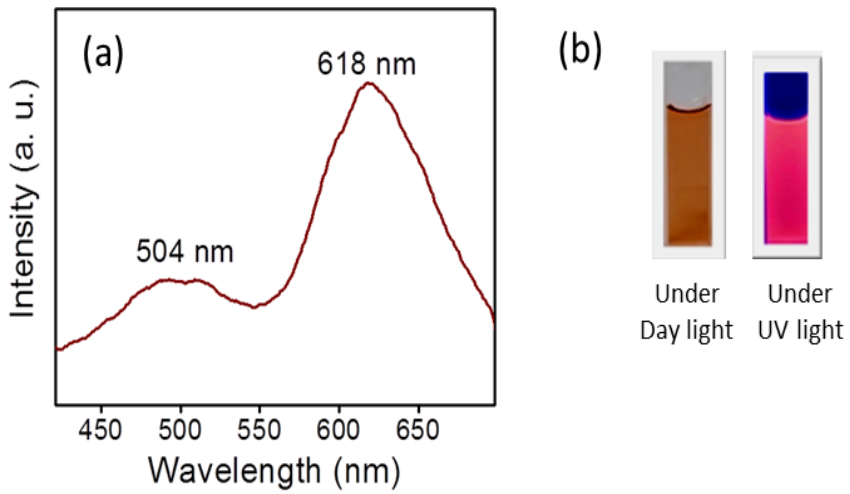

Figure 3.8 (a) Photoluminescence spectrum of PD-CND at an excitation of 360 nm, (b) Digital photographs of PD-CND solution under daylight and UV light exposure

The dual emissive nature of carbon nanodots may be attributed to the control of surface states involving nitrogen and oxygen-related

groups, or to the regulation of the carbonized structure and polymer chains of the precursors, as reported in the literature [22, 23]. Under UV light illumination, the overall emission of PD-CND appears orange-red colour (**Figure 3.8(b)**). The quantum yield of PD-CNDs, determined using Rhodamine 6G in water as the reference, was found to be 61%.

3.9. Photoluminescnce excitation spectrum of p-phenylenediamine derived carbon nanodots

The photoluminescence excitation spectrum of p-phenylenediamine derived carbon nanodots (PD-CNDs) was given in **Figure 3.9.** The excitation bands in the 250–320 nm region are believed to correspond to the π → π* (HOMO → LUMO) transition of C=C bonds in the sp^2 carbon domain.

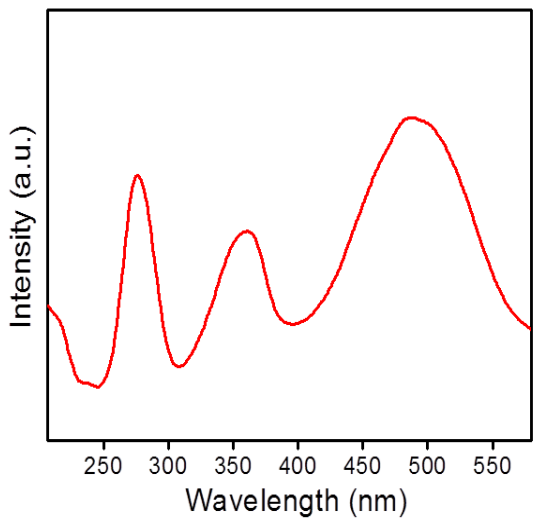

Figure 3.9 Photoluminescence excitation spectrum of PD-CNDs

The excitation bands in the 320−420 nm and 420−500 nm regions are attributed to transitions from π states to oxygen and nitrogen related defect states on the surfaces of the carbon nanodots. Subsequently, electrons in the π* and oxygen defect states can non-radiatively relax to the nitrogen-related defect state, resulting in long-wavelength orange-red emission [22].

3.10. Excitation wavelength-dependent emission of p-phenylenediamine derived carbon nanodots

Analysis of the excitation dependency nature of p-phenylenediamine derived carbon nanodots (PD-CNDs) (**Figure 3.10**) reveals that the emission peak at 504 nm is dependent on the excitation wavelength, whereas the position of the second emission peak at 618 nm remains unchanged. This behavior is typically due to the presence of different emissive states on the CNDs and is attributed to functional groups within the structure. The peak at the lower wavelength exhibits a red shift and gradually diminishes as the excitation wavelength increases. The peak exhibits excitation wavelength-dependent photoluminescence (PL) properties, which likely originates from the surface states. The FT-IR spectrum shows that the as-synthesized CNDs possess various functional groups, such as C-H, C=O, C-NH_2, and C-OH, on their surface. These functional groups could form a series of energy levels within the surface states, leading to corresponding emissive traps. When CNDs are excited by light at a specific wavelength, a particular surface state emissive

trap dominates the emission. As a result, different excitation wavelengths can produce different emission behaviors, leading to the observed excitation-dependent properties. The excitation independent behaviour can be associated with the uniform size distribution and a similar kind of functional group present on the surface with defects being passivated [24].

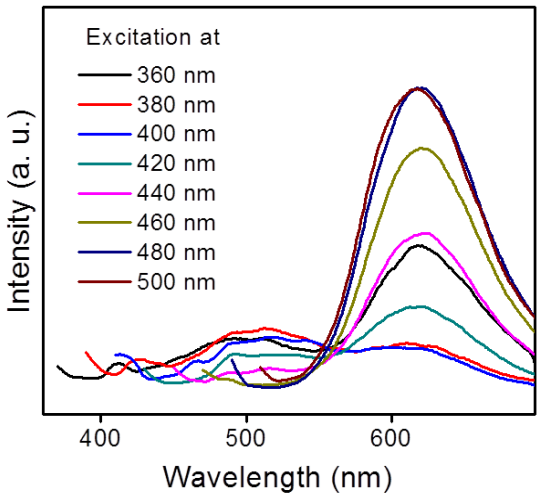

Figure 3.10 Excitation wavelength dependent emission spectra of PD-CNDs

A notable characteristic of the system is the absence of an emission peak at higher energy (lower wavelength region), even when high-energy radiation is used for excitation. Emissions from the carbon core, which are typically expected at higher energies, are not observed in this case. This can be explained by the considerable sp^3 character of the carbon core, where emission may occur from the isolated sp^2 clusters with a large energy gap at the periphery of the carbon particles. The HOMO–LUMO π–π*

energy gap of such sp^2 clusters, similar to pyridine moieties anchored on the carbon core, which is significantly higher than the emission energy from the surface states. Therefore, the absence of an emission peak below 300 nm indicates the lack of high-energy emission from the core, attributed to radiative excitonic recombination across the core band gap. The emission in the 400–500 nm region corresponds to edge-state excitation, while the higher wavelength emission (above 500 nm) observed in **Figure 3.8(a)** originates from surface fluorophores. Compared to surface group participation, edge group emission is significantly lower.

3.11. Photostability analysis of p-phenylenediamine derived carbon nanodots

Luminescence based fine applications require the photostability of the fluorophore species. Therefore, the photostability of CNDs was tested by continuously exposing the solution to UV radiation. The data presented in **Figure 3.11** demonstrate that the emission intensity (λ_{max} = 618 nm) of these particles remains significantly stable when dispersed in an aqueous medium.

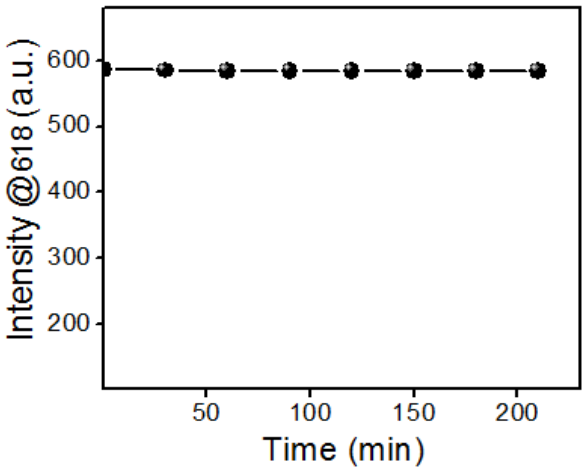

Figure 3.11 The dependence of luminescence intensity on prolonged UV light irradiation

3.12. Time-correlated single photon counting (TCSPC) measurements

Time correlated single photon counting (TCSPC) analysis was carried out to measure the average fluorescence lifetime of the synthesized carbon nanodots. Fluorescence decay profile of PD-CND is depicted in **Figure 3.12**. Instrument response function (prompt) is obtained at 368 nm (excitation wavelength) using milk powder suspension (black circles). The observed lifetime data of PD-CND was very well fitted to a mono-exponential function and the observed average life time value of PD-CND was 2.40 ns.

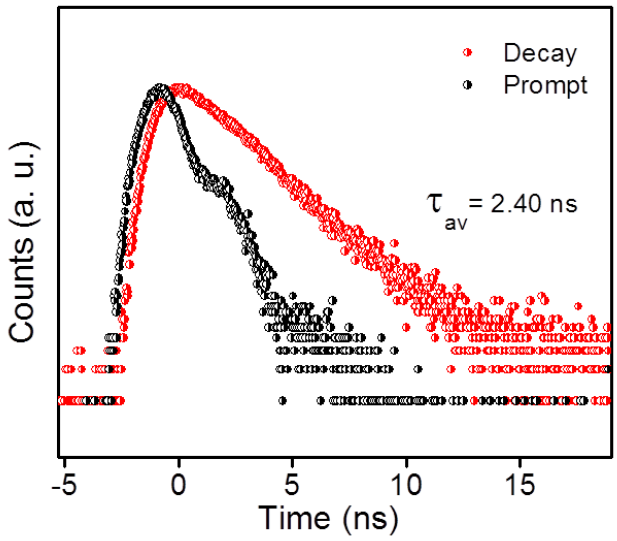

Figure 3.12 Fluorescence life-time decay profile of PD-CNDs (λ_{em}= 618 nm)

3.13. Conclusions

This chapter details the characterization of p-phenylenediamine derived carbon nanodots (PD-CNDs). HR-TEM analysis confirms their spherical morphology with an average particle size of 2.8 nm, all being under 10 nm. FT-IR spectroscopy and XPS analysis reveal the presence of oxygen and nitrogen containing functional groups, including amino, carboxyl and hydroxyl groups and the presence of pyridinic, pyrrolic nitrogens. These functional groups contribute to the good water solubility and long-term stability of the synthesized CNDs. XRD analysis indicates a significant amorphous nature, while Raman spectroscopy confirms the structure of the carbon core. Zeta potential measurements show a positive surface charge (ζ

potential = +55 mV). PD-CNDs exhibit orange-red luminescence with dual emission peaks at 504 nm and 618 nm upon excitation at 365 nm. The 504 nm peak is excitation-dependent, while the 618 nm peak is excitation-independent. The photo stability of the emission peak was monitored under continuous UV light exposure and the average lifetime value of PD-CND was observed to be 2.40 ns.

References

1. Fan, W., et al., *Broadband nonlinear optical properties of red fluorescent carbon dots.* Results in Physics, 2022. **38**: p. 105591.

2. Vedamalai, M., et al., *Carbon nanodots prepared from o-phenylenediamine for sensing of Cu $^{2+}$ ions in cells.* Nanoscale, 2014. **6**(21): p. 13119-13125.

3. An, Y., et al., *Red, green, and blue light-emitting carbon dots prepared from o-phenylenediamine.* RSC advances, 2021. **11**(43): p. 26915-26919.

4. Liu, H., et al., *Hydrogen-bond-induced emission of carbon dots for wash-free nucleus imaging.* Analytical chemistry, 2019. **91**(14): p. 9259-9265.

5. Raveendran, V., C. Anjali, and R.N. Kizhakayil, *Fe $^{3+}$-induced luminescence quenching in carbon dots–mechanism unveiled.* Analytical Methods, 2024. **16**(15): p. 2349-2358.

6. Qu, S., et al., *Toward efficient orange emissive carbon nanodots through conjugated sp^2-domain controlling and surface charges engineering.* Advanced materials, 2016. **28**(18): p. 3516-3521.

7. Wang, J., et al., *Lignin-derived red-emitting carbon dots for colorimetric and sensitive fluorometric detection of water in organic solvents.* Analytical Methods, 2020. **12**(25): p. 3218-3224.

8. Bai, J., et al., *Solvent-controlled and solvent-dependent strategies for the synthesis of multicolor carbon dots for pH sensing and cell imaging.* Journal of Materials Chemistry C, 2019. **7**(31): p. 9709-9718.

9. VA, A., et al., *Acetic acid derived carbon dots as efficient pH and bio-molecule sensor.* International Journal of Environmental Analytical Chemistry, 2021. **101**(4): p. 506-512.

10. Phull, M., A. Ali, and B. Maity, *Sustainable synthesis of carbon dots from Ananas Comosus as renewable biomass: nanomolar level detection of glutathione.* RSC Sustainability, 2024. **2**(5): p. 1599-1612.

11. Popova, A., *Crystallographic analysis of graphite by X-Ray diffraction.* Coke and Chemistry, 2017. **60**(9): p. 361-365.

12. Li, Z., et al., *X-ray diffraction patterns of graphite and turbostratic carbon.* Carbon, 2007. **45**(8): p. 1686-1695.

13. Ramanan, V., et al., *Outright green synthesis of fluorescent carbon dots from eutrophic algal blooms for in vitro imaging.* ACS Sustainable Chemistry & Engineering, 2016. **4**(9): p. 4724-4731.

14. Kalytchuk, S., et al., *Purple-emissive carbon dots enhance sensitivity of Si photodetectors to ultraviolet range.* Nanoscale, 2020. **12**(15): p. 8379-8384.

15. Clogston, J.D. and A.K. Patri, *Zeta potential measurement.* Characterization of nanoparticles intended for drug delivery, 2011: p. 63-70.

16. Gopal, R., et al., *Aggregation-Induced White Light Emission and Solvent-Induced Dual Mode Multi-Analyte Sensing by Highly Crystalline Single Component Derived N, S Co-Doped Carbon Nanodots.* ACS Applied Optical Materials, 2023. **1**(3): p. 701-714.

17. Raveendran, V. and R.N. Kizhakayil, *Fluorescent carbon dots as biosensor, green reductant, and biomarker.* ACS omega, 2021. **6**(36): p. 23475-23484.

18. Han, L., et al., *Facile synthesis of multicolor photoluminescent polymer carbon dots with surface-state energy gap-controlled emission.* Journal of Materials Chemistry C, 2017. **5**(41): p. 10785-10793.

19. Jiao, Y., et al., *Novel processing for color-tunable luminescence carbon dots and their advantages in biological systems.* ACS Sustainable Chemistry & Engineering, 2020. **8**(23): p. 8585-8592.

20. Li, X., et al., *Dual-excitation and dual-emission carbon dots for Fe $^{3+}$ detection, temperature sensing, and lysosome targeting.* Analytical Methods, 2021. **13**(37): p. 4246-4255.

21. Zhou, W., et al., *Towards efficient dual-emissive carbon dots through sulfur and nitrogen co-doped.* Journal of Materials Chemistry C, 2017. **5**(32): p. 8014-8021.

22. Chen, D., et al., *Excitation-independent dual-color carbon dots: surface-state controlling and solid-state lighting.* ACS Photonics, 2017. **4**(9): p. 2352-2358.

23. Shuang, E., et al., *Carbon dots with tunable dual emissions: from the mechanism to the specific imaging of endoplasmic reticulum polarity.* Nanoscale, 2020. **12**(12): p. 6852-6860.

24. Singh, A., et al., *Ultra-bright green carbon dots with excitation-independent fluorescence for bioimaging.* Journal of Nanostructure in Chemistry, 2023. **13**(3): p. 377-387.

CHAPTER 4

p-PHENYLENEDIAMINE DERIVED CARBON NANODOTS AS SENSOR

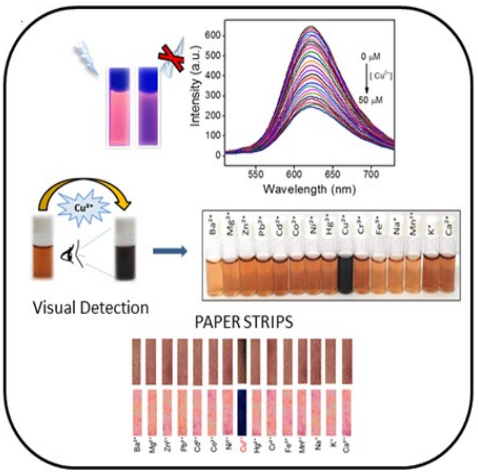

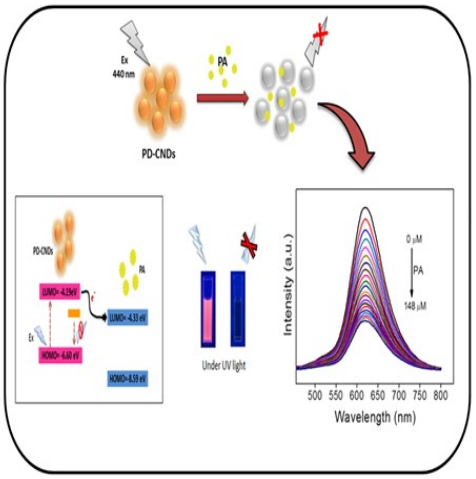

Sensing is one of the most extensively utilized applications of carbon nanodots. This chapter explores the sensing applications of the prepared carbon nanodots (PD-CNDs). The fluorescence of these carbon nanodots was tested in the presence of a variety of significant analytes. Notably, a significant reduction in fluorescence intensity was observed with cupric ions and picric acid, enabling their fluorimetric detection.

4.1. Introduction

A sensor is a device capable of measuring various parameters and converting these measurements into precise signals. Key requirements for sensors include sensitivity, diversity, selectivity, stability, and accuracy, all of which are essential for effective environmental monitoring. Innovative sensor devices with certain qualities like low cost, high sensitivity, improved reliability, shorter reaction times, smaller size, faster recovery, easier operation, and real-time analysis are in greater demand. These properties of chemical and biological sensors can be further enhanced by nanostructured materials, which have demonstrated considerable promise. Numerous sensing methods have shown to be trustworthy and sensitive. However, they often suffer from drawbacks such as high cost, expensive equipment, the need for specific sample preparation, and labor-intensive procedures. This has led to a need for procedures that are quicker, easier, less expensive, and more efficient. It is now crucial to build straightforward and affordable sensors for the detection of chemical and biological substances. The creation and use of chemical sensors is an essential component of analytical chemistry, as they offer precise information about the kind and abundance of chemical species in their surroundings. Selectivity and sensitivity to a particular analyte determine the efficiency of a sensor. Based on the parameters they monitor, chemical sensors can be roughly categorized as electrochemical, optical/ fluorescence, thermal, and pH sensors. Fluorescence-based sensing

techniques have recently gained significant attention due to their high sensitivity, cost-effectiveness, speed, and ease of use.

Carbon nanodots (CNDs) are extensively studied as active materials for sensors, as evidenced by the increasing number of published papers on carbon nanodot-based sensors. The annual publication trend of articles is illustrated in **Figure 4.1** that shows the boom in the works in this area. The data pertaining to the role of "carbon nanodots as a sensor" from 2010 to 2020 was obtained from the Scopus database [1]. Several types of carbon nanodot based sensors have been thoroughly studied, including colorimetric [2-5], electrochemical [4, 6-8], and fluorescence sensors [9, 10]. A colorimetric sensor uses the shift in the absorbance/fluorescence peak of CNDs as a sensing signal, whereas a fluorescence sensor uses the variation in the fluorescence intensity/quenching of CNDs on absorption and desorption of analytes. Optical sensors are appealing due to their simplicity, cost-effectiveness, and ability to rapidly provide qualitative information. Additionally, results for various chemical species can be visually observed on-site with the naked eye [2, 3]. In contrast to colorimetric and fluorescence sensors, which rely on visual signals, electrochemical sensors use the variation in the resistance or impedance of CNDs deposited on glassy carbon electrodes to recognize analytes.

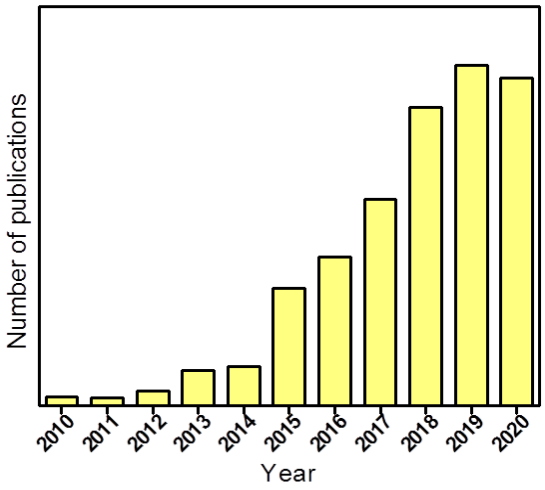

Figure 4.1 Annual distributions of published articles

As a new fluorescent nanomaterial, carbon nanodots have an intriguing application in fluorescence based sensing. The design of fluorescent carbon nanodots based sensors typically employs three strategies. Firstly, analytes directly interact with carbon nanodots, leading to changes in the fluorescence signals of the CNDs [11, 12]. Secondly, post-functionalization of carbon nanodots is utilized, where specific receptors are conjugated with CNDs to construct fluorescent nanosensors with high sensitivity and specificity [13]. The third strategy involves integrating CNDs with other materials such as quenchers, fluorophores, or substrates. For instance, the fluorescence of quenched CND complexes can be recovered upon breaking of quenching and interaction with targeted analytes. Additionally, the fluorescence of CNDs can be quenched by the addition of certain metal ions, making them applicable in sensing various analytes such as anions, biomolecules

[14-16] etc. By combining the phenomena of quenched and recovered fluorescence, CNDs can serve as dual-mode sensors capable of detecting multiple analytes simultaneously.

Fluorescent carbon nanodot sensors have been used for the detection of metal ions and anions. Researchers have developed a variety of fluorescent sensors for detecting metal ions. Carbon nanodot based probes are synthesized to selectively recognize ions such as Hg^{2+} [17-22], Ag^{+} [23-26], Au^{3+} [27, 28], Cd^{2+} [29], Co^{2+} [30], Cu^{2+} [31-34], Fe^{3+} [16, 35-37], Cr^{6+} [38-40], Zn^{2+} [41], Pb^{2+} [17, 41, 42] and so on. In addition, CNDs are also utilized for fluorescence determination of various anions, such as superoxide anions [43], I^{-} [44], CN^{-} [45], S^{2-} [46], PO_4^{3-} [47, 48] etc. Compared to metal ion detection, the application of CNDs for anion detection has been much less prevalent. CNDs are also widely used in the detection of small organic and biological molecules. Some important small molecules, such as volatile organic compounds, explosive chemicals, pesticides, antioxidants, and biological reagents, pose serious threats to human health, the environment, water quality, and ecological stability, despite their significant economic benefits. Therefore, proper utilization and post-treatment of these small molecules are crucial. To identify these molecules, different CNDs are designed and synthesized. Numerous reports exist on the sensing of various small molecules which include the detection of glucose [49], ascorbic acid [50, 51], folic acid [52, 53], proteins [54], DNA [55], cholesterol [56, 57], nitro-explosives including trinitrotoluene [58] and picric acid [59], antibiotics like amoxicillin

[60] and tetracycline [61-63] as well as dopamine [64], vitamin B_{12} [65], glutathione [66], lysine [67], histidine [68] and others.

4.2 p-Phenylenediamine derived carbon nanodots as sensor

p-Phenylenediamine (p-PD) derived CNDs are extensively used as fluorescent probes for detecting various analytes in environmental and biological systems. This is due to their adjustable PL properties and ease of functionalization. Compared to other PL probes, p-PD-derived CNDs offer several advantages: a larger specific surface area, greater resistance to photo-bleaching, enhanced chemical inertness, superior biocompatibility, and better environmental friendliness. Moreover, the PL of p-PD-derived CNDs is more responsive to changes in the surrounding environment, resulting in faster response times and higher sensitivity when used as probes. In recent years, numerous studies have reported the use these CNDs for various ion detection. This is largely due to the abundant oxygen/nitrogen-related groups on the surface and their efficient photoluminescent (PL) properties. Zhu *et al.* [69] used p-PD and ammonium thiocyanate as precursors to synthesize CNDs via the hydrothermal method. These CNDs exhibited red photoluminescence (PL) emission at 618 nm when excited at 598 nm and were developed as a selective sensor for detecting Sn^{2+} ions. Ludmerczki *et al.* [70] reported a method for detecting nitrite ions using CNDs prepared from p-PD as the carbon source and ethanol as the reaction solvent. Their studies found that the CNDs could detect nitrite ions through the

quenching of photoluminescence at 535 nm, caused by diazotization. Nitrite ions pose serious threat to human health, making their rapid and reliable detection in freshwater essential. Huo *et al.* [71] prepared CNDs using p-PD and citric acid, exploiting quenching effect of phoxim on the inner filter effect induced photoluminescence (PL) emission of CNDs. Within the concentration range of 1–10 μM and 10–98 μM, CNDs shown high sensitivity and selectivity for the detection of phoxim, they exhibited a dual linear relationship. The suggested assay was further extended to detect phoxim in real samples. Yu *et al.* [72] synthesized CNDs using a phenylenediamine isomer through Fe^{3+} catalyzed oxidative polymerization at 80°C. Among this, p-PD-derived CNDs were employed to detect the water content in D_2O. Superoxide anion ($O_2^{\bullet-}$) stands out as one of the most crucial reactive oxygen species. In the realm of environmental and hazardous chemical monitoring, the sensitive detection of $O_2^{\bullet-}$ presents both significance and challenge. Yue *et al.* [73] devised a "turn-on" photoluminescence (PL) probe utilizing CNDs, synthesized from p-PD, as a key material for detecting $O_2^{\bullet-}$.

4.3 Exploring diverse mechanisms of fluorescence quenching

The fluorescence by carbon nanodots acts as a sensing signal, responding dynamically upon interactions with the analytes. These interactions, termed quenching, enhancement, or recovery, are driven by the interplay between CNDs and analytes. Potential interactions encompass dipole-dipole interactions and

charge transfer phenomena. Theoretically, any alteration in fluorescence properties (intensity, wavelength or lifetime) in response to varying analyte concentrations holds promise for sensor applications. Carbon nanodots exhibit various mechanisms underlying fluorescence changes, which have found utility in sensing applications. Mainly there exist four mechanisms: (i) static and dynamic quenching, (ii) fluorescence resonance energy transfer (FRET), (iii) photo-induced electron transfer (PET) and (iv) inner filter effect (IFE).

4.3.1. Static and Dynamic Quenching

Static quenching in carbon nanodots (CNDs) occurs when an interaction with a quencher results in the formation of a non-fluorescent ground state complex. This formation alters the absorption spectrum of the CNDs. In dynamic quenching, the excited state of CNDs returning to the ground state due to collisions with the quencher, facilitated by charge transfer or energy transfer. Unlike static quenching, dynamic quenching does not alter the absorption spectra of CNDs, affecting only the excited state. Additionally, the presence of the quencher changes the fluorescence lifetime of the CNDs [74, 75].

4.3.2. Fluorescence Resonance Energy Transfer

Fluorescence resonance energy transfer (FRET) is the process where an initially excited molecule (donor) returns to its ground state while also stimulating an electron in the acceptor

molecule via energy transfer. FRET is driven by long range dipolar interactions between the excited donor and acceptor molecules. According to FRET theory, the rate of energy transfer is determined by three factors: the distance between the donor and the acceptor, the extent of overlap between the fluorescence emission spectrum of the donor (the fluorophore) and the absorption spectrum of the acceptor (the analyte), and the relative orientation of the donor and acceptor dipoles. Additionally, the fluorescence lifetime changes with an increase in quencher concentration [76, 77].

4.3.3. Photo-induced Electron Transfer

In photo-induced electron transfer (PET), electrons typically get transferred from a ground state molecule (the electron donor) to an excited state fluorescent molecule (the electron acceptor). Upon excitation, the electron from the HOMO of the electron donor moves to the HOMO of the fluorescent molecule, while the electron from the LUMO of the fluorescent molecule jumps to the HOMO of the electron provider, resulting in fluorescence quenching. When a third species (guest) is present, the HOMO energy level of the electron provider adjusts to be approximately equal to or lower than that of the fluorescent molecule, suppressing or preventing the PET process and recovering or enhancing fluorescence. The pre-requisites for PET involvement in fluorescence quenching are: (a) shorter carbon nanodot (CND) lifetimes in the presence of the target analyte, and

(b) a definite energy gap between the energy levels of the CNDs and the quencher molecule, particularly between their LUMO and HOMO levels or between their LUMO levels [75, 78]. There are two main types of PET reactions: reductive and oxidative. In reductive PET, the quencher is the electron donor, and the CNDs are the electron acceptors. In oxidative PET, the target analyte is the electron acceptor, and the CNDs are the electron donor. The energy gap between the LUMO of the quencher and the HOMO of the donor drives reductive PET, while the gap between the LUMOs of the CNDs and the quencher causes oxidative electron transfer.

4.3.4. Inner Filter Effect

When the excitation or emission spectra of CNDs and absorption spectrum of the quencher in the detection system overlap, it is known as the inner filter effect (IFE). IFE, also known as apparent quenching, is the result of either an excess concentration of CNDs or the quencher in solution attenuating the excitation beam or absorbing the radiation emitted; it is not an actual quenching process. This effect reduces intensity (but not decay time) and should not be termed "quenching". Instead, a second absorber is simply filtering the emission of a particle. Chromophores, typically the target analyte in the solution, can act as a filter and influence the fluorescence emission of the fluorophore by absorbing light within either the excitation or emission wavelength range of the fluorophore. As a result, it is possible to create IFE assisted fluorescent sensors for particular

analytes by skillfully modifying the absorber or fluorophore concentration [79].

4.4. Present work

Preliminary studies revealed that the fluorescence of PD-CNDs is stable under continuous UV light irradiation. The well-defined emission properties of these carbon nanodots (PD-CNDs) prompted us to explore their potential in sensing applications for identifying various analytes. Our observations indicate that PD-CNDs are sensitive to metal ion and nitroaromatic compound. This chapter is divided in to two parts. Part I discusses PD-CNDs as a turn-off sensor for cupric ions, which also enable the naked eye detection of Cu^{2+}. Part II covers the theoretical and experimental investigation of PD-CNDs as sensors for nitroaromatic compounds.

PART I

4.5. p-Phenylenediamine derived carbon nanodots as turn-off sensor for Cu (II) ions

4.5.1. Introduction

Metal ion detection is one of the most common applications of carbon nanodots (CNDs) in both chemical and biological environments. This widespread use is partly due to the coordination and affinity of different metal ions for functional groups, which are the key structural components of CNDs. Metal binding to CNDs often results in luminescence quenching, even at very low metal ion concentrations, making CNDs a useful platform for metal ion detection. The observation of ionic selectivity in various systems further supports the use of CNDs as metal ion sensors. The unique optical properties, especially their tunable fluorescence, make CNDs ideal for detecting and measuring a wide range of metal ions. CNDs are at the forefront of advanced sensing technologies due to their inherent high sensitivity and ease of surface functionalization. A fundamental feature of CNDs is their ability to selectively interact with specific metal ions, which can be precisely adjusted by modifying their surface. By introducing functional groups onto the CND surface, researchers can enhance the affinity of CNDs for the particular metal ion, enabling selective binding and chelation processes. This selectivity often results in noticeable changes in the fluorescence properties of CNDs, providing a robust foundation for reliable metal ion detection.

Here we monitored the response of PD-CNDs towards fifteen selected metal ions. Analyte solutions of specified concentrations were added to PD-CNDs and the response was monitored using fluorescence spectroscopy by exciting the samples at 440 nm. It was observed that Cu^{2+} ions can efficiently quench the luminescence of PD-CNDs within seconds, even at low concentrations, acting as turn-off sensor for Cu^{2+} ions. Naked eye sensing of cupric ions was also enabled at higher concentrations.

4.5.2. Relevance of Copper ion

Copper ions have garnered significant attention from the researchers due to their critical role in various biological processes. Copper is essential for the proper functioning of numerous enzymes and is indispensable for maintaining the strength of skin, blood vessels, epithelial tissues, and connective tissues throughout the body. It plays a vital role in the synthesis of hemoglobin, myelin, and melanin, and is necessary for the normal functioning of the thyroid gland. After iron and zinc, copper is the third most abundant essential transition metal ion in the human body, playing a crucial role in several physiological processes. As a prerequisite nutrient for life, copper is involved in many fundamental physiological processes across diverse organisms and biological systems [80, 81]. It is essential for the structural and catalytic properties of numerous significant enzymes [82]. However, excessive intake of copper can be detrimental due to its ability to generate reactive oxygen species and disrupt cellular

metabolism. Consuming copper contaminated water or food can lead to acute gastrointestinal symptoms, acute tubular necrosis in the kidney, liver cirrhosis, hemolytic anemia, and acute renal failure. Copper poisoning can also cause weakness, lethargy, and anorexia [83-86]. Furthermore, even short-term exposure to excess copper can contribute to various neurodegenerative disorders, including Wilson's disease, Alzheimer's disease, Parkinson's disease, and Menkes disease [87-91]. The US Environmental Protection Agency (USEPA) has set the tolerable concentration limit for copper ions in drinking water at 20 μM (1.3 ppm) [92]. In light of these considerations, numerous optical and electrochemical sensors have been developed for Cu^{2+} monitoring to ensure safe levels in the environment and prevent adverse health effects. **Figure 4.2** shows the adverse effect of copper ion in human health and environment.

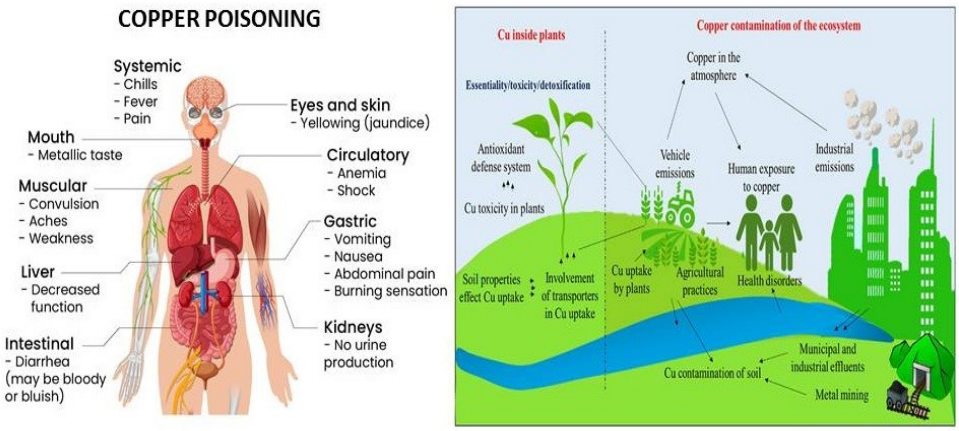

Figure 4.2 Adverse effect of copper [Credits: DOI:10.1016/ j.chemosphere.2020.127436]

4.5.3. Fluorimetric methods for the detection of Cu (II) ions with carbon nanodots

The shifts towards simpler yet effective detection methods are particularly crucial and demanding for universally acceptable onsite applications. Recent investigations focus on fluorescence and absorption spectral methods as viable techniques for tracing cupric ions. In contrast, fluorescent sensors for Cu^{2+} detection have gained popularity due to their high sensitivity, simplicity, rapid response, and excellent selectivity. Sai *et al.* [93] reported the use of protein-derived, hydrothermally fabricated carbon dots (CDs) for the fluorimetric detection of Cu^{2+}. The first Cu^{2+} probe, developed in 2012, had a limit of detection (LOD) of 1 nM [94]. Nitrogen-rich carbon dots (NCDs) were initially used by Ganiga *et al.* [95] to detect Cu^{2+} ions; this was the first work to investigate the relationship between Cu^{2+} ions and NCD-based fluorescent nanomaterials. Their detailed investigations showed that both the direct recombination of excitons and the participation of defect states are the sources of the steady-state photoluminescence emission of NCDs. The detection limit for Cu^{2+} ions was determined to be 10 μM within a dynamic range of 10 μM to 0.4 mM. Dong *et al.* [96] reported an effective method for detecting trace amounts of Cu^{2+} ions using branched poly(ethyleneimine) functionalized carbon nanodots (BPEI-CDs) as fluorescent probes. The abundant amine groups on the surface of BPEI-CDs can interact with cupric ions to form cupric amine complexes. The BPET-CDs sensor enabled rapid, reliable, and selective detection of

Cu^{2+} with a low limit of detection (LOD) as 6 nM. Additionally, they tested the probe in real river water samples, demonstrating a linear response to Cu^{2+} concentrations ranging from 0 to 9 μM. Zong *et al*. [97] reported on the detection of Cu^{2+} using pristine carbon nanodots that contain surface groups such as hydroxyl, amine, and carboxyl. The diverse sensitivities are attributed to the presence of different functional groups on various CND surfaces. These groups could form complexes with Cu^{2+}, resulting in the fluorescence quenching of CNDs, and a limit of detection of 23 nM was achieved. Tian and colleagues [98] developed a ratiometric sensor with dual emission colors from blue carbon nanodots and red quantum dots embedded in silica nanoparticles. This innovative approach aimed to enhance the reliability of visual detection methods for Cu^{2+}. These studies highlight the versatility and potential of CNDs in creating sensitive and selective sensors for monitoring essential trace elements like Cu^{2+} in biological and environmental samples. Huang *et al.* [99] synthesized fluorescent carbon nanodots from poly (vinylpyrrolidone) and l-cysteine via carbonization. Cupric ions interacted with the nitrogen (N) and sulfur (S) atoms on the surface of CNDs through complexation. The emission of CNDs was efficiently quenched due to the high metal-to-ligand binding affinity. Liu developed nitrogen-doped carbon dots (NCDs) using electrospun carbon nanofibers. The strong interaction between Cu^{2+} ions and the surface functional groups of the CNDs induced fluorescence quenching upon the addition of Cu^{2+}[100].

4.5.4. Detection of Cu (II) ions using p-phenylenediamine derived carbon nanodots

Upon exposure to 365 nm UV light, the p-phenylenediamine derived carbon nanodots (PD-CNDs) exhibited a distinctive orange-red luminescence. It was observed that Cu^{2+} ions can efficiently quench the luminescence of PD-CNDs within seconds, even at lower concentrations. The luminescence quenching of PD-CND after the addition of Cu^{2+} ion solution at an excitation of 440 nm is shown in **Figure 4.3(a).** The fluorescence intensity gradually decreased to approximately 25% of its initial value when the concentration of Cu^{2+} ions reached around 50 μM, as depicted in **Figure. 4.3**. This decrease was visually evident under UV radiation at a wavelength of 365 nm (**Figure 4.3 (b)**). The plot of relative fluorescence intensity (F_0-F/F_0) vs. concentration of Cu^{2+} ions shown in **Figure 4.3 (c)** exhibited a commendable linearity in lower concentrations. The experimentally determined limit of detection for Cu^{2+} ions under the current experimental condition was 2.28 μM, which is significantly less than the permissible limit of Cu^{2+} ions in drinking water (~20 μM) set by the US Environmental Protection Agency [101]. To assess the selectivity of the fluorimetric detection method, the response of the sensor to potentially interfering ions was examined using the following metal ions: Ba^{2+}, Mg^{2+}, Zn^{2+}, Pb^{2+}, Cd^{2+}, Co^{2+}, Ni^{2+}, Hg^{2+}, Cr^{3+}, Fe^{3+}, Na^{+}, Mn^{2+}, K^{+} and Ca^{2+} ions. **Figure 4.3 (d)** illustrates the selectivity of PD-CND for the target analyte.

Notably, Cu^{2+} ions significantly quenched the fluorescence of PD-CND, whereas other metal ions had a negligible effect.

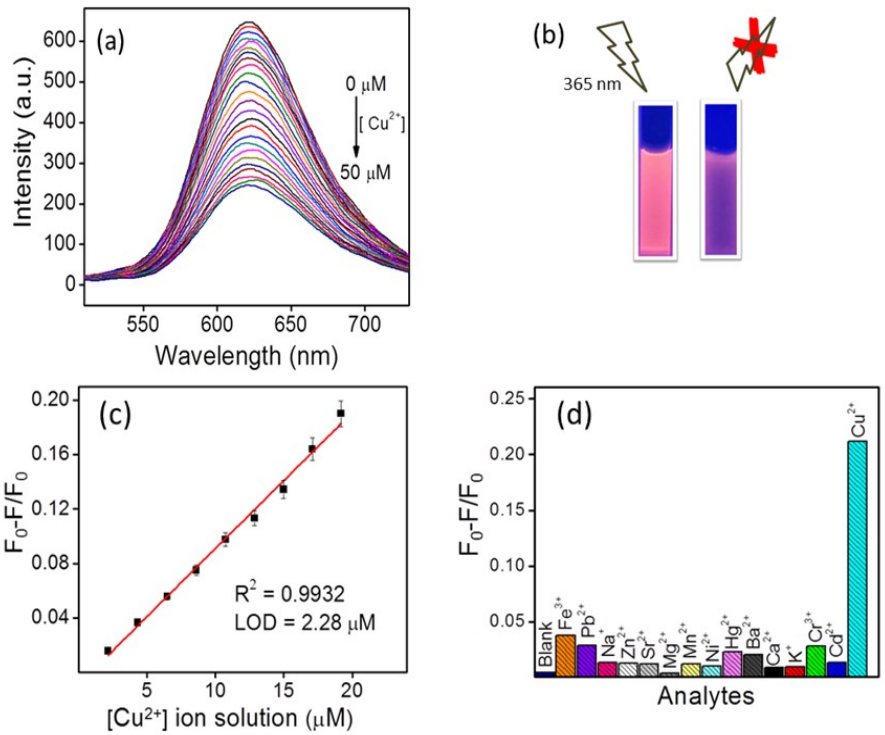

Figure 4.3 (a) Photoluminescence spectra of PD-CND in presence of Cu^{2+} at 440 nm excitation, (b) luminescence quenching of PD-CND under 365 nm exposure of UV radiation, (c) Stern-Volmer plot of luminescence quenching, (d) selectivity of PD-CNDs towards selected analytes.

4.5.5. Investigation of quenching mechanism

The fluorescence quenching phenomenon encompasses various interactions, including inner filter effects, non-radiative combination pathways, electron transfer processes, and ion binding interactions. To explore this further, fluorescence lifetime

decay analysis was conducted, with a particular focus on charge transfer and exciton recombination processes, both in the presence and absence of Cu^{2+} ions. **Figure 4.4** illustrates the fluorescence lifetime decays of PD-CNDs obtained using TCSPC. The lifetime studies reveal a mono-exponential decay with minimal shift upon the introduction of Cu^{2+} ions. Specifically, the fluorescence lifetime (τ) remains nearly constant before and after the addition of Cu^{2+} ions (τPD-CND = 2.40 ns, τPD-CND @Cu = 2.47 ns). This consistency suggests that the quenching mechanism involves complex formation (static quenching) rather than dynamic quenching . The examination of UV-visible absorption and photoluminescence spectra, both in the absence and presence of Cu^{2+} ions, supports this static quenching hypothesis. The absence of fluorescence resonance energy transfer (FRET) is further confirmed by the negligible overlap between the absorbance spectrum of Cu^{2+} and the emission spectrum of PD-CNDs. Additionally, the inner filter effect is ruled out, as there is no overlap between the excitation curve of PD-CNDs and the absorbance curve of Cu^{2+} ions, depicted in **Figure 4.5 (a).** An intriguing observation in the study is the blue shift in the π-π* transition of PD-CNDs in the presence of Cu^{2+} ions, accompanied by absorbance quenching (**Figure 4.5 (b)**). This shift, denoted as Δλ = 3 nm for a 100 μM addition, is attributed to the formation of the complex PD-CND@Cu resulting from the interaction between Cu^{2+} ions and PD-CNDs. These findings collectively contribute to a

comprehensive understanding of the quenching mechanisms involving complex formation.

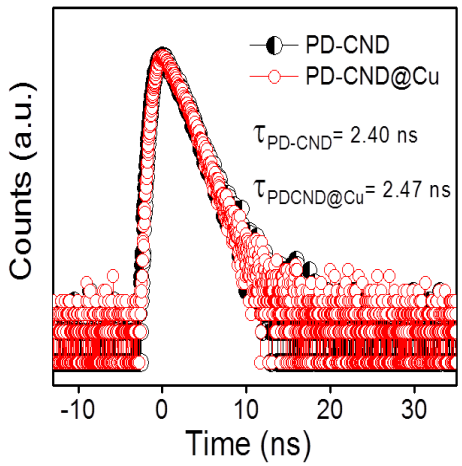

Figure 4.4. Fluorescence decay profile of PD-CNDs before and after the addition of Cu^{2+} ion solution

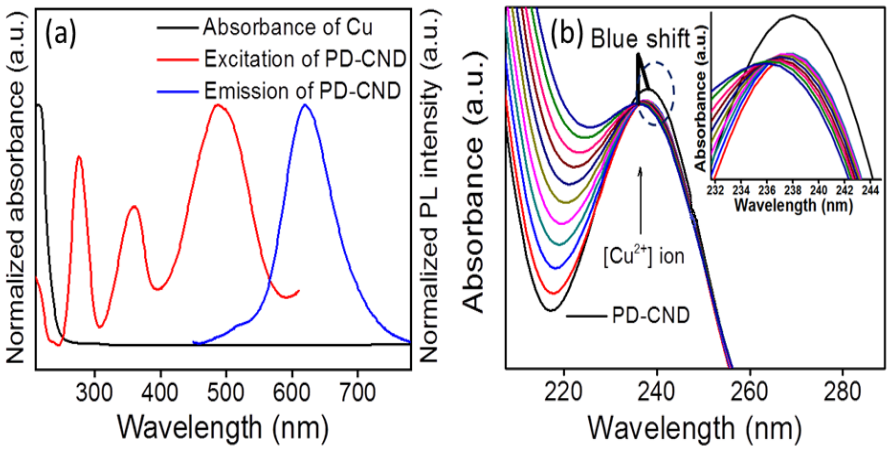

Figure 4.5 (a) The absorption spectrum of copper along with the excitation and emission spectra of PD-CNDs, (b) Variation of UV-visible absorption spectrum of PD-CND after addition of Cu^{2+} ion solution

4.5.6. Copper hydroxynitrate-Carbon nanodot complex formation

p-Phenylenediamine derived carbon nanodots (PD-CNDs) serve as an excellent tool for detecting the heavy metal ion Cu^{2+}. Interestingly, the carbon nanodot solution turns black and forms a black precipitate within a minute in the presence of copper ions, a change that can be easily observed with the naked eye. **Figure 4.6** shows the interaction of various metal ions with PD-CNDs. As indicated in this figure, no other ions could evoke such a response when in contact with PD-CND solution at this much dilution.

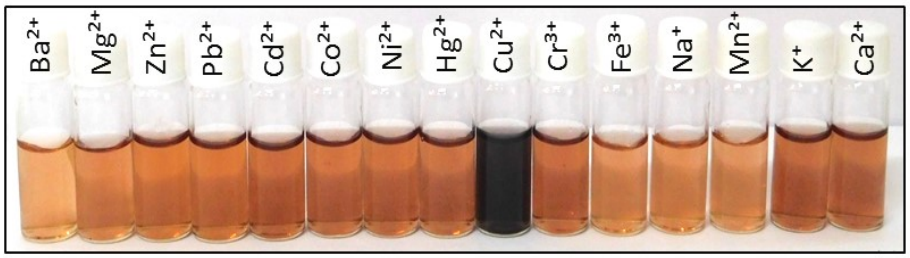

Figure 4.6 Interaction of selected metal ion solutions with PD-CNDs

The lowest concentration of copper ions that could induce this color change was 1.3 ppm (~20μM). To test the interference of other ions in the visible detection of copper ions, a mixture of metal ions (Ba^{2+}, Mg^{2+}, Zn^{2+}, Pb^{2+}, Cd^{2+}, Co^{2+}, Ni^{2+}, Hg^{2+}, Cr^{3+}, Fe^{3+}, Na^{+}, Mn^{2+}, K^{+}, and Ca^{2+}) was introduced into the PD-CND solution, both with and without Cu^{2+} ions. The mixture without Cu^{2+} ions showed no color change, while the mixture containing traces of

Cu^{2+} exhibited a drastic color change. This interference-free performance and reliability of the method are demonstrated in **Figure 4.7(a).** The development of the black color is easily visualized within a short period of time as shown in **Figure 4.7 (b).**

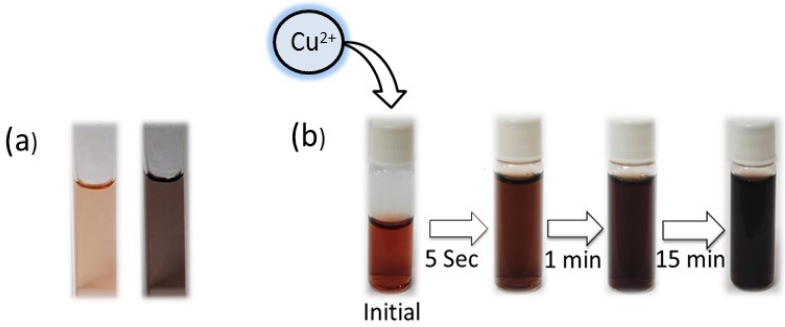

Figure 4.7 (a) PD-CND solution and mixture of selected metal ions without Cu^{2+} ions (left) and with Cu^{2+} ions (right),(b) Photographs of the black solution developed after the addition of Cu^{2+} solution captured at a particular time interval

The visual detection of Cu^{2+} ions is suggested to stem out from the complex formation between carbon nanodots and copper ions. This hypothesis finds support in various analytical results depicted in the accompanying figures. A comparison between the XRD patterns of PD-CND@Cu and PD-CND (**Figure 4.8 (a)**) reveals a broad peak centered at a 2θ value of 23.4°, corresponding to the (002) plane of graphitic carbon in PD-CND. Additionally, sharp crystalline peaks are observed at 12.73°, 15.97°, 17.69°, 21.45°, 22.81°, 25.71°, 29.30°, 32.03°, 33.56°, 36.47°, 39.55°, 43.65°, 53.56°, 58.68°, 60.73°, and 62.61°, which match with copper

hydroxynitrate [102, 103]. The Raman spectrum (**Figure 4.8 (b)**) exhibited a comparable correlation with the reported vibrational frequencies associated with each peak. Bands indicative of Cu-O (279 cm^{-1}, 498 cm^{-1}) and Cu-ONO_2 bonds (385 cm^{-1}), as well as vibrations from the nitrate groups (613 and 1010 cm^{-1}), and were observed [103-105]. Furthermore, the D and G bands, already present in the PD-CND system, were retained as weak signals with slight shifts in PD-CND@Cu.

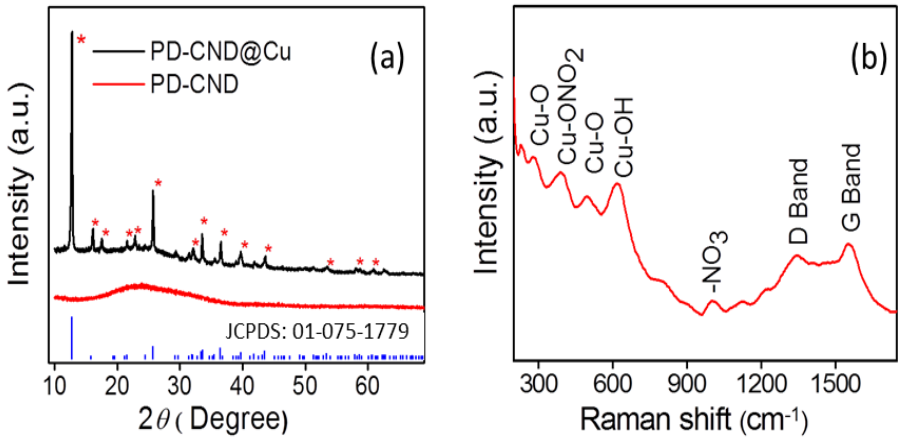

Figure 4.8(a) XRD pattern of PD-CND and PD-CND@Cu, (b) Raman spectrum of PD-CND@Cu.

The FT-IR spectrum (**Figure 4.9(a)**) clearly shows additional bands corresponding to –Cu-O and –NO_2 vibrations, indicating the successful complex formation between carbon nanodots and cupric moieties. The broad band in the range of 3600-3200 cm^{-1} denotes –O-H and/or –N-H stretching. The Cu-O-H bonds present in PD-CND@Cu give rise to bending absorptions at various frequencies, depending on the degree of H-bonding, which

correlates with the band width. These bands are located at 878, 784, and 672 cm^{-1}, respectively. The bands at 1451, 1385, and 1019 cm^{-1} indicate the presence of different $–ONO_2$ stretching vibrations in PD-CND@Cu [106, 107]. The UV-visible absorption spectrum of PD-CND in the presence and absence of Cu^{2+} ions in water are shown in **Figure 4.9 (b).** PD-CND exhibits an absorption band at 240 nm, while Cu^{2+} ions are known not to show any absorption band near this wavelength. However, the noticeable blue shift observed upon the addition of Cu^{2+} ions (already mentioned above) is attributed to their interaction with PD-CND, leading to the complex formation.

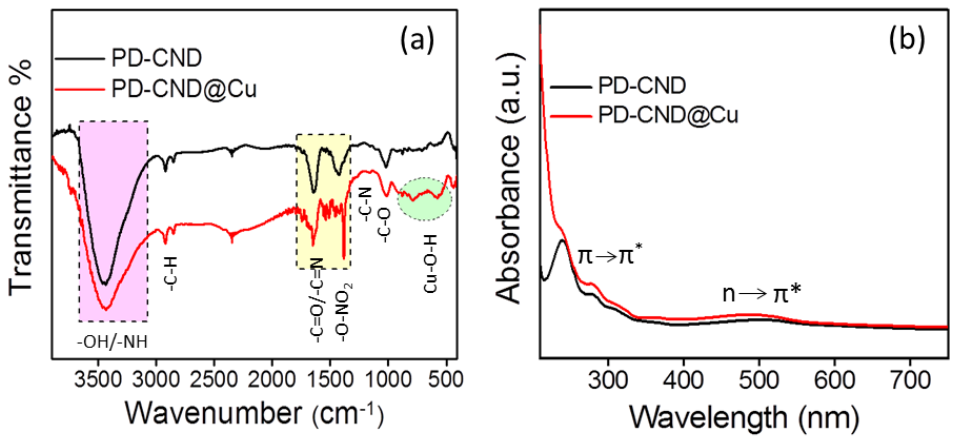

Figure 4.9 (a) FT-IR spectra and (b) UV-visible absorption spectra of PD-CND and PD-CND@Cu.

The morphology of the complex was analyzed using TEM and FE-SEM analysis. The results reveal that PD-CND@Cu exhibits a plate-like morphology (**Figure 4.10 (a), (b) and (c)**). The presence of copper in the complex was visualized through EDX

analysis (**Figure 4.11 (a)**) and further confirmed by elemental mapping (**Figure 4.11 (b)-(e)**). The experiment indirectly facilitated the facile synthesis of copper hydroxynitrate-functionalized carbon nanodots, which exhibit characteristics similar to layered materials.

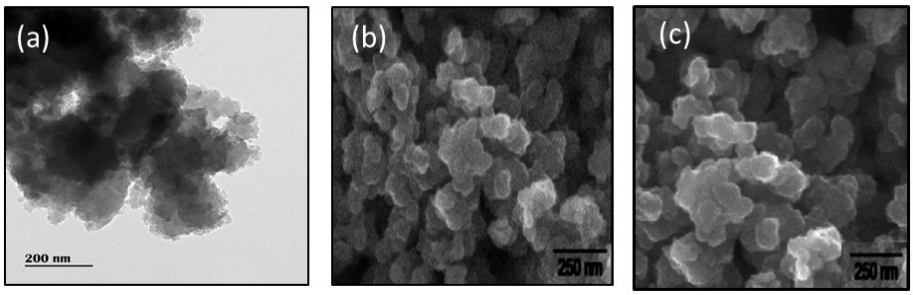

Figure 4.10 (a) TEM image of PD-CND@Cu, (b) and (c) FE-SEM images of PD-CND@Cu.

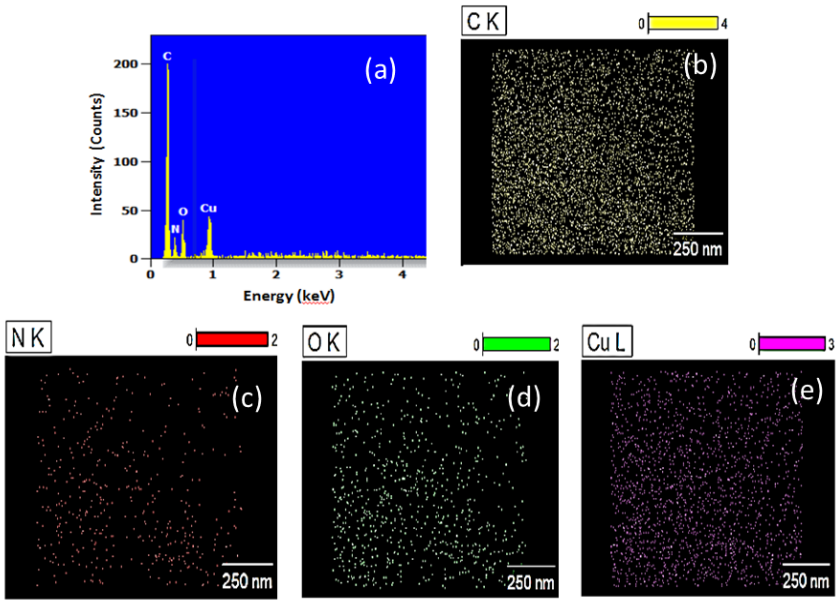

Figure 4.11 (a) EDS Analysis of PD-CND@Cu, (b)-(e) elemental mapping of C, N, O and Cu in PD-CND@Cu

Copper hydroxynitrate salts have diverse applications across various fields and can also serve as precursors for synthesizing copper hydroxides or copper oxide nanoparticles. To validate this, in this study, copper oxide nanoparticles were obtained by carbonizing PD-CND@Cu at 500 °C for 2 hours, as confirmed by the XRD pattern (**Figure 4.12**). Thus, the utility of the complex, an indirect outcome of naked-eye copper sensing, is established.

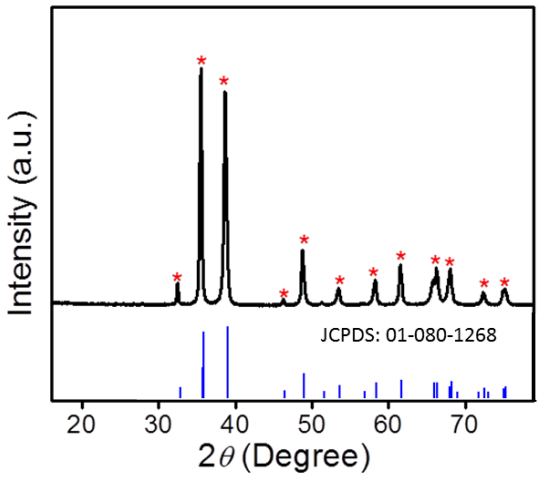

Figure 4.12 XRD pattern of CuO obtained after carbonization of PD-CND@Cu.

4.5.7. Development of solid-state paper strips

The naked-eye detection of Cu^{2+} ions was further extended to a solid-state sensor strip. This strip is prepared by coating ordinary filter paper with a PD-CND solution, followed by drying in a hot air oven. When exposed to UV light, the strip exhibits orange-red luminescence. When the filter paper strips came in contact

with the metal ion solutions and properly dried, the strip treated with copper ions appears black under UV light, indicating the quenched luminescence (**Figure 4.13**). The lowest concentration of cupric ions that causes this color change is noted to be 1 mM.

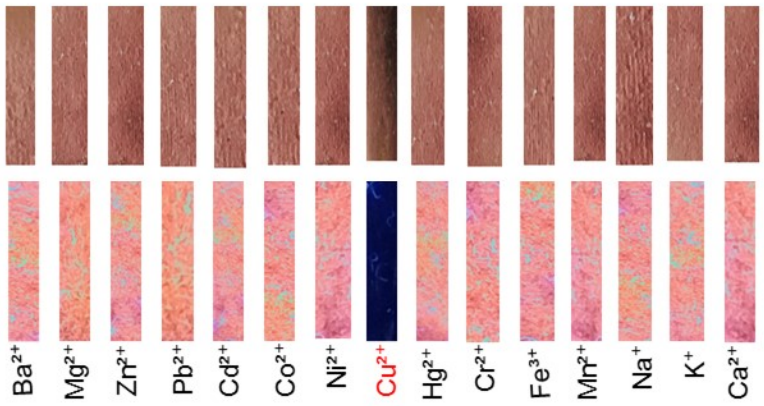

Figure 4.13 Photographs of solid paper strip under daylight (upper panel) and 365 nm UV light exposures after coating with various metal ion solutions.

PART II

4.6. p-Phenylenediamine derived carbon nanodots as picric acid sensor; an experimental and theoretical approach

4.6.1. Introduction

Nitroaromatic compounds (NACs) are aromatic compounds that contain one or more nitro groups. The presence of these nitro groups lends NACs a wide range of applications. They are used as precursors, intermediates, or starting materials in a variety of production sectors [108, 109]. NACs are also widely used in explosives. The nitro group supplies available oxygen to oxidize the aromatic ring, forming a self-oxidant. This feature gives explosive properties to NACs like 2,4-dinitrophenol (DNP), 2,4,6-trinitrotoluene (TNT) and 2,4,6-trinitrophenol (TNP) [110]. The nitroaromatic compound parathion is used as a pesticide, while nitrobenzene (NB) serves as an intermediate in the production of fungicides and linear alkyl benzene detergents [111]. Pentachloronitrobenzene (PCNB) is used to control a variety of plant diseases [112, 113]. Parkinson's disease and many other diseases are treated with some drugs that contain nitro groups. Similarly, drugs for treating parasite infections include NACs such as nifurtimox, metronidazole, and nitazoxanide. A wide range of compounds such as dyes, cosmetics, paints, preservatives, antioxidants, fungicides, pesticides can be chemically synthesized using NACs as valuable raw matrials. Though NACs have diverse

applications, their extensive use leads to continuous environmental discharge through various means such as agricultural runoffs, industrial discharges, improper waste disposal practices, and activities like packaging, loading, and transportation. This results in significant pollution of surrounding water, soil, and air. The application of nitroaromatic pesticides contaminates the soil, which is further spread by agricultural runoff. Consumption of crops contaminated with these nitro-pesticides, herbicides, and fungicides poses toxic risk to humans and animals. The release of NACs from manufacturing industries, shipping, warehousing, and other activities, coupled with improper waste disposal, exacerbates environmental pollution. These compounds contaminate water, soil, and air, presenting hazards to humans and other living organisms. NACs are particularly concerned due to their mutagenic, carcinogenic, and toxic properties. As a result, the United States Environmental Protection Agency (USEPA) has listed them as priority pollutants [114].

The hazards of NACs on human health can be consolidated like this. NACs are known for their hepatotoxicity, carcinogenicity, and potent mutagenicity. Chronic exposure to nitrotoluenes has been shown to cause cancer in mice and rats. In humans, dinitrotoluenes (DNT) are associated with several adverse health effects, including cancer, liver cytotoxicity, anemia, leukocytosis, cyanosis, dark urine, diarrhea, headache, insomnia, labored breathing, nausea, orange feces, prostrate posture and red

discharge around the nose, squinting, and weakness. Exposure to DNT is also reported to be nephrotoxic and carcinogenic to the urinary tract. It can cause methemoglobinemia, as well as discoloration of hair and skin in humans [115]. Additionally, certain NACs impact the reproductive system, resulting in reduced sperm count, altered sperm morphology, and aspermatogenesis. Several NACs can disrupt the nervous system by inhibiting the enzyme acetylcholinesterase. They are also known to exert endocrine-disrupting activities and cytotoxic effects. Chronic health effects of NACs following occupational exposure are well-documented. Workers in DNT manufacturing plants have exhibited symptoms such as unpleasant taste, weakness, head-ache, loss of appetite, nausea, insomnia, vomiting, and cyanosis [116]. While the carcinogenicity of some NACs, like nitrobenzene, in humans remains uncertain, others such as TNT are well-established carcinogens. Bharadiya *et al.* [117] reported symptoms such as methemoglobinemia, epigastric discomfort, and nausea following the ingestion of nitrobenzene by a 17-year-old patient. Overall, the chronic exposure to NACs in occupational settings has been linked to a wide range of adverse health effects, underscoring the need for stringent safety presence of NACs in the air is a major concern due to their mutagenic and carcinogenic properties. Emissions from sources such as diesel exhaust and cigarette smoke release NACs into the atmosphere, and their subsequent inhalation can impair lung function. Studies have shown that NACs can suppress the immune system and induce tumors in human bronchial

epithelial cells. Additionally, NACs are toxic to aquatic animals and plants, with extensive research documenting their harmful effects on fish. Tiwari *et al.* [118] have well described the mechanism of measures and regulations to mitigate their impact on human health. The toxicity of NACs is represented in **Figure 4.14.**

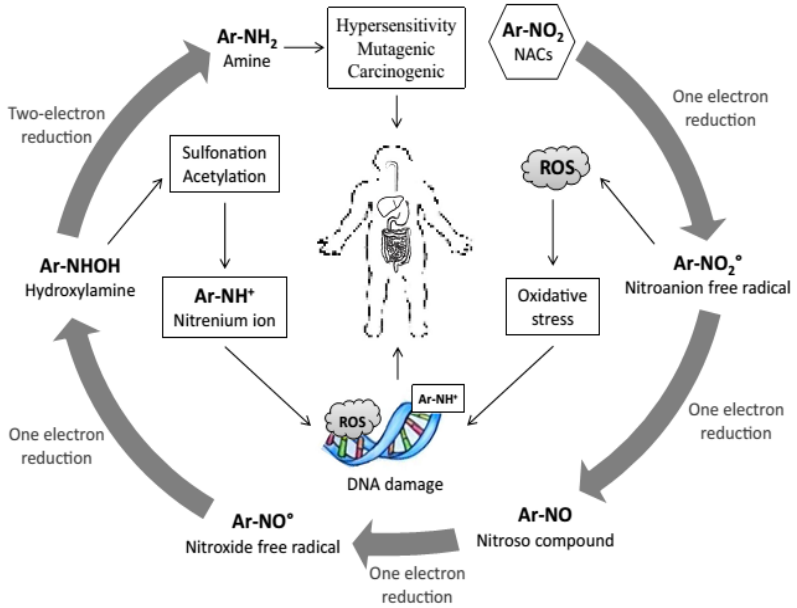

Figure 4.14 Key mechanisms of NACs toxicity

Various detection methods have been explored for NACs including electrochemical, chemical, biosensors, spectrophotometric, and analytical techniques such as gas chromatography (GC) and liquid chromatography etc [119-121]. The analytical methods mentioned earlier necessitate trained personnel, advanced analytical equipment, lengthy analysis times, and the extraction and concentration of environmental samples for detecting NACs. Moreover, these methods often involve the use of hazardous solvents during labor-intensive sample preparation.

Challenges such as matrix effects, co-elution, and co-extraction of interferences are also common in certain cases. In contrast, sensor-based detection methods offer an appealing alternative for on-site detection [122]. They are noted for their increased sensitivity and selectivity, quicker analysis times, and portability in field settings. Chemosensors for NACs exploit their electron deficient nature, causing fluorescence quenching in electron rich moieties. Li *et al.* [123] developed metal-organic frameworks to achieve sensitive detection of NACs, particularly TNT. Molecularly imprinted polymer-based sensors have also been reported for detecting 2, 4-DNT and TNT, achieving detection limits of 30–40 μM [124]. Electrochemical detectors are proposed for rapid and cost-effective on-site detection of NACs. Mesoporous SiO_2, specifically of MCM-41 type, offers a large surface area with strong NAC adsorption capability, enabling electrochemical detection down to nanomolar levels [125]. Despite the high sensitivity offered by chemical and electrochemical sensors, the preparation and functionalization of sensor materials can be challenging and expensive. Additionally, many sensor materials are non-biodegradable and toxic, potentially leading to secondary pollution concerns. In recent years, nanosensors have garnered significant attention for detecting environmental pollutants, including NACs, at trace levels. Sangili *et al.* [126] demonstrated the effective use of cerium oxide nanoparticles for detecting Nitrobenzene. Nanosensors, such as nanofibers, nanotubes, nanowires, and nanodots, are known for their stability and cost-effective

functionalization. They offer advantages such as real-time monitoring, high sensitivity, and eliminate the need for extensive sample preparation.

4.6.2. Carbon nanodots as fluorescent sensor for nitroaromatic compounds

The fluorimetric detection of nitroaromatic compounds using carbon nanodots has been extensively studied. Here, we examine some works in this area. Carbon nanodots derived from malonic acid and urea precursors demonstrated high selectivity for picric acid (PA) due to energy transfer (ET) and inner filter effect (IFE) mechanisms. The synthesized fluorescent probe exhibited selectivity for PA with a limit of detection (LOD) of 51 nM [127]. Carbon nanodots from polyacrylamide and citric acid precursors exhibit bright blue fluorescence with an emission peak at 415 nm. However, the introduction of TNP significantly reduces this fluorescence due to inner filter effects (IFE) [128]. Apple seed pyrolysis was utilized to create CNDs, which were then used as a sensing probe for 4-nitrophenol (4-NP) [129]. Microwave synthesis of sustainable carbon nanodots from sewage sludge was employed as a fluorescent probe for 4-nitrophenol (4-NP). This method demonstrated quenching with a limit of detection of 0.069 μM in the linear range from 0.2 to 20 μM due to inner filter effects [130]. Wang *et al.* [131] developed a ratiometric fluorescence sensor for more efficient and accurate explosive detection. The CNDs synthesized via a solvothermal route using o-

phenylenediamine and ethanolamine, exhibited emission peaks at 430 nm (yellow photoluminescence) and 550 nm (blue photoluminescence). This sensor demonstrated an excellent limit of detection (LOD) of 50 nM. Yellow emissive carbon nanodots (Y-CDs) synthesized via solvothermal synthesis using o-phenylenediamine and urea exhibited photoluminescence emission at 565 nm. The addition of TNP quenched this emission, achieving a limit of detection of up to 57 nM [132]. Hydrothermal synthesis using m-phenylenediamine as a carbon and nitrogen source was employed for detecting TNP, achieving a limit of detection of 2.45 μM [133]. Meng *et al.* [134] utilized ammonia with phenylenediamine as a nitrogen precursor in their studies. Fluorescence intensity quenching occurred due to inner filter effect (IFE), resulting in a limit of detection of 3.69 μM for TNP. Wang *et al.* [135] conducted an analysis for TNP detection using nitrogen-doped carbon nanodots (N-CDs), where TNP acts as a quencher through FRET. Babar *et al.* [136] synthesized water-soluble nitrogen and phosphorus co-doped carbon nanodots (N, P-CDs) to enhance optical properties for detecting TNP with LOD of 23 μM. The fluorescence lifetime exhibited no significant change after adding TNP, suggesting static quenching via ground-state complex formation between the donor and acceptor [136]. By employing L-lysine and thiourea as precursors, N, S co-doped carbon quantum dots (CQDs) were synthesized, exhibiting strong blue photoluminescence with a quantum yield (QY) of 53.19%. The presence of TNP in an aqueous medium selectively quenched the

photoluminescence via FRET, achieving a limit of detection of 0.24 μM [137]. Keerthana *et al.* [138] synthesized nitrogen-doped carbon quantum dots (N-CQDs) and subsequently functionalized them with boron using a microwave reactor, resulting in bright green fluorescence. Detection of TNP was achieved through turn-off sensing via FRET, which was validated by a significant change in fluorescent lifetime and the formation of a complex between the donor and acceptor molecules [138]. Hydrothermal synthesis of N,S-co-doped carbon quantum dots using citric acid and thiosemicarbazide precursors resulted in strong blue photoluminescence with a quantum yield of 37.8%. TNP selectively absorbed onto the N, S co-doped CQDs, forming a non-fluorescent complex through electrostatic interactions. The detection of TNP was achieved via FRET mechanism, with an estimated LOD of 0.22 μM [139].

4.6.3. p-Phenylenediamine derived carbon nanodots as picric acid sensor

Among the NACs, 2, 4, 6-trinitrophenol, also known as picric acid (PA), has the highest potential for explosion. For long years, PA has been a part of landmines. In addition, it is utilized in the manufacturing of matches, fireworks, rocket fuel, leather, and dye industries, among other businesses. PA is dangerous to human health since it is very acidic and easily soluble in water because it contains strong nitro groups that suck electrons. This can happen through soil and ground water. Long-term exposure to PA can

cause serious health problems, such as irritation of the eyes and skin, respiratory problems, liver problems, neurological disorders, infertility, and chronic illnesses including cancer, anaemia, and cyanosis. Even in small concentrations, PA can be detrimental to human health. Hence, there is a significant demand for designing a sensor capable of easy, rapid, selective, and sensitive detection of PA in aqueous solutions.

In this section, the application of PD-CNDs is explored as sensors for nitroaromatic compounds, focusing particularly on picric acid. A set of nitroaromatic and aromatic compounds were chosen for this purpose, to examine their response towards CNDs. The details of the selected compounds are enlisted in **Table 4.1**:

Table 4.1. Details of nitroaromatic and aromatic compounds involved in the experiments.

No	Compound	Abbr.	Molecular weight	Structure
1	o-Nitrotoluene	o-NT	137.14	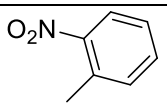
2	m-Nitrotoluene	m-NT	137.14	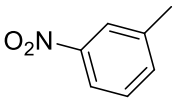
3	p-Nitrotoluene	p-NT	137.14	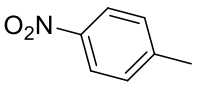
4	m-Nitrobenzaldehyde	m-NBZA	151.12	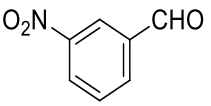

5	p-Nitrobenzaldehyde	p-NBZA	151.12	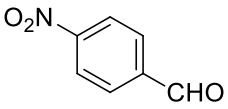
6	Nitrobenzene	NB	123.11	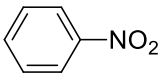
7	p-Nitrophenol	p-NP	139.11	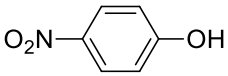
8	p-Nitrobenzoic acid	p-NBA	167.12	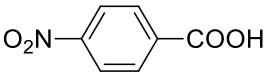
9	Picric acid	PA	229.11	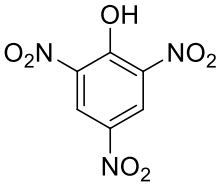
10	1-chloro-2,4-dinitrobenzene	CDNB	202.55	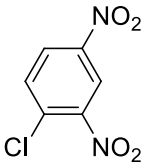
11	Benzaldehyde	BZA	106.12	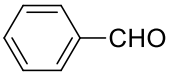
12	Toluene	T	92.14	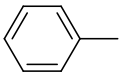
13	Aniline	A	93.14	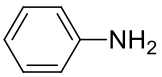
14	Benzoic acid	BA	122.12	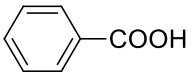

Here, the change in the luminescence intensity of PD-CND is monitored in presence of these analytes at an excitation of 440 nm. The concentration of all the analytes were fixed at 1 mM. Interestingly, the luminescence of the carbon nanodots decreased gradually with increasing concentration of picric acid (**Figure 4.15 (a)**). The corresponding changes in luminescence under UV light exposure are depicted in **Figure 4.15(b)**.

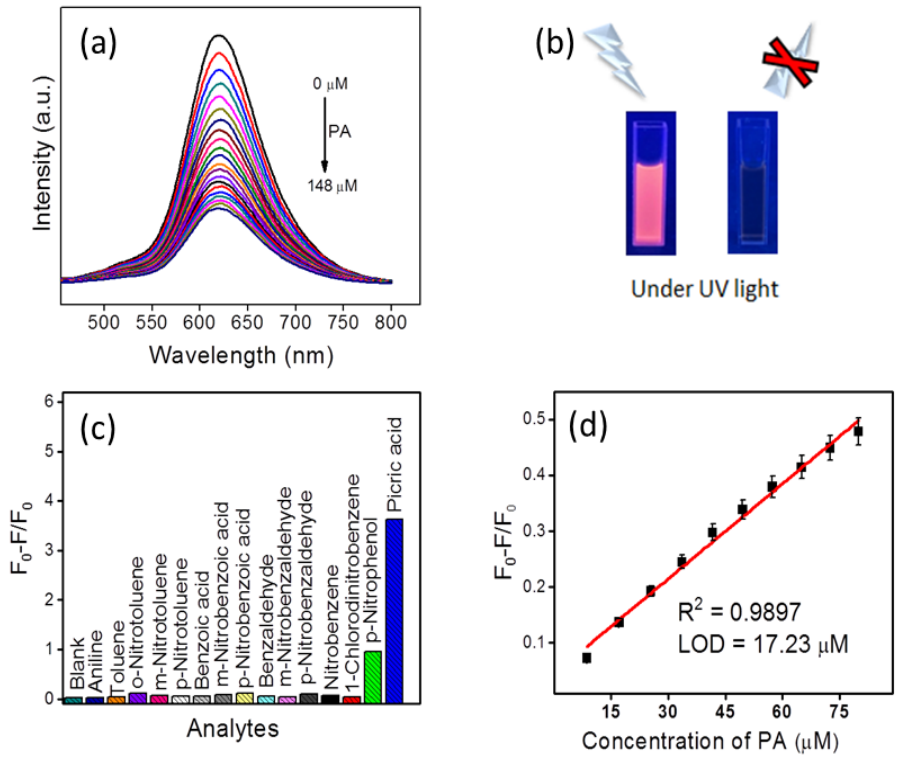

Figure 4.15(a) Photoluminescence spectrum of PD-CND after the addition of PA, (b) Quenching of the luminescence visualized under UV light exposure, (c) selectivity of PD-CNDs for PA, (d) Stern-Volmer plot of relative fluorescence quenching as a function of concentration of PA.

Selectivity was examined by monitoring the change in fluorescence intensity of PD-CNDs upon the addition of 20 μL of the analytes. The bar diagram in **Figure 4.15(c)** shows that maximum luminescence quenching occurs in the aqueous dispersion of PD-CNDs in the presence of PA. When plotting the relative fluorescence quenching efficiency as a function of the analyte concentration, good linearity is observed at lower concentrations (**Figure 4.15(d)**). This Stern-Volmer plot exhibit good linearity in the concentration range 10-75 μM and the limit of detection (LOD) was estimated to be 17.68 μM, calculated using the equation LOD = 3 σ /m, where σ is the standard deviation of the blank sample and 'm' is the slope of the calibration curve.

4.6.4 Possible quenching mechanism

The next step is to identify the mechanism behind the significant fluorescence quenching of PD-CNDs in aqueous dispersion upon the addition of the analyte picric acid (PA). Typically, luminescence quenching occurs through various processes such as: (a) electrostatic interaction or electron transfer, (b) resonance energy transfer, or (c) inner filter effect (IFE). Picric acid (PA) acts as a strong protonic acid in aqueous solution due to the presence of three electron-withdrawing nitro groups on the benzene ring. According to Niu *et al.*, the interaction between electron-rich functional groups on the carbon nanodots and the picric acid moiety involves the formation of a picrate-carbon nanodot-NH_3^+ ion pair through strong electrostatic interactions

leading to the quenching of luminescence [140]. Another report also substantiates the electrostatic interaction between carbon nanodots and nitroaromatic compounds [141]. In this case, there is a possibility for such interactions. To investigate the possibility of complex formation, the UV-visible absorption spectrum of the aqueous solution of PD-CNDs was recorded with and without PA of various concentrations (**Figure 4.16(a)**).

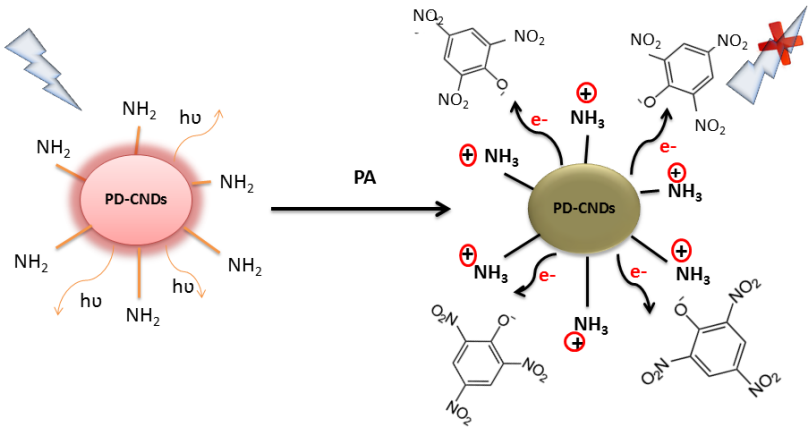

Scheme 4.1 Interaction between PA and PD-CNDs

Upon adding the analyte, an absorption peak appears around 355 nm, which is likely corresponding to the analyte itself, along with slight variations in other peaks. These results suggest that the analyte may form a non- fluorescent complex, such as a Meisenheimer complex, with the electron-rich surface functional groups on PD-CNDs, leading to fluorescence quenching [142, 143]. The possible electrostatic interaction and the proposed structure of the non-fluorescent complex are illustrated in **Scheme 4.1 and 4.2**

Fluorescence lifetime measurements of PD-CNDs with and without PA were performed using the time-correlated single photon counting technique (TCSPC). The corresponding decay curve is shown in **Figure 4.16(b)**. It was noted that the average lifetime remained almost the same in the absence and presence of the analyte, ruling out the possibility of FRET. Meanwhile, the excitation spectrum of PD-CNDs was scanned, revealing a large spectral overlap with the PA absorption band (**Figure 4.16(c)**), indicating a possibility for IFE. It also seen that these type of overlap is nil/minimum for other compounds selected, which supports the selectivity towards PA. Therefore, the quenching

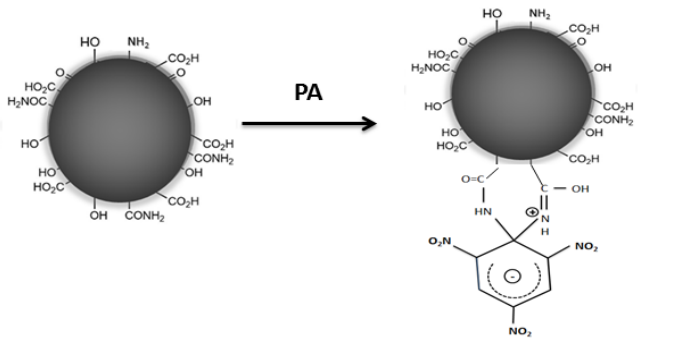

Scheme 4.2 Proposed structure for the non-fluorescent complex.

process of PD-CNDs caused by PA is presumably dominated by mechanisms such as electrostatic interaction, electron transfer, and IFE.

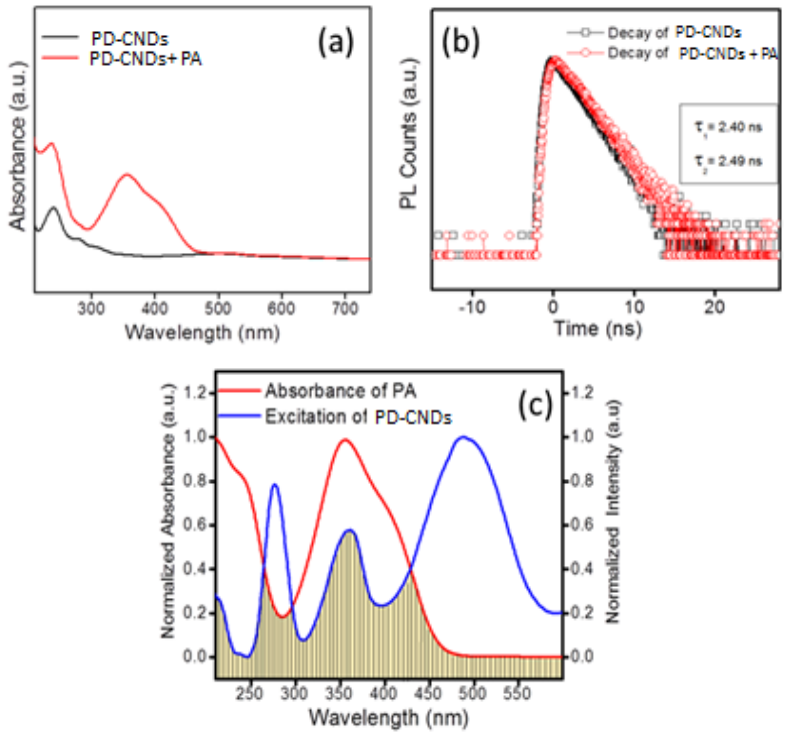

Figure 4.16 (a) UV-visible spectra of PD-CNDs with and without PA, (b) fluorescence lifetime decay curves, (c) combination of the excitation spectrum of PD-CNDs and absorbance of PA.

4.7. Theoretical studies to probe the selective sensing

4.7.1. Frontier molecular orbital analysis

The details regarding the Frontier molecular orbital (FMO) analysis are given in Chapter 2 section 2.4.4.1. HOMO and LUMO have been obtained from the Gaussian output file of FMO analysis and were analyzed to predict the pathway of electron transfer in the studied system. The optimized structure of nitroaromatics

along with their HOMO-LUMO energies in eV depicted in **Table 4.2**.

Table 4.2 Optimized structure of selected nitroaromatics with HOMO and LUMO energies in eV

Compound	HOMO	LUMO
 *o*-NT	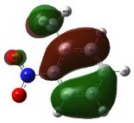 -7.5562	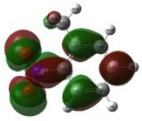 -2.7563
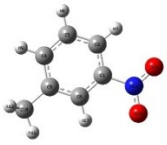 *m*-NT	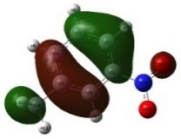 -7.5507	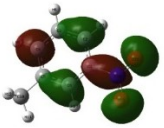 -2.8434
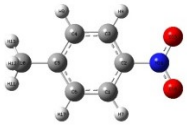 *p*-NT	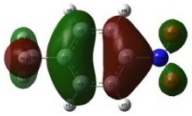 -7.6541	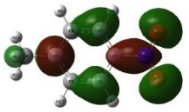 -2.7917
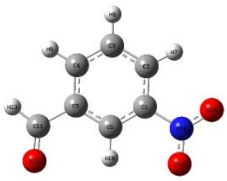 *m*-NBZA	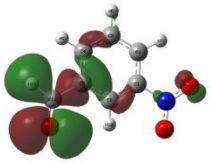 -7.8664	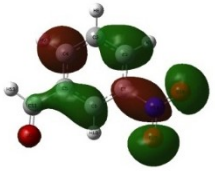 -3.2189
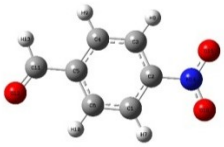	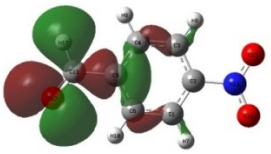 -7.9371	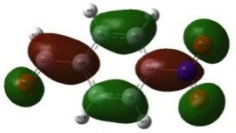 -3.5672

p-NBZA		
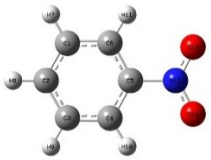 NB	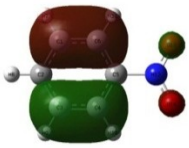 -7.8963	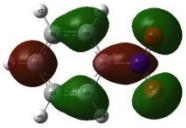 -2.9223
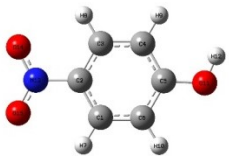 *p*-NP	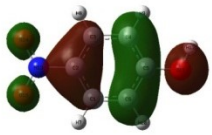 -7.2950	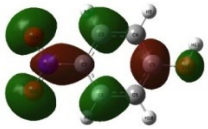 -2.7454
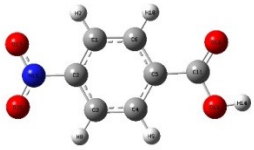 *p*-NBA	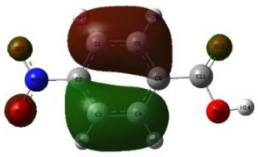 -8.2010	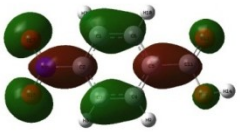 -3.3985
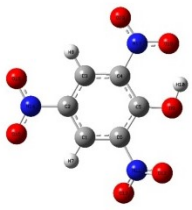 PA	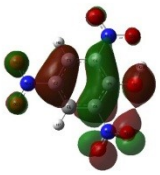 -8.5929	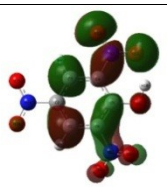 -4.3399
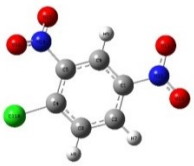 CDBA	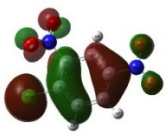 -8.4242	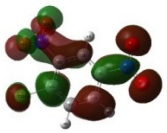 -3.6679

The E_{HOMO} and E_{LUMO} of CNDs can be determined with the help of Cyclic Voltametry measurements [144, 145]. **Figure 4.17** represents the cyclic voltammogram of PD-CNDs. The HOMO and LUMO energy levels of PD-CNDs could be estimated according to the empirical formula:

$$E_{HOMO} = -e(E_{ox}+4.4) \quad (1)$$

$$E_{LUMO} = -e(E\text{red}+4.4) \quad (2)$$

Where E_{ox} and E_{red} are the onset of oxidation and reduction potential for PD-CNDs respectively. The E_{red} was determined to be -0.21 V. The corresponding E_{LUMO} was calculated to be -4.19 eV. To determine the HOMO levels, we combined the E_{red} with the optical energy band gap (E_g, resulting from the absorption edge in the absorption spectrum):

$$E_{HOMO} = E_{LUMO} - E_g \quad (3)$$

E_g was estimated to be 2.41 eV. So, the E_{HOMO} was calculated to be -6.60 eV. Comparing these values with those of nitroaromatics, it has been confirmed that LUMO of picric acid is the only one which is lower than the LUMO of CNDs. So as per the principle, an oxidative pathway can be possible here and which is not possible for other. These results are in good agreement with the experimental results which also shows preferential sensing of picric acid by CNDs than the rest of the studied compounds. In the experimental result, p-NP is the one which is being sensed by

CNDs next to picric acid, but the sensing effect is lower than that with picric acid. Examination of the energy values of MOs of p-NP makes clear that its LUMO is more energetic than that of CNDs which in turn prevents the oxidative pathway. Then comparing the HOMO energy values, there may be a chance of transferring electron from the HOMO of p-NP to the HOMO of CNDs. Thus, there is a chance of reductive pathway of electron transfer and which may be the reason for its sensing. All other compounds could not be sensed by CNDs or there is no significant quenching.

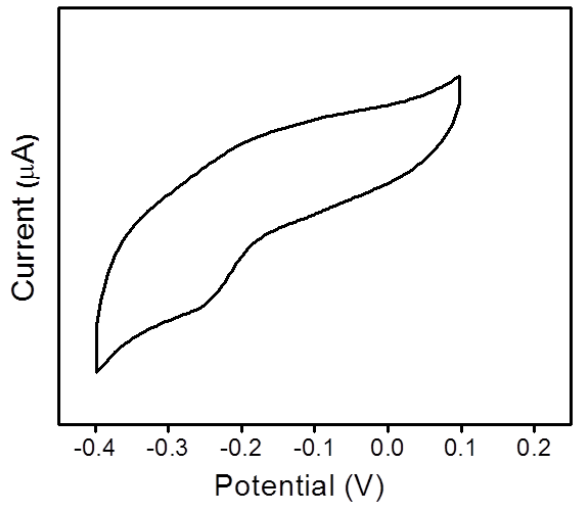

Figure 4.17 Cyclic voltammograme of PD-CNDs

4.7.2. Global descriptive parameters and Donor Acceptor Map

The utility of global descriptive parameters of a molecule open up a way to get the relation between the chemical reactivity of a molecule and its sensitiveness to structural

perturbations and responses to the changes in external conditions. The detailed description of the global descriptive parameters and donor acceptor map (DAM) given in Chapter 2 (section 2.4.4.2) including the reference DAM. Donor Acceptor Map is a plot which simultaneously shows the electron acceptance and electron donating power of studied molecules. The global reactive descriptors of the selected nitroaromatic compounds are tabulated in **Table 4.3.**

Table 4.3 Global reactive descriptors of nitroaromatics in eV

No	Name	IP	EA	η	S	χ	μ	ω	Ra	Rd
1	o-NT	9.31	1.10	4.10	0.12	5.21	-5.21	3.30	0.83	0.85
2	m-NT	9.34	1.17	4.08	0.12	5.25	-5.25	3.38	0.86	0.85
3	p-NT	9.32	1.12	4.10	0.12	5.22	-5.22	3.32	0.84	0.85
4	m-NBZA	9.89	1.60	4.14	0.12	5.74	-5.74	3.98	1.14	0.99
5	p-NBZA	9.88	2.03	3.92	0.12	5.96	-5.96	4.52	1.28	0.96
6	NB	9.83	1.20	4.31	0.11	5.52	-5.52	3.53	1	1
7	p-NP	9.06	1.05	4.00	0.12	5.05	-5.05	3.19	0.76	0.78
8	p-NBA	9.85	1.88	3.98	0.12	5.87	-5.87	4.32	1.22	0.96
9	PA	10.12	2.97	3.57	0.13	6.54	-6.54	5.99	1.65	0.97
10	CDNB	10.02	2.16	3.93	0.12	6.09	-6.09	4.72	1.37	1.00

The corresponding DAM is shown in **Figure 4.18**. Here nitrobenzene (NB) has been taken as a reference/parent compound with which the reactivity was being compared. In DAM there are four quadrants: I, II, III and IV. Our compounds lie in I, III and IV which respectively denotes good electron acceptor, good electron donor and good electron donor/acceptor (depending upon the situation they may either accept or donate electrons). CDNB is the only one showing electron accepting capacity whereas o-NT, m-NT, p-NT and p-NP show electron donating capacity, all others except nitrobenzene show dual character. The 'S' value shows that all are reactive than the reference compound nitrobenzene. The presence of chlorine makes compound CDNB more electron acceptor. In the other hand, the -CH_3 group makes the compounds o-NT, m-NT and p-NT good electron donors. Similarly -OH group in PA makes it a good donor.

The theoretical findings align well with the experimental results. There are only a few reports on nitroaromatic compound sensing that combine both theoretical and experimental outcomes in a single study, making this work particularly noteworthy.

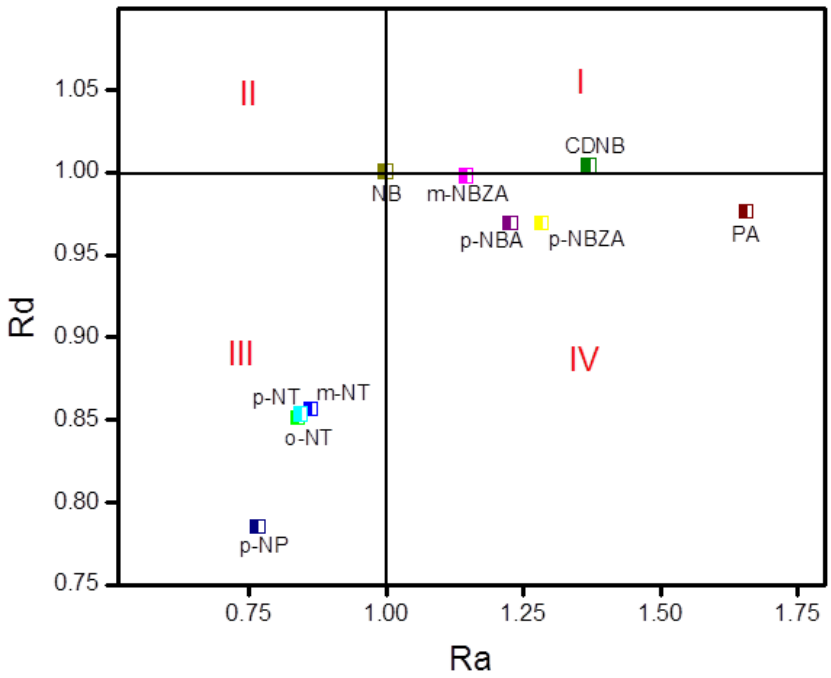

Figure 4.18 DAM of selected nitroaromatics

4.8. Conclusions

In summary, the study introduces fluorescent N-doped carbon nanodots (PD-CNDs) synthesized from p-phenylenediamine for the rapid visual detection and quantification of Cu (II) ions. PD-CNDs exhibit orange-red luminescence under UV light, which is quenched upon the introduction of cupric ions. Visual detection of Cu (II) ions is achieved through the formation of a black precipitate attributed to the complex PD-CNDs@Cu. The system demonstrates high selectivity for Cu (II) ions, even in the presence of other metal ions. Detection is extended to a solid-state using PD-CNDs-coated filter paper strips, enabling easy visual

detection of copper ions. The complex formation is supported by FE-SEM, XRD, FT-IR, and Raman spectroscopy. The quantification of Cu (II) ions by fluorimetric analysis shows a linear response at lower concentrations. The study suggests a static quenching mechanism through complex formation between PD-CNDs and Cu (II) ions, supported by fluorescence lifetime analysis and UV-visible absorption studies, ruling out dynamic quenching and inner filter effects. The observed blue shift in the π-π* transition of PD-CNDs upon Cu (II) ion addition further elucidates the quenching process. Hence, the presented fluorescent N-doped carbon nanodots offer a promising platform for the rapid and selective visual detection of Cu(II) ions, with potential applications in environmental monitoring and water quality assessment.

p-Phenylenediamine derived carbon nanodots (PD-CNDs) also serve as effective sensor for picric acid (PA). The orange-red luminescence of PD-CNDs diminishes in the presence of PA, enabling fluorimetric detection of PA at micromolar concentrations. The investigation explores the sensing mechanism, indicating that fluorescence quenching is due to electrostatic interaction, electron transfer, and inner filter effect (IFE). Theoretical studies further corroborate these findings.

References

1. Putro, P.A., et al., *A Bibliometric Analysis of Carbon Dots in Sensors Application.* Jurnal Penelitian Fisika dan Aplikasinya (JPFA), 2022. **12**(2): p. 138-155.

2. Junaid, H.M., A.R. Solangi, and M. Batool, *Carbon dots as naked eye sensors.* Analyst, 2021. **146**(8): p. 2463-2474.

3. Huang, G., et al., *Carbon dots based multicolor fluorescence sensor for ratiometric and colorimetric dual-model detection of Cu^{2+}.* Dyes and Pigments, 2022. **203**: p. 110381.

4. Lin, X., et al., *Carbon dots based on natural resources: Synthesis and applications in sensors.* Microchemical Journal, 2021. **160**: p. 105604.

5. Li, X., et al., *Carbon dot-based fluorescent and colorimetric sensor for sensitive and selective visual detection of benzoyl peroxide.* Chinese Chemical Letters, 2022. **33**(3): p. 1632-1636.

6. Huang, Q., et al., *Graphene quantum dots/multiwalled carbon nanotubes composite-based electrochemical sensor for detecting dopamine release from living cells.* ACS sustainable chemistry & engineering, 2020. **8**(3): p. 1644-1650.

7. Huang, Q., et al., *Pd-Au@ carbon dots nanocomposite: Facile synthesis and application as an ultrasensitive electrochemical biosensor for determination of colitoxin DNA in human serum.* Biosensors and Bioelectronics, 2017. **94**: p. 507-512.

8. Bilal, S., et al., *Assessment of pesticide induced inhibition of Apis mellifera (honeybee) acetylcholinesterase by means of N-doped carbon dots/BSA nanocomposite modified electrochemical biosensor.* Bioelectrochemistry, 2022. **144**: p. 107999.

9. Abbasi, A. and M. Shakir, *Simple one-step solid-state synthesis of highly crystalline N doped carbon dots as selective turn off-sensor for picric acid and metanil yellow.* Journal of Fluorescence, 2022. **32**(3): p. 1239-1246.

10. Huang, Q., et al., *High quantum yield nitrogen-doped carbon dots: green synthesis and application as "off-on" fluorescent sensors for*

the determination of Fe^{3+} and adenosine triphosphate in biological samples. Sensors and Actuators B: Chemical, 2018. **276**: p. 82-88.

11. da Silva, J.C.E. and H.M. Gonçalves, *Analytical and bioanalytical applications of carbon dots.* TrAC Trends in Analytical Chemistry, 2011. **30**(8): p. 1327-1336.

12. Zhu, S., et al., *Highly photoluminescent carbon dots for multicolor patterning, sensors, and bioimaging.* Angewandte Chemie International Edition, 2013. **52**(14): p. 3953-3957.

13. Qu, Z.-b., et al., *Boronic acid functionalized graphene quantum dots as a fluorescent probe for selective and sensitive glucose determination in microdialysate.* Chemical communications, 2013. **49**(84): p. 9830-9832.

14. Mohapatra, S., et al., *Design of Fe_3O_4@ SiO_2@ carbon quantum dot based nanostructure for fluorescence sensing, magnetic separation, and live cell imaging of fluoride ion.* Langmuir, 2015. **31**(29): p. 8111-8120.

15. Wang, Q., et al., *Microwave-assisted synthesis of carbon nanodots through an eggshell membrane and their fluorescent application.* Analyst, 2012. **137**(22): p. 5392-5397.

16. Raveendran, V., C. Anjali, and R.N. Kizhakayil, *Fe^{3+}-induced luminescence quenching in carbon dots–mechanism unveiled.* Analytical Methods, 2024. **16**(15): p. 2349-2358.

17. Wang, Z., et al., *Fluorescence sensor array based on amino acid derived carbon dots for pattern-based detection of toxic metal ions.* Sensors and Actuators B: Chemical, 2017. **241**: p. 1324-1330.

18. Zhao, J., et al., *Unique approach to develop carbon dot-based nanohybrid near-infrared ratiometric fluorescent sensor for the detection of mercury ions.* Analytical chemistry, 2017. **89**(15): p. 8044-8049.

19. Wang, W., et al., *Carbon dots functionalized by organosilane with double-sided anchoring for nanomolar Hg^{2+} detection.* Journal of colloid and interface science, 2015. **437**: p. 28-34.

20. Hua, J., et al., *Highly fluorescent carbon quantum dots as nanoprobes for sensitive and selective determination of mercury*

(II) in surface waters. Spectrochimica Acta Part A: Molecular and Biomolecular Spectroscopy, 2017. **187**: p. 149-155.

21. He, J.H., et al., *Functional preserving carbon dots-based fluorescent probe for mercury (II) ions sensing in herbal medicines via coordination and electron transfer.* Analytica Chimica Acta, 2018. **1035**: p. 203-210.

22. Chandra, S., et al., *Sulphur and nitrogen doped carbon dots: A facile synthetic strategy for multicolour bioimaging, tiopronin sensing, and Hg^{2+} ion detection.* Nano-Structures & Nano-Objects, 2017. **12**: p. 10-18.

23. Dang, D.K., et al., *One pot solid-state synthesis of highly fluorescent N and S co-doped carbon dots and its use as fluorescent probe for Ag^{+} detection in aqueous solution.* Sensors and Actuators B: Chemical, 2018. **255**: p. 3284-3291.

24. Liao, S., et al., *Novel S, N-doped carbon quantum dot-based" off-on" fluorescent sensor for silver ion and cysteine.* Talanta, 2018. **180**: p. 300-308.

25. Bian, S., et al., *Facile synthesis of sulfur-doped graphene quantum dots as fluorescent sensing probes for Ag^{+} ions detection.* Sensors and Actuators B: Chemical, 2017. **242**: p. 231-237.

26. Cayuela, A., et al., *Fluorescent carbon quantum dot hydrogels for direct determination of silver ions.* Talanta, 2016. **151**: p. 100-105.

27. Gao, W., et al., *Carbon dots with red emission for sensing of Pt^{2+}, Au^{3+}, and Pd^{2+} and their bioapplications in vitro and in vivo.* ACS applied materials & interfaces, 2018. **10**(1): p. 1147-1154.

28. Liao, J., Z. Cheng, and L. Zhou, *Nitrogen-doping enhanced fluorescent carbon dots: green synthesis and their applications for bioimaging and label-free detection of Au3+ ions.* ACS Sustainable Chemistry & Engineering, 2016. **4**(6): p. 3053-3061.

29. Gaddam, R.R., et al., *Facile synthesis of carbon dot and residual carbon nanobeads: Implications for ion sensing, medicinal and biological applications.* Materials Science and Engineering: C, 2017. **73**: p. 643-652.

30. Chen, Y., et al., *Regulating the overlap between the absorption spectrum of metal ion-chromogenic agent and the emission*

spectrum of carbon-based dots to improve the sensing performance for metal ions. Sensors and Actuators B: Chemical, 2017. **242**: p. 1210-1215.

31. Ma, Y., et al., *A dual-emissive fluorescent sensor fabricated by encapsulating quantum dots and carbon dots into metal–organic frameworks for the ratiometric detection of Cu^{2+} in tap water.* Journal of Materials Chemistry C, 2017. **5**(33): p. 8566-8571.

32. Gui, R., et al., *Ions-induced two-photon fluorescence dual-switching for reversible and simultaneous sensing of Cu^{2+} and Hg^{2+} based on dual-emitting carbon dot/carbon dot conjugates.* Sensors and Actuators B: Chemical, 2017. **100**(245): p. 386-394.

33. Gedda, G., et al., *Green synthesis of carbon dots from prawn shells for highly selective and sensitive detection of copper ions.* Sensors and Actuators B: Chemical, 2016. **224**: p. 396-403.

34. Singh, V., et al., *Sensitive and selective detection of copper ions using low cost nitrogen doped carbon quantum dots as a fluorescent sensing plateform.* ISSS Journal of Micro and Smart Systems, 2017. **6**: p. 109-117.

35. Mohammed, L.J. and K.M. Omer, *Dual functional highly luminescence B, N Co-doped carbon nanodots as nanothermometer and Fe^{3+}/Fe^{2+} sensor.* Scientific reports, 2020. **10**(1): p. 3028.

36. Wang, Y., Q. Chang, and S. Hu, *Carbon dots with concentration-tunable multicolored photoluminescence for simultaneous detection of Fe^{3+} and Cu^{2+} ions.* Sensors and Actuators B: Chemical, 2017. **253**: p. 928-933.

37. Pang, S. and S. Liu, *Dual-emission carbon dots for ratiometric detection of Fe^{3+} ions and acid phosphatase.* Analytica Chimica Acta, 2020. **1105**: p. 155-161.

38. Gong, X., et al., *An "on-off-on" fluorescent nanoprobe for recognition of chromium (VI) and ascorbic acid based on phosphorus/nitrogen dual-doped carbon quantum dot.* Analytica Chimica Acta, 2017. **968**: p. 85-96.

39. Xiao, D., et al., *Porous carbon quantum dots: one step green synthesis via L-cysteine and applications in metal ion detection.* RSC advances, 2015. **5**(3): p. 2039-2046.

40. Fang, L., et al., *Ammonium citrate derived carbon quantum dot as on-off-on fluorescent sensor for detection of chromium (VI) and sulfites.* Materials Letters, 2017. **191**: p. 1-4.

41. Kumar, V.V., T. Raman, and S.P. Anthony, *Fluorescent carbon quantum dots chemosensor for selective turn-on sensing of Zn^{2+} and turn-off sensing of Pb^{2+} in aqueous medium and zebrafish eggs.* New Journal of Chemistry, 2017. **41**(24): p. 15157-15164.

42. Kumar, A., et al., *Green synthesis of carbon dots from Ocimum sanctum for effective fluorescent sensing of Pb^{2+} ions and live cell imaging.* Sensors and Actuators B: Chemical, 2017. **242**: p. 679-686.

43. Zhang, W., et al., *Te-containing carbon dots for fluorescence imaging of superoxide anion in mice during acute strenuous exercise or emotional changes.* Chemical Science, 2018. **9**(3): p. 721-727.

44. Du, F., et al., *Carbon dots-based fluorescent probes for sensitive and selective detection of iodide.* Microchimica Acta, 2013. **180**: p. 453-460.

45. Dong, Y., et al., *"Turn-on" fluorescent detection of cyanide based on polyamine-functionalized carbon quantum dots.* RSC Advances, 2014. **4**(8): p. 3701-3705.

46. Barati, A., M. Shamsipur, and H. Abdollahi, *Metal-ion-mediated fluorescent carbon dots for indirect detection of sulfide ions.* Sensors and Actuators B: Chemical, 2016. **230**: p. 289-297.

47. Chen, B.B., et al., *Highly selective detection of phosphate ion based on a single-layered graphene quantum dots-Al^{3+} strategy.* Talanta, 2018. **178**: p. 172-177.

48. Chai, L.J., et al., *A reversible fluorescence nanoswitch based on carbon quantum dots nanoassembly for detection of pyrophosphate ion.* Sensors and Actuators B: Chemical, 2015. **220**: p. 138-145.

49. Buiculescu, R., et al., *Controlling carbon nanodot fluorescence for optical biosensing.* Analyst, 2016. **141**(13): p. 4170-4180.

50. Kong, W., et al., *A facile carbon dots based fluorescent probe for ultrasensitive detection of ascorbic acid in biological fluids via non-oxidation reduction strategy.* Talanta, 2017. **165**: p. 677-684.

51. Xie, Z., et al., *Ionic liquid-functionalized carbon quantum dots as fluorescent probes for sensitive and selective detection of iron ion and ascorbic acid.* Colloids and Surfaces A: Physicochemical and Engineering Aspects, 2017. **529**: p. 38-44.

52. Gopal, R., et al., *Aggregation-Induced White Light Emission and Solvent-Induced Dual Mode Multi-Analyte Sensing by Highly Crystalline Single Component Derived N, S Co-Doped Carbon Nanodots.* ACS Applied Optical Materials, 2023. **1**(3): p. 701-714.

53. Wang, M., et al., *Nitrogen-doped carbon quantum dots as a fluorescence probe combined with magnetic solid-phase extraction purification for analysis of folic acid in human serum.* Analytical and bioanalytical chemistry, 2017. **409**: p. 7063-7075.

54. Freire, R., et al., *NH_2-rich Carbon Quantum Dots: A protein-responsive probe for detection and identification.* Sensors and Actuators B: Chemical, 2018. **255**: p. 2725-2732.

55. Huang, S., et al., *A ratiometric nanosensor based on fluorescent carbon dots for label-free and highly selective recognition of DNA.* RSC Advances, 2015. **5**(55): p. 44587-44597.

56. Sun, Q., et al., *Fluorometric detection of cholesterol based on β-cyclodextrin functionalized carbon quantum dots via competitive host-guest recognition.* Talanta, 2017. **167**: p. 513-519.

57. Sun, L., et al., *Fluorescence detection of cholesterol using a nitrogen-doped graphene quantum dot/chromium picolinate complex-based sensor.* Journal of materials chemistry B, 2017. **5**(45): p. 9006-9014.

58. Ran, X., et al., *Water-soluble pillar [6] arene functionalized nitrogen-doped carbon quantum dots with excellent supramolecular recognition capability and superior electrochemical sensing performance towards TNT.* Sensors and Actuators B: Chemical, 2018. **257**: p. 362-371.

59. Liang, Q., et al., *A facile microwave-hydrothermal synthesis of fluorescent carbon quantum dots from bamboo tar and their application.* Analytical methods, 2017. **9**(24): p. 3675-3681.

60. Niu, J. and H. Gao, *Synthesis and drug detection performance of nitrogen-doped carbon dots.* Journal of luminescence, 2014. **149**: p. 159-162.

61. Lin, M., et al., *An inner filter effect based sensor of tetracycline hydrochloride as developed by loading photoluminescent carbon nanodots in the electrospun nanofibers.* Nanoscale, 2016. **8**(5): p. 2999-3007.

62. Yang, J., et al., *Detection of trace tetracycline in fish via synchronous fluorescence quenching with carbon quantum dots coated with molecularly imprinted silica.* Spectrochimica Acta Part A: Molecular and Biomolecular Spectroscopy, 2018. **190**: p. 450-456.

63. Liu, M.L., et al., *One-pot carbonization synthesis of europium-doped carbon quantum dots for highly selective detection of tetracycline.* Methods and Applications in Fluorescence, 2017. **5**(1): p. 015003.

64. Tian, T., et al., *One-pot synthesis of boron and nitrogen co-doped carbon dots as the fluorescence probe for dopamine based on the redox reaction between Cr (VI) and dopamine.* Sensors and Actuators B: Chemical, 2017. **240**: p. 1265-1271.

65. Kalaiyarasan, G. and J. Joseph, *Determination of vitamin B_{12} via pH-dependent quenching of the fluorescence of nitrogen doped carbon quantum dots.* Microchimica Acta, 2017. **184**: p. 3883-3891.

66. Li, J., et al., *A photoluminescence "switch-on" nanosensor composed of nitrogen and sulphur co-doped carbon dots and gold nanoparticles for discriminative detection of glutathione.* Analyst, 2018. **143**(9): p. 2083-2089.

67. Song, W., et al., *Ratiometric detection of intracellular lysine and pH with one-pot synthesized dual emissive carbon dots.* Analytical chemistry, 2017. **89**(24): p. 13626-13633.

68. Zhu, X., et al., *Nitrogen-doped carbon nanoparticle modulated turn-on fluorescent probes for histidine detection and its imaging in living cells.* Nanoscale, 2016. **8**(4): p. 2205-2211.

69. Zhu, P., et al., *Nitrogen, sulfur co-doped red carbon dots for sensitive and selective detection of Sn_{2+} ions.* Optical Materials, 2021. **121**: p. 111543.

70. Ludmerczki, R., et al., *Fluorescence-based selective nitrite ion sensing by amino-capped carbon dots.* Environmental Nanotechnology, Monitoring & Management, 2021. **16**: p. 100573.

71. Huo, X., et al., *Facile synthesis of yellowish-green emitting carbon quantum dots and their applications for phoxim sensing and cellular imaging.* Analytica Chimica Acta, 2022. **1206**: p. 338685.

72. Xia, J., Y.-L. Yu, and J.-H. Wang, *Fe^{3+}-Catalyzed low-temperature preparation of multicolor carbon polymer dots with the capability of distinguishing D_2O from H_2O.* Chemical communications, 2019. **55**(83): p. 12467-12470.

73. Yue, J., et al., *Superoxide anion turns on the fluorescence of carbon dots-ferric complex for sensing.* Microchemical Journal, 2021. **168**: p. 106412.

74. Zu, F., et al., *The quenching of the fluorescence of carbon dots: a review on mechanisms and applications.* Microchimica Acta, 2017. **184**: p. 1899-1914.

75. Lakowicz, J.R., *Principles of fluorescence spectroscopy*. 2006: Springer.

76. Misra, G., *Fluorescence spectroscopy*, in *Data Processing Handbook for Complex Biological Data Sources*. 2019, Elsevier. p. 31-37.

77. Miao, S., K. Liang, and B. Kong, *Förster resonance energy transfer (FRET) paired carbon dot-based complex nanoprobes: versatile platforms for sensing and imaging applications.* Materials Chemistry Frontiers, 2020. **4**(1): p. 128-139.

78. Kavarnos, G.J., *Fundamental concepts of photoinduced electron transfer*, in *Photoinduced electron transfer I*. 2005, Springer. p. 21-58.

79. Panigrahi, S.K. and A.K. Mishra, *Inner filter effect in fluorescence spectroscopy: As a problem and as a solution.* Journal of Photochemistry and Photobiology C: Photochemistry Reviews, 2019. **41**: p. 100318.

80. Krupanidhi, S., A. Sreekumar, and C. Sanjeevi, *Copper & biological health.* Indian Journal of Medical Research, 2008. **128**(4): p. 448-461.

81. Kelkar, P., S. Chang, and S.A. Muley, *Response to oral supplementation in copper deficiency myeloneuropathy.* Journal of Clinical Neuromuscular Disease, 2008. **10**(1): p. 1-3.

82. Gaetke, L.M. and C.K. Chow, *Copper toxicity, oxidative stress, and antioxidant nutrients.* Toxicology, 2003. **189**(1-2): p. 147-163.

83. Karakuş, E., *A rhodamine based fluorescent chemodosimeter for the selective and sensitive detection of copper (II) ions in aqueous media and living cells.* Journal of Molecular Structure, 2021. **1224**: p. 129037.

84. Kumar, V., et al., *Relationship of antioxidant and oxidative stress markers in different organs following copper toxicity in a rat model.* Toxicology and Applied Pharmacology, 2016. **293**: p. 37-43.

85. Yu, J., et al., *Fabrication of the Ni-based composite wires for electrochemical detection of copper (Ⅱ) ions.* Analytica Chimica Acta, 2021. **1143**: p. 45-52.

86. Stern, B.R., *Essentiality and toxicity in copper health risk assessment: overview, update and regulatory considerations.* Journal of Toxicology and Environmental Health, Part A, 2010. **73**(2-3): p. 114-127.

87. Barnham, K.J., C.L. Masters, and A.I. Bush, *Neurodegenerative diseases and oxidative stress.* Nature reviews Drug discovery, 2004. **3**(3): p. 205-214.

88. Viles, J.H., *Metal ions and amyloid fiber formation in neurodegenerative diseases. Copper, zinc and iron in Alzheimer's, Parkinson's and prion diseases.* Coordination Chemistry Reviews, 2012. **256**(19-20): p. 2271-2284.

89. Madsen, E. and J.D. Gitlin, *Copper and iron disorders of the brain.* Annu. Rev. Neurosci., 2007. **30**: p. 317-337.

90. Lee, J.C., H.B. Gray, and J.R. Winkler, *Copper (II) binding to α-synuclein, the Parkinson's protein.* Journal of the American Chemical Society, 2008. **130**(22): p. 6898-6899.

91. Hung, Y.H., A.I. Bush, and R.A. Cherny, *Copper in the brain and Alzheimer's disease.* JBIC Journal of Biological Inorganic Chemistry, 2010. **15**: p. 61-76.

92. Fawell, J.K., *Drinking water quality and health.* 2013.

93. Sai, L., et al., *Protein-derived carbon nanodots with an ethylenediamine-modulated structure as sensitive fluorescent probes for Cu^{2+} detection.* RSC advances, 2017. **7**(27): p. 16608-16615.

94. Liu, S., et al., *Hydrothermal treatment of grass: a low-cost, green route to nitrogen-doped, carbon-rich, photoluminescent polymer nanodots as an effective fluorescent sensing platform for label-free detection of Cu (II) ions.* Advanced materials, 2012. **24**(15): p. 2037.

95. Ganiga, M. and J. Cyriac, *Understanding the Photoluminescence Mechanism of Nitrogen-Doped Carbon Dots by Selective Interaction with Copper Ions.* ChemPhysChem, 2016. **17**(15): p. 2315-2321.

96. Dong, Y., et al., *Polyamine-functionalized carbon quantum dots as fluorescent probes for selective and sensitive detection of copper ions.* Analytical chemistry, 2012. **84**(14): p. 6220-6224.

97. Zong, J., et al., *Carbon dots as fluorescent probes for "off–on" detection of Cu^{2+} and l-cysteine in aqueous solution.* Biosensors and Bioelectronics, 2014. **51**: p. 330-335.

98. Zhu, A., et al., *Carbon-dot-based dual-emission nanohybrid produces a ratiometric fluorescent sensor for in vivo imaging of cellular copper ions.* Angewandte Chemie (International ed. in English), 2012. **51**(29): p. 7185-7189.

99. Huang, S.-W., et al., *Synthesis of fluorescent carbon dots as selective and sensitive probes for cupric ions and cell imaging.* Molecules, 2019. **24**(9): p. 1785.

100. Li, Y., et al., *Nitrogen-doped carbon dots derived from electrospun carbon nanofibers for Cu (ii) ion sensing.* New Journal of Chemistry, 2019. **43**(4): p. 1812-1817.

101. Liu, J. and Y. Lu, *A DNAzyme catalytic beacon sensor for paramagnetic Cu^{2+} ions in aqueous solution with high sensitivity and selectivity.* Journal of the American Chemical Society, 2007. **129**(32): p. 9838-9839.

102. Zheng, X., et al., *Improved electrochemical property of copper nitrate hydrate by multi-wall carbon nanotube.* Electrochimica Acta, 2014. **147**: p. 765-772.

103. Pereira, D.C., D.L.A.d. Faria, and V.R. Constantino, *CuII hydroxy salts: characterization of layered compounds by vibrational spectroscopy.* Journal of the Brazilian Chemical Society, 2006. **17**: p. 1651-1657.

104. Videira-Quintela, D., et al., *Silver, copper, and copper hydroxy salt decorated fumed silica hybrid composites as antibacterial agents.* Colloids and Surfaces B: Biointerfaces, 2020. **195**: p. 111216.

105. Santos, X., et al., *Capability of Copper Hydroxy Nitrate ($Cu_2(OH)_3NO_3$) as an Additive to Develop Antibacterial Polymer Contact Surfaces: Potential for Food Packaging Applications.* Polymers, 2023. **15**(7): p. 1661.

106. Henrist, C., et al., *Study of the morphology of copper hydroxynitrate nanoplatelets obtained by controlled double jet precipitation and urea hydrolysis.* Journal of crystal growth, 2003. **254**(1-2): p. 176-187.

107. Güner, E.K. and A.K. Özer, *SYNTHESIS AND CHARACTERIZATION OF COPPER HYDROXYNITRATE BY HYDROTHERMAL METHOD.* Journal of the Turkish Chemical Society Section B: Chemical Engineering, 2017. **1**(1): p. 183-192.

108. Arora, P.K., et al., *Metabolism of 4-chloro-2-nitrophenol in a Gram-positive bacterium, Exiguobacterium sp. PMA.* Microbial Cell Factories, 2012. **11**: p. 1-10.

109. Ju, K.-S. and R.E. Parales, *Nitroaromatic compounds, from synthesis to biodegradation.* Microbiology and molecular biology reviews, 2010. **74**(2): p. 250-272.

110. Singh, S., *Sensors—An effective approach for the detection of explosives.* Journal of hazardous materials, 2007. **144**(1-2): p. 15-28.

111. Wu, J.-f., et al., *Novel partial reductive pathway for 4-chloronitrobenzene and nitrobenzene degradation in Comamonas sp. strain CNB-1.* Applied and environmental microbiology, 2006. **72**(3): p. 1759-1765.

112. McNeil, E.M., A.-M. Ritchie, and D.W. Melton, *The toxicity of nitrofuran compounds on melanoma and neuroblastoma cells is enhanced by Olaparib and ameliorated by melanin pigment.* DNA repair, 2013. **12**(11): p. 1000-1006.

113. Zhou, L., et al., *ALDH2 mediates 5-nitrofuran activity in multiple species.* Chemistry & biology, 2012. **19**(7): p. 883-892.

114. Al, M.F., et al., *Impact of Fenton and ozone on oxidation of wastewater containing nitroaromatic compounds.* Journal of Environmental Sciences, 2008. **20**(6): p. 675-682.

115. McGee, L.C., et al., *Metabolic disturbances in workers exposed to dinitrotoluene.* The American Journal of Digestive Diseases, 1942. **9**(10): p. 329-332.

116. Tchounwou, P.B., et al., *Environmental toxicology and health effects associated with dinitrotoluene exposure.* Reviews on environmental health, 2003. **18**(3): p. 203-229.

117. Bharadiya, A.A., et al., *Nitrobenzene poisoning presenting as methemoglobinemia.* Muller Journal of Medical Sciences and Research, 2014. **5**(2): p. 185-187.

118. Tiwari, J., et al., *Environmental persistence, hazard, and mitigation challenges of nitroaromatic compounds.* Environmental Science and Pollution Research, 2019. **26**: p. 28650-28667.

119. Wang, T., et al., *Aggregation-enhanced FRET-active conjugated polymer nanoparticles for picric acid sensing in aqueous solution.* Journal of Materials Chemistry C, 2018. **6**(2): p. 266-270.

120. Woltman, S.J., et al., *Chromatographic detection of nitroaromatic and nitramine compounds by electrochemical reduction combined with photoluminescence following electron transfer.* Analytical chemistry, 2000. **72**(20): p. 4928-4933.

121. Saravanan, N.P., et al., *Voltammetric determination of nitroaromatic and nitramine explosives contamination in soil.* Talanta, 2006. **69**(3): p. 656-662.

122. Sun, R., et al., *Recyclable fluorescent paper sensor for visual detection of nitroaromatic explosives.* Sensors and Actuators B: Chemical, 2018. **265**: p. 476-487.

123. Li, J., et al., *Two metal–organic frameworks with structural varieties derived from cis–trans isomerism nodes and effective detection of nitroaromatic explosives.* Crystal Growth & Design, 2018. **18**(3): p. 1857-1863.

124. Stringer, R.C., S. Gangopadhyay, and S.A. Grant, *Detection of nitroaromatic explosives using a fluorescent-labeled imprinted polymer.* Analytical Chemistry, 2010. **82**(10): p. 4015-4019.

125. Zhang, H.-X., et al., *Electrochemical sensor for detecting ultratrace nitroaromatic compounds using mesoporous SiO_2-modified electrode.* Analytical chemistry, 2006. **78**(6): p. 1967-1971.

126. Sangili, A., et al., *A Facile synthesis of ultra-small cerium oxide nanoparticles for enhanced Electrochemical Detection of Nitrobenzene in water samples.* International Journal of Electrochemical Science, 2018. **13**(6): p. 6135-6143.

127. Fan, Y.Z., et al., *A facile synthesis of water-soluble carbon dots as a label-free fluorescent probe for rapid, selective and sensitive detection of picric acid.* Sensors and Actuators B: Chemical, 2017. **240**: p. 949-955.

128. Wang, X., et al., *A reliable and facile fluorescent sensor from carbon dots for sensing 2, 4, 6-trinitrophenol based on inner filter effect.* Science of the total environment, 2020. **720**: p. 137680.

129. Chatzimarkou, A., et al., *Selective FRET-based sensing of 4-nitrophenol and cell imaging capitalizing on the fluorescent properties of carbon nanodots from apple seeds.* Sensors and Actuators B: Chemical, 2018. **258**: p. 1152-1160.

130. Hu, Y. and Z. Gao, *Sewage sludge in microwave oven: A sustainable synthetic approach toward carbon dots for fluorescent sensing of para-Nitrophenol.* Journal of hazardous materials, 2020. **382**: p. 121048.

131. Wang, K., et al., *Facile synthesis of dual emission carbon dots for the ratiometric fluorescent detection of 2, 4, 6-trinitrophenol and cell imaging.* Journal of Molecular Structure, 2022. **1263**: p. 133167.

132. Zhang, S., et al., *Bright-yellow-emissive carbon dots with a large Stokes shift for selective fluorescent detection of 2, 4, 6-trinitrophenol in environmental water samples.* Materials Letters, 2020. **263**: p. 127208.

133. Saravanan, A., et al., *Applications of N-doped carbon dots as antimicrobial agents, antibiotic carriers, and selective fluorescent probes for nitro explosives.* ACS Applied Bio Materials, 2020. **3**(11): p. 8023-8031.

134. Meng, Y., et al., *Multi-sensing function integrated nitrogen-doped fluorescent carbon dots as the platform toward multi-mode detection and bioimaging.* Talanta, 2020. **210**: p. 120653.

135. Wang, D., et al., *An efficient fluorescent nano-sensor of N-doped carbon dots for the determination of 2, 4, 6-trinitrophenol and other applications.* Analytical Methods, 2020. **12**(43): p. 5195-5201.

136. Babar, D.G. and S.S. Garje, *Nitrogen and phosphorus co-doped carbon dots for selective detection of nitro explosives.* ACS omega, 2020. **5**(6): p. 2710-2717.

137. Khan, Z.M., et al., *A facile one step hydrothermal synthesis of carbon quantum dots for label-free fluorescence sensing approach to detect picric acid in aqueous solution.* Journal of Photochemistry and Photobiology A: Chemistry, 2020. **388**: p. 112201.

138. Keerthana, P., et al., *Detection of picric acid in industrial effluents using multifunctional green fluorescent B/N-carbon quantum dots.* Journal of Environmental Chemical Engineering, 2022. **10**(2): p. 107209.

139. Chandra, S., et al., *Nitrogen/sulfur-co-doped carbon quantum dots: a biocompatible material for the selective detection of picric acid in aqueous solution and living cells.* Analytical and Bioanalytical Chemistry, 2020. **412**: p. 3753-3763.

140. Niu, Q., et al., *Amine-capped carbon dots as a nanosensor for sensitive and selective detection of picric acid in aqueous solution via electrostatic interaction.* Analytical methods, 2013. **5**(21): p. 6228-6233.

141. Roshni, V., et al., *Novel and reliable chemosensor based on C. dots from Sunflower seeds for the distinct detection of picric acid and bilirubin.* Spectrochimica Acta Part A: Molecular and Biomolecular Spectroscopy, 2021. **250**: p. 119354.

142. Ahmed, G.H.G., et al., *Highly fluorescent carbon dots as nanoprobes for sensitive and selective determination of 4-nitrophenol in surface waters.* Microchimica Acta, 2015. **182**: p. 51-59.

143. Al-Kaysi, R.O., I. Gallardo, and G. Guirado, *Stable spirocyclic Meisenheimer complexes.* Molecules, 2008. **13**(6): p. 1282-1302.

144. Ju, B., et al., *Photostable and low-toxic yellow-green carbon dots for highly selective detection of explosive 2, 4, 6-trinitrophenol based on the dual electron transfer mechanism.* ACS applied materials & interfaces, 2018. **10**(15): p. 13040-13047.

145. Chen, B.B., et al., *Highly selective detection of 2, 4, 6-trinitrophenol by using newly developed terbium-doped blue carbon dots.* Analyst, 2016. **141**(9): p. 2676-2681.

CHAPTER 5

SOLVENT RELAXATION AND ASSOCIATED APPLICATIONS OF p-PHENYLENEDIAMINE DERIVED CARBON NANODOTS

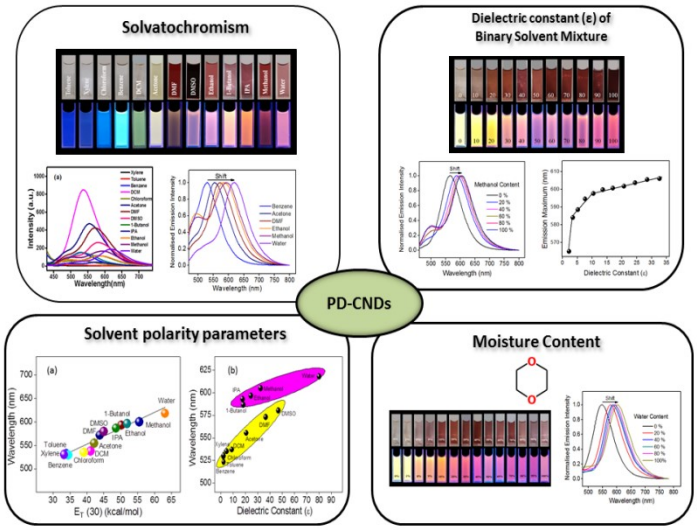

In this chapter, investigations carried out using a collection of solvents, categorized into polar and nonpolar, indicated the potential of the system for applications based on its solvatochromic nature. The feature enabled the determination of different polarity parameters as well as dielectric constants of solvents and solvent mixtures, with considerable accuracy. The system was potent for predicting the composition of a given pair of solvents. The service of the system is also extended for moisture sensing in organic solvents.

5.1. Introduction

5.1.1. Solvatochromism and solvent relaxation.

Different solvents have varying effects on the electronic ground state and excited state of the solute, altering the energy gap between them. This change is reflected in the absorption or emission spectrum of the solute, manifesting as variations in the position, intensity, and shape of the spectroscopic bands. Solvatochromism is the phenomenon where the color of a solution changes when a solute is dissolved in different solvents, *ie*., "change in color due to solvent effects", which appears as a change in absorbance/emission wavelength. There are mainly two types of solvatochromism exist, negative solvatochromism and positive solvatochromism. The former corresponds to a hypsochromic shift (or blue shift) in absorbance or emission wavelength with increasing solvent polarity, while the later corresponds to a bathochromic shift (or red shift) with increasing solvent polarity. Generally this phenomenon exhibited by fluorescent dyes and some organic molecules.

The fluorescence solvatochromism is caused by dipole interactions between the solvent molecules and the fluorophore. The dipole moment substantially affects the electrical structure of the surface as the solvent polarity increases. It also shrinks the energy gap, which causes the red-shift of fluorescence emission wavelength. The ground and excited states of the fluorophore have different energies, resulting in a change in the molecular dipole

moment, which eventually causes the solvent molecules in the vicinity to rearrange. However, as per the Franck–Condon principle, the time frame for the excitation of the molecule to a higher electronic level is much less when compared to the time taken for the solvent molecules to reorient around the former. The dipole moment of the fluorophore in the excited state is much higher than that in the ground state, which quickly transfers the excess vibrational energy to nearby solvent molecules, as it gradually relaxes to the lowest vibrational energy level (occurring in the picosecond time scale). By slowly rotating (a process known as solvent relaxation) around the excited fluorophore, which takes between 10 and 100 picoseconds, solvent molecules stabilize and lower the energy level of the excited state. Owing to the reduced energy gap between the ground and excited states, the fluorescence emission is red-shifted

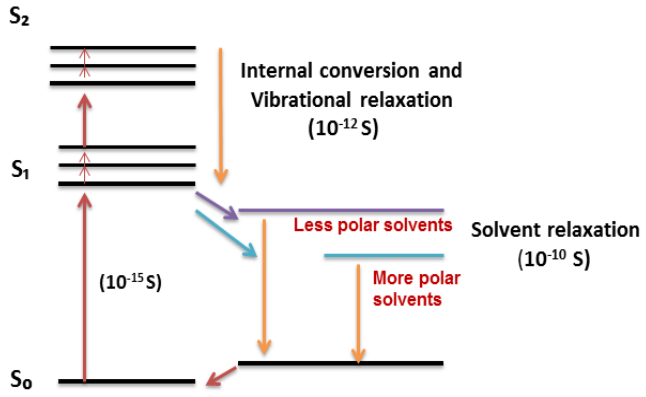

Figure 5.1 Jablonski diagram for fluorescence with solvent relaxation

(λ_{max} shifted to longer wavelength). The Jablonski diagram for fluorescence with solvent relaxation and fluorophore-solvent excited state interactions is depicted in **Figure 5.1** and **Figure 5.2** respectively.

Recently, many research groups have reported that CNDs also exhibit solvatochromism. For example, Sato *et al.* [1] synthesized CNDs from a phenylenediamine isomer, which exhibited fluorescence emission at longer wavelengths and are solvatochromic, with red-shifted emission as the solvent polarity increased. Pramanik *et al.* [2] synthesized CNDs via hydrothermal carbonization of naturally occurring bio-waste which showed solvatochromism. This solvatochromic behavior has been utilized for the fluorescence sensing of ethanol and tetrahydrofuran (THF) in water. Kundu *et al.* [3] synthesized nitrogen functionalized

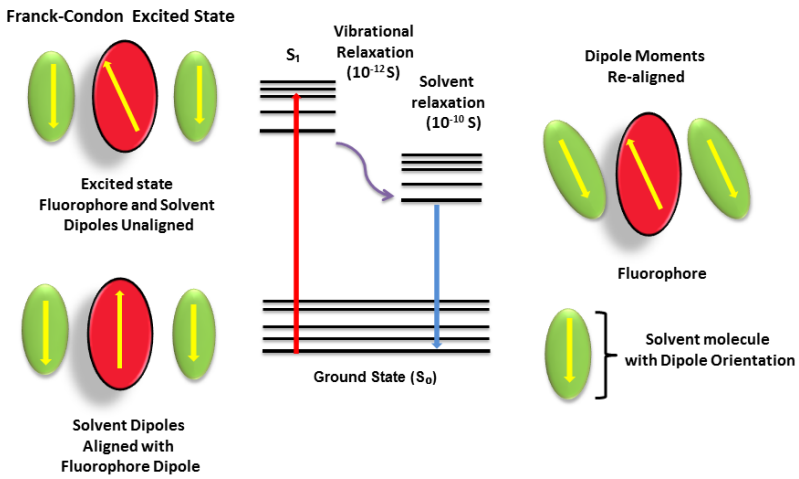

Figure 5.2 Fluorophore-solvent excited state interaction

carbon nanodots (NCDs), which exhibit excellent solubility in a series of organic solvents and have extensively investigated the NCDs-solvent interactions to understand the solvatochromic behavior of CNDs. Sciortino *et al.* [4] studied various interactions of carbon nanodots with their environment in a wide range of solvents to elucidate the nature of the electronic transitions.

In the present study, thirteen solvents categorized into polar and non-polar are examined for their interaction with CNDs, where the emission wavelength varied almost in the entire VIBGYOR region, depending on the solvent polarity. A detailed investigation supported by spectral data in the previous chapter reveals that the photoluminescence of the system originates from edge group/midlevel and surface functional group participation. The most important properties of the solvent are its dielectric constant (ε) and hydrogen bonding capacity. The system could predict the solvent parameters, such as dielectric constant (ε) and Reichardt's empirical E_T (30) polarity parameter, based on the molar transition energies (E_T) of the Betaine 30 dye in the solvents. Another noteworthy application is the accurate determination of the dielectric constant and composition of solvent mixtures, as exemplified by a methanol-1,4-Dioxane system. Apart from these, the application is further extended for tracing moisture content in dioxane, which is a commercially significant achievement. An error percentage < 1 assures the proven potential of the system for the above mentioned applications.

PART A

5.2. Solvatochromism in p-phenylenediamine derived carbon nanodots- Influence of solvent polarity

An in-depth analysis of the solvent induced luminescence characteristics of p-Phenylenediamine derived carbon nanodots (PD-CNDs) was conducted using solvents of varying polarity, including benzene, toluene, xylene, chloroform, dichloromethane (DCM), DMSO, ethanol, methanol, isopropyl alcohol (IPA), 1-butanol, DMF, acetone and water. The characteristics of these solvents, including dielectric constant, E_T (30) and relative polarity are listed in **Table 5.1.**

The photographs of PD-CND dispersions (0.1 mg/mL) in these selected solvents, shown in **Figure 5.3**, demonstrate that the system exhibits different colors in different solvents, indicating solvatochromic character. This property is consistent across all the thirteen solvents tested and is visible both under daylight and UV light; suggesting that the polarity of the solvent influences the ground state and excited states of PD-CNDs. Interestingly, the luminescence color of the system spans almost the entire VIBGYOR region.

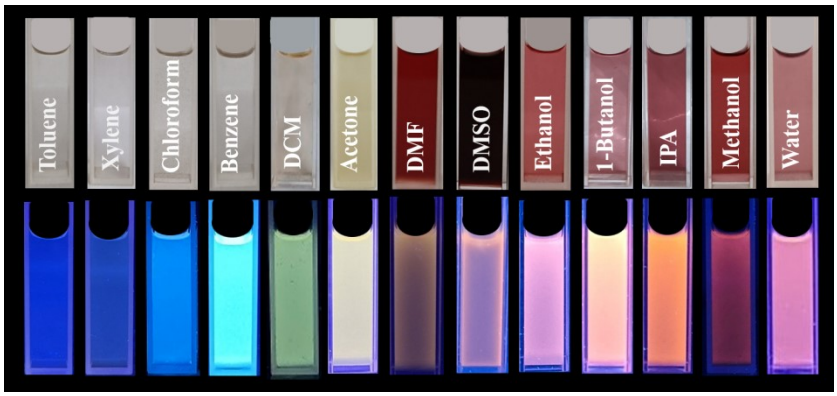

Figure 5.3 Photographs of dispersion of PD-CNDs in selected solvents under daylight (upper panel) and UV illumination (lower panel)

Table 5.1 Solvent polarity parameters of selected solvents and fluorescence emission peak maximum (λ_{max} (em)) of PD-CNDs in the solvents.

No	Solvent	Dielectric constant (ε)	Relative polarity	$E_T(30)$	Kamlet Taft parameters			λ_{max} (em) (nm)
					α	β	π^*	
1	Toluene	2.38	0.099	33.9	0	0.11	0.54	532.76
2	Benzene	2.28	0.111	34.5	0	0.10	0.59	529.55
3	Xylene	2.37	0.074	33.3	0	0	0.47	530.54
4	DCM	8.93	0.309	41.1	0.13	0.10	0.82	537.66
5	Chloroform	4.81	0.259	39.1	0.44	0	0.58	535.00
6	Acetone	20.7	0.355	42.2	0.08	0.43	0.71	555.00
7	DMF	36.7	0.386	43.8	0	0.69	0.88	571.64
8	DMSO	47.0	0.444	45.0	0	0.76	1.00	579.87
9	1-Butanol	17.8	0.586	50.2	0.79	0.88	0.47	593.00
10	IPA	18.3	0.546	48.6	0.8	0.5	0.5	586.60
11	Ethanol	24.6	0.654	51.9	0.86	0.75	0.54	596.50
12	Methanol	32.6	0.762	55.5	0.98	0.66	0.60	605.53
13	Water	78.54	1.000	63.1	1.17	0.47	1.09	618.01

Analysis of the absorption spectral features provides insights into solute solvent interactions, as indicated by the absorption maximum wavelength. Solvents are categorized based on the polarity for a fair comparison of the data. The absorption spectrum of PD-CNDs recorded in these selected solvents (**Figure 5.4 (a) and (b)**) shows that the intensity, shape and position of the absorption peaks of PD-CNDs vary significantly with the nature of the solvents. The wavelength corresponding to the absorption maximum increased sequentially for protic solvents, though this effect is less pronounced for aprotic solvents. Intermolecular solute-solvent interactions, primarily affecting the ground state and excited state energy differences of the species, are instrumental for these variations. The **Figure 5.4 (a)** represents the UV-visible absorption spectrum of PD-CND in nonpolar solvents, in which they can be dispersed to some extent, showing π- π* and n-π* transitions. Nonpolar solvents can interact with CNDs via dipole-dipole interactions, stabilizing the ground state of PD-CNDs and causing a slight hypsochromic shift in the π-π* transition peak in these solvents [5]. **Figure 5.4 (b)** shows the absorption spectra of PD-CND in polar solvents, with the inset highlighting the absorption spectra in the visible region. A pronounced shift in the absorbance maxima is evident, indicating significant differences in the interaction of PD-CNDs with various solvents.

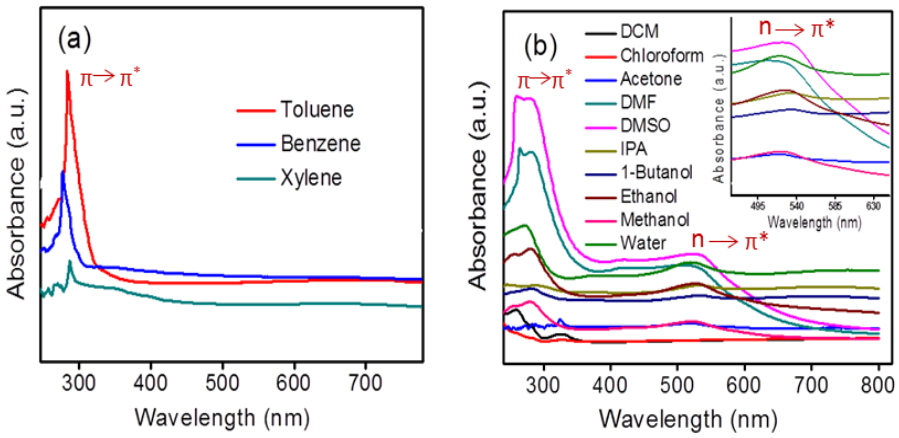

Figure 5.4 UV-visible absorption spectra of PD-CND dispersions in **(a)** nonpolar solvents and **(b)** in polar solvents. The inset in (b) indicates the absorption spectra in the visible region.

The influence of solvent polarity on absorbance, especially in hydrogen-bonding solvents, is attributed to the n-π* transition occurring from the edge atom into the π* orbital of the core. This charge movement induces a change in dipole moment, favoring the absorption of energy corresponding to this transition [6]. **Figure 5.5 (a)** represents the fluorescence spectra of PD-CNDs in various solvents, at an excitation of 420 nm, highlighting the influence of solvent polarity. **Figure 5.5 (b)** displays the corresponding normalized spectra of PD-CNDs in these selected solvents. Notably, weak fluorescence emission is observed in solvents with both low and high polarity. Previous studies have linked this observation to reduced dispersibility of carbon particles in these solvents due to the amphiphilic and polarized surface of the particles. Additionally, the presence of twisted intra-molecular charge transfers between the solvent and carbon particles, along with proximity effects,

contribute to this phenomenon [7, 8]. Proximity effects involve non-radiative energy loss when fluorophores are in close proximity, generating additional non-radiative relaxation pathways, particularly pronounced with increasing solvent polarity. Quantum yield values in representative solvents support these observations. The quantum yield values determined in benzene and water are 0.82 and 0.61 respectively.

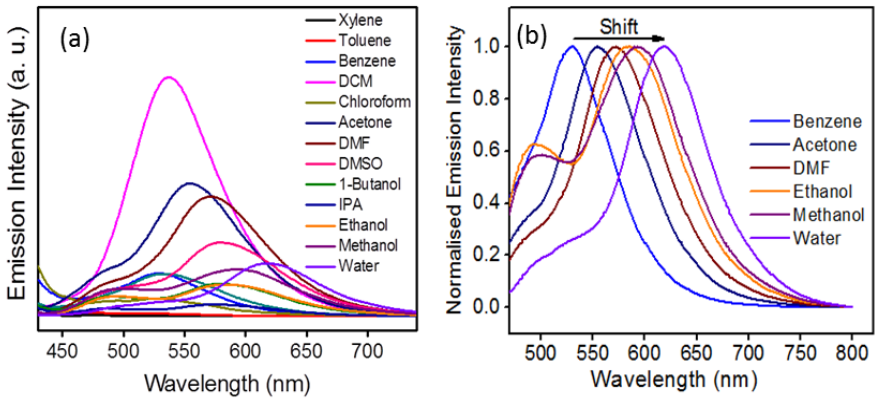

Figure 5.5 (a) Fluorescence spectra of PD-CNDs (λ_{ex} = 420 nm) in selected solvents and **(b)** corresponding normalized fluorescence spectra to explicitly mark the wavelength shift with change in solvent polarity.

The spectra reveal a visible bathochromic shift in fluorescence, changing from blue to red, as the polarity of the medium increases. This shift is attributed to hydrogen bonding induced emission, facilitated by interactions between the carbon particle surface and hydrogen bond-dominant protic solvents in polar environments [9, 10]. The fluorescence maxima in various solvents are listed in the **Table 5.1.** As solvent polarity increases, the emission wavelength shifts to longer values. Notably, the

intervals between fluorescence peak positions are smaller for aprotic solvents, while the differences are significantly larger for protic solvents. When the dispersion medium changes from toluene to water, the emission peaks are red-shifted by 86 nm, indicating a maximum shift of 0.33 eV with increased solvent polarity.

The observed red-shift of emission in protic solvents indicates that the hydrogen bonding acceptor character of PD-CND is enhanced by photo-excitation. This enhancement is due to an increase in the negative charge localized on the hydrogen bonding acceptor group on the carbon surface, as supported by UV-visible absorbance and photoluminescence spectral methods [11, 12]. This shift is significantly larger than those observed in other CNDs exhibiting solvatochromic behavior [6]. **Figure 5.5 (b)** clearly demonstrates that PD-CNDs exhibit a shift in the emission maxima when the solvent is changed from toluene to water, typically from nonpolar to polar solvents.

The emission exhibited by PD-CNDs in selected solvents is also excitation wavelength dependent, as shown in **Figure 5.6.** When the excitation wavelength shifts from 360 to 500 nm, the emission peaks of CNDs in a given solvent display a clear red shift. Emission is observed in two regions: the 400-500 nm range and at around 500-700 nm when excited with wavelength scanning from 360-420 nm, the shift was observed for the first region, while the peak in 500-700 nm was almost unaltered in the emission maximium wavelength. This observation was also noted previously in water. The excitation wavelength dependence in the

edge emission state suggests that the fluorescent centers responsible for edge state emissions are widely distributed, illustrating the red edge excitation shift. In the range of λ_{exc} = 420-500 nm, the emission spectra show only one peak at a higher wavelength region, with the intensity steadily decreasing as the emission energy decreases.

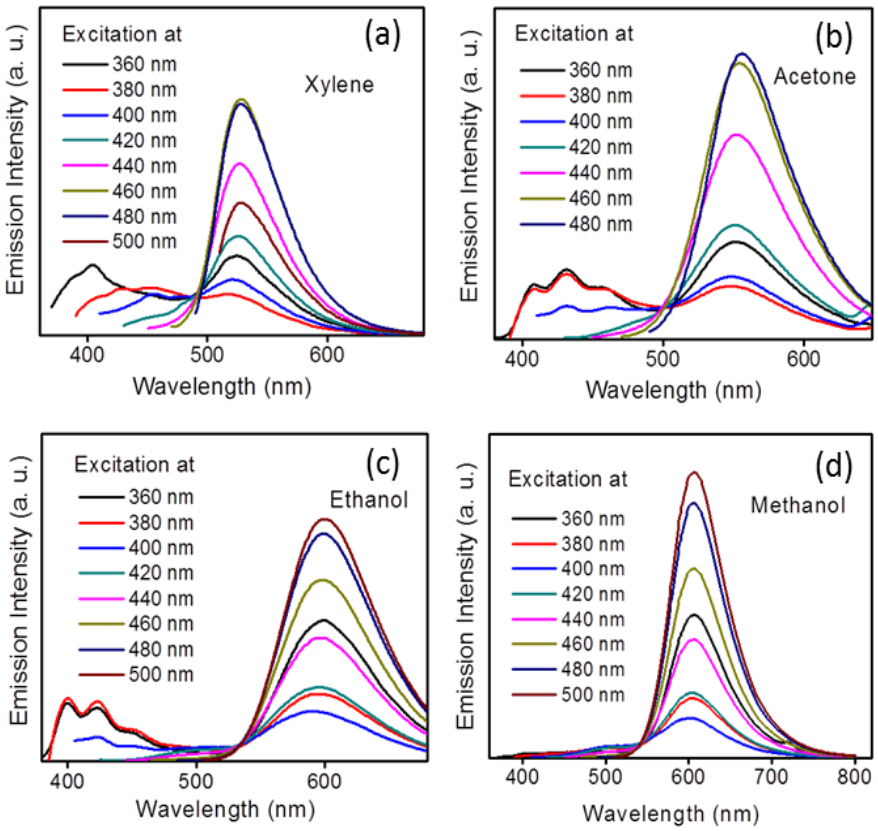

Figure 5.6 Fluorescence emission spectra of PD-CND dispersions in (a) xylene, (b) acetone, (c) ethanol and (d) methanol at different excitation levels.

5.3. Correlation between solvent polarity parameters and emission maxima of p-phenylenediamine derived carbon nanodots

The polarity-dependent solvatochromic character can be explained using the qualitative solvent polarity parameter, E_T (30) [13]. The E_T (30) scale models the solvent polarity effect on a Betaine dye's S_0 to S_1 transition. When plotting fluorescence and absorption maxima against the E_T (30) scale, solvatochromic behavior can be predicted. **Figure 5.7 (a)** shows the plot of emission maximum values *versus* the E_T (30) polarity parameter of the solvents used for dispersing PD-CND. The E_T (30) values for various solvents, adopted from the literature [13], are listed in **Table 5.1**. A fairly good linear relationship is observed between the emission maximum wavelengths of PD-CND and the corresponding E_T (30) values of different solvents, indicating the specific nature of interaction between the solvent and the solute. The linear trend in fluorescence suggests that the red-shift in emission depends on solvent polarity [1]. Another parameter that best describes solvent polarity is the dielectric constant (ε), which quantifies the polar nature in terms of the amount of electrical energy stored in the electric field of the solvent. Two distinct variations are evident, when plotting dielectric constant (ε) values of the selected solvents against their emission maxima values (**Figure 5.7 (b)**), signifying polar protic solvents and polar aprotic/non-polar solvents. This unambiguously proves the influence of hydrogen bonding in determining the emission maximum in different solvents. From the plot, dielectric constant

values of solvents can be indirectly predicted. Polar protic solvents can be distinguished from others by their emission maxima values falling higher than 580 nm. In polar protic solvents, more specific interactions between PD-CND and the solvent can be identified, with hydrogen bonding interactions highly probable between alcoholic solvents and oxygen or nitrogen rich functional groups in PD-CNDs [2].

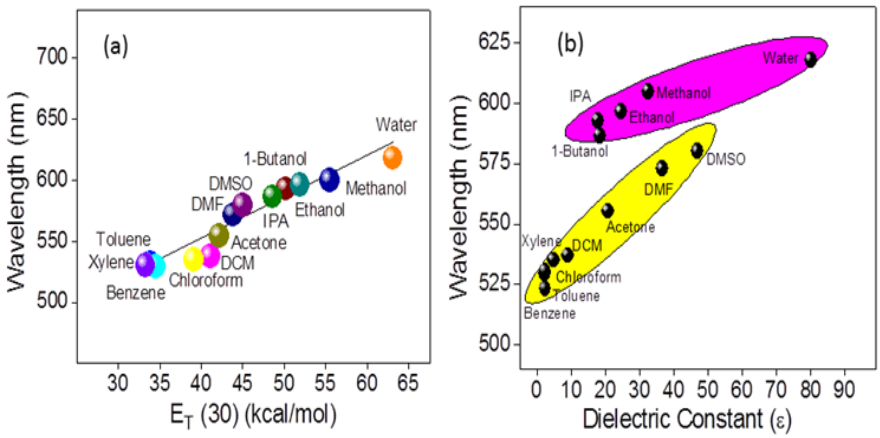

Figure 5.7 (a) Plot of fluorescence emission maximum values, λ_{max} (em), of PD-CNDs dispersion in selected solvents versus E_T (30) and **(b)** λ_{max} (em) values versus dielectric constant of solvents used for dispersing the PD-CNDs.

PART B

5.4. Solvatochromism mediated applications of p-phenylenediamine derived carbon nanodots

5.4.1. Determination of dielectric constant of alcohol-1, 4-dioxane binary solvent mixtures

The significant shift in the emission maximum with changes in solvent polarity allows for the analysis of solvent mixture properties. This material can be directly applied to estimate the dielectric constant values of primary alcohols. In addition to the previously selected solvents, the optical properties of PD-CND in other n-alcohols (n-propanol, n-butanol, n-pentanol, n-hexanol and n-heptanol) were further investigated. Although the polarities of these alcoholic solvents are different, the absorption and PL spectra in these alcoholic solvents are very close (**Figure 5.8 (a) and (b)**). This may arise due to the formation of hydrogen bonds between oxygen and nitrogen atoms on the surface of PD-CNDs and alcohol molecules. A linear relationship between dielectric constant (one parameter that best describes solvent polarity) and emission maxima of alcohols was also observed (**Figure 5.8 (c)**). This material can be directly applied to estimate the dielectric constant values of primary alcohols. The linear relationship observed between the emission maxima and the dielectric constant values of primary alcohols supports this proposal. The corresponding values of the physical parameters are given in **Table 5.2**.

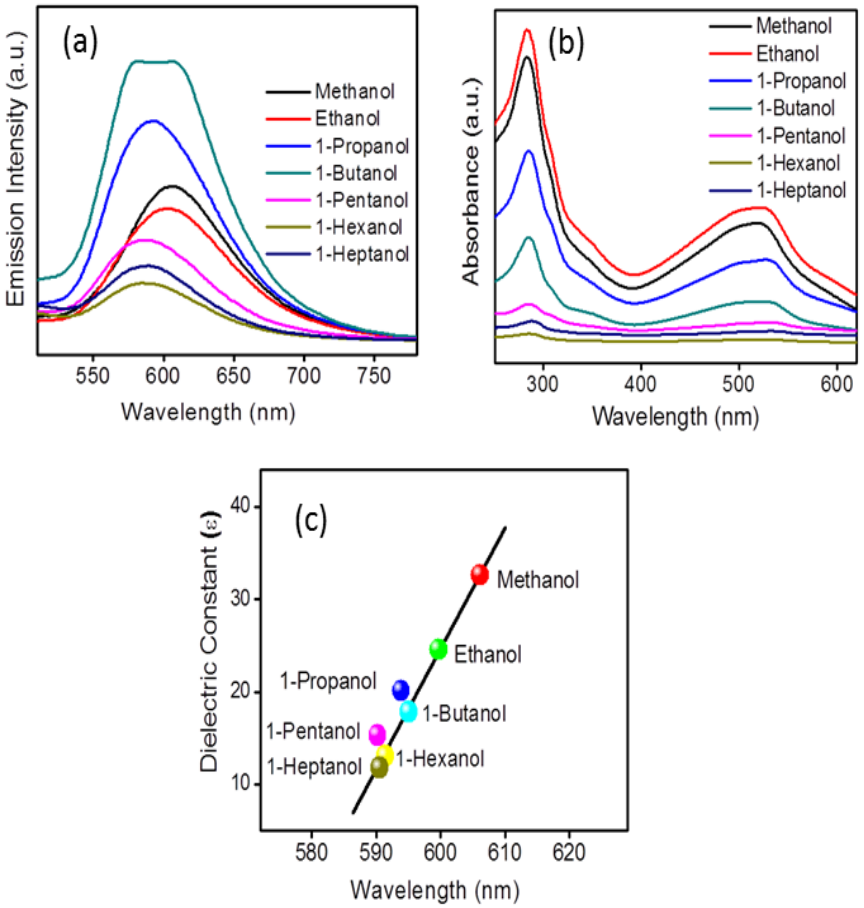

Figure 5.8 (a) Fluorescence spectra (λ_{exc}=440 nm) and **(b)** UV-visible absorption spectra of PD-CND dispersion in n-alcohol, **(c)** Correlation between dielectric constant of n-alcohols and λ_{em}(max) of PD-CNDs.

Table 5.2 Fluorescence emission maximum of PD-CNDs, λ_{max} (em) in different n-alcohols and the dielectric constant values of respective n-alcohols.

No.	Name	λ_{max}(em) (nm)	Dielectric Constant (ε)
1	Methanol	606.16	32.60
2	Ethanol	596.68	24.55
3	1-Propanol	592.89	20.10
4	1-Butanol	593.10	17.80
5	1-Pentanol	590.2	15.30
6	1-Hexanol	591.46	13.03
7	1-Heptanol	590.54	11.75

The scope of the results extends further to alcohol–dioxane mixtures. The solvatochromic effect of PD-CNDs is evident in daylight and becomes more pronounced under UV light illumination. This is illustrated in **Figure 5.9**, which shows photographs of PD-CND dispersions (0.05 mg/mL) in mixtures of 1, 4-dioxane and methanol at varying ratios (0%, 10%, 20%,…,100% v/v, with 10% increments) under both daylight and 365 nm UV light.

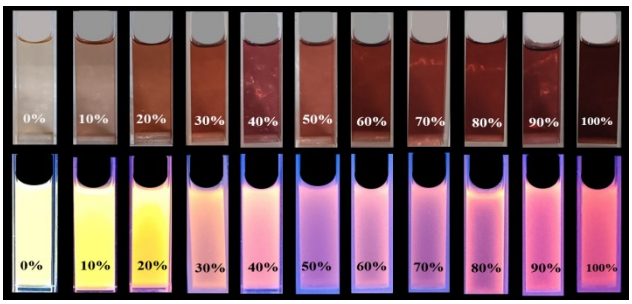

Figure 5.9 Photographs of PD-CND dispersions in various compositions of methanol–1,4-dioxane mixtures (0% to 100% methanol, in 10% increments) arranged in increasing order of methanol content. Images are presented under daylight (upper panel) and 365 nm UV light illumination (lower panel).

Figure 5.10 (a) shows the fluorescence emission spectra of these dispersions excited at the optimal wavelength of 460 nm, **Figure 5.10 (b)** presents the normalized spectra of the selected compositions. **Figure 5.10 (c)** summarizes the changes in emission wavelength and methanol content in the binary mixture. The bathochromic shift of the emission maximum varies linearly with methanol content in three ranges: 0 to 5%, 5 to 40%, and 40 to 100%. These results demonstrate that p-phenylenediamine derived CNDs can be used to quantify the solvent composition in the mixture. Additional experiments with mixtures containing 33% and 52% methanol confirm the reliability of the results, yielding compositions of 33.03% and 52.09%, respectively, as shown in **Figure 5.10 (c).** Apart from these, another significant result is derived from these observations. Since the emission feature is related to the polarity of the medium, it is reasonable to expect that the trend in the variation of the dielectric constant with composition should be reflected in the emission maxima of the mixtures. The polarity of the solvents greatly influences the emission features of these particles. The dielectric constants of dioxane–methanol mixtures with varying compositions, as reported by Papanastasiou *et al*. [14], are used as a reference here. The related parameters are presented in **Table 5.3. Figure 5.10 (d)** illustrates the relationship between these values. The same trend is observed for compositions and dielectric constants when plotted against the λ_{max} obtained for various mixtures, enabling the

determination of dielectric constant values for a given methanol–1, 4-dioxane mixture.

Table 5.3 The methanol content (%), fluorescence emission maximum of PD-CNDs, λ_{max} (em) and dielectric constant of methanol-1, 4-dioxane mixture.

No.	Methanol Content (%)	λ_{max}(em) (nm)	Dielectric Constant (ε)
1	0	565.00	2.209
2	10	584.07	3.500
3	20	588.44	5.215
4	30	594.5	7.622
5	40	597.52	10.408
6	50	599.65	13.560
7	60	600.57	16.945
8	70	601.77	20.672
9	80	603.59	24.440
10	90	605.41	28.516
11	100	606.00	32.634

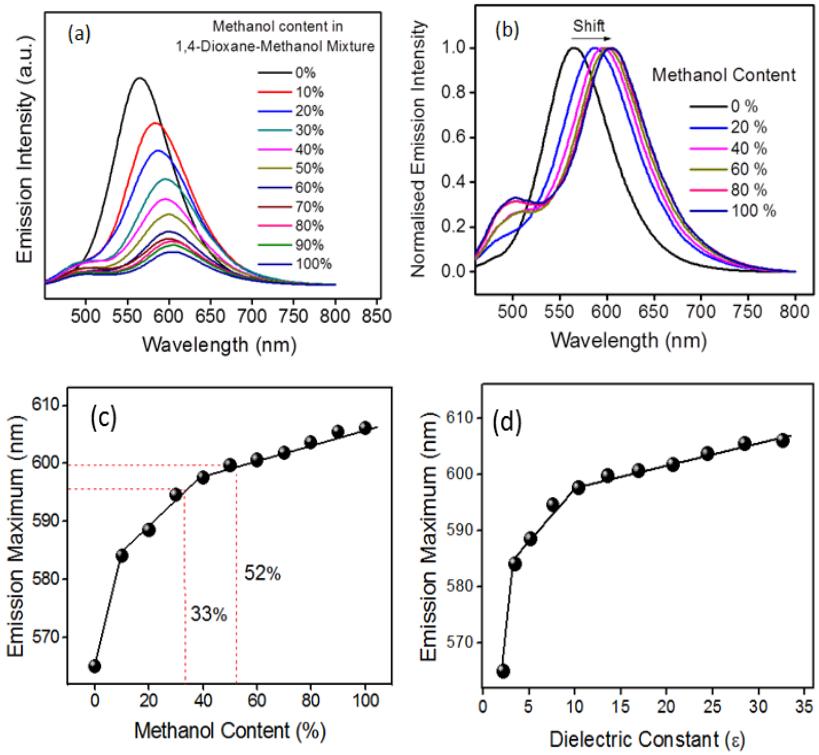

Figure 5.10 (a) Fluorescence emission spectra of PD-CNDs at selected compositions (0.05 to 100% with 10% increment), and **(b)** normalised emission spectra of PD-CNDs in selected composition of methanol–1, 4-dioxane mixture (0.05, 20, 40, 60, 80 and 100% v/v) (λex = 460 nm). **(c)** Plot showing the relationship of emission peak maximum versus methanol content in the binary mixture and **(d)** plot of emission peak maximum versus dielectric constant.

5.4.2. Determination of moisture content in organic solvents

Moisture content in organic solvents can adversely affect various chemical reactions by not only reducing yield but also slowing reaction rates and limiting their applications. This necessitates a straightforward, fast, and reliable analytical method for accurately quantifying water in organic solvents for both synthetic laboratories and industrial applications. Karl-Fischer titration [15] is one of the most widely used techniques for water detection, known for its excellent selectivity and accuracy. Fluorescence-based techniques have been proposed as an alternative to Karl-Fischer titration for determining moisture content due to their advantages, including high sensitivity, operational simplicity, rapid response, and low cost [16]. Here, PD-CND system is used as fluorescent probe to determine moisture content in an organic solvents: 1, 4-Dioxane.

5.4.3. Determination of moisture content in 1, 4-Dioxane

A simple and efficient fluorescence-based technique is presented to measure moisture content in 1, 4-Dioxane using PD-CNDs. Typically, 0.05 mg/ml of PD-CND powder was dispersed in 10 mL of different compositions of the 1,4-Dioxane–water mixture (ranging from 0.05% to 100% v/v, with 10% increments), and changes in the fluorescence wavelengths were recorded. Photographs of the PD-CND dispersion at these compositions under visible and UV light illumination are shown in **Figure 5.11**. There is a significant difference in the color of the dispersions both

in visible light and under UV light. As the water content in 1, 4-Dioxane increased, a gradual shift to a dark brown color was observed, indicating that the absorbance of these systems varies with the composition of the mixture. The solvatochromic effect is even more pronounced in the fluorescence images recorded under UV light (365 nm) illumination. A gradual change in the luminescence color from yellow to pink is clearly observed as the water percentage increases in the mixture.

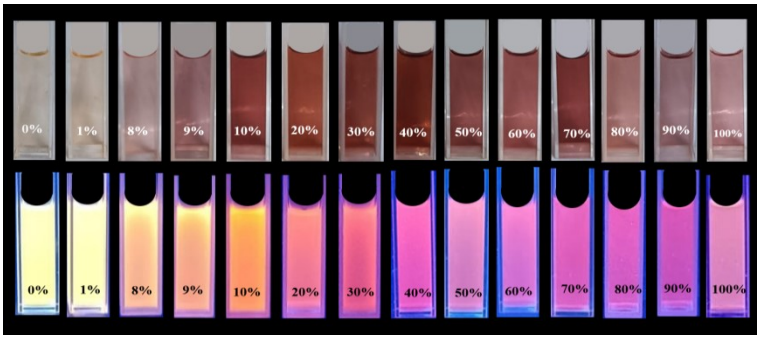

Figure 5.11 Photographs of PD-CND dispersions in different compositions of 1, 4-dioxane–water mixture (0.05, 1, 8, 9, 10 and thereafter with an increment of 10% up to 100% v/v) in the increasing order of water content. Images under day light (upper panel); under 365 UV illumination (lower panel)

The fluorescence spectrum of each composition, excited at 420 nm (**Figure 5.12 (a)**), shows a dramatic decrease in the fluorescence intensities of PD-CNDs in 1,4-Dioxane, accompanied by a small bathochromic shift as the water content in the mixture increases from 0.05% to 100% v/v. The normalized emission spectrum for various compositions, displayed in **Figure 5.12 (b),** indicates a significant variation in emission wavelength even with

very small amounts of water, as low as 1%. As shown in **Figure 5.12 (c)**, the red shift in the emission maximum with increasing water content in 1, 4-Dioxane reveals two linear variations in different ranges: 0– 10% and 11–100% water content, with R^2 values of 0.9673 and 0.9953 respectively. The difference in slope

may be due to the preferential solvation of PD-CNDs by

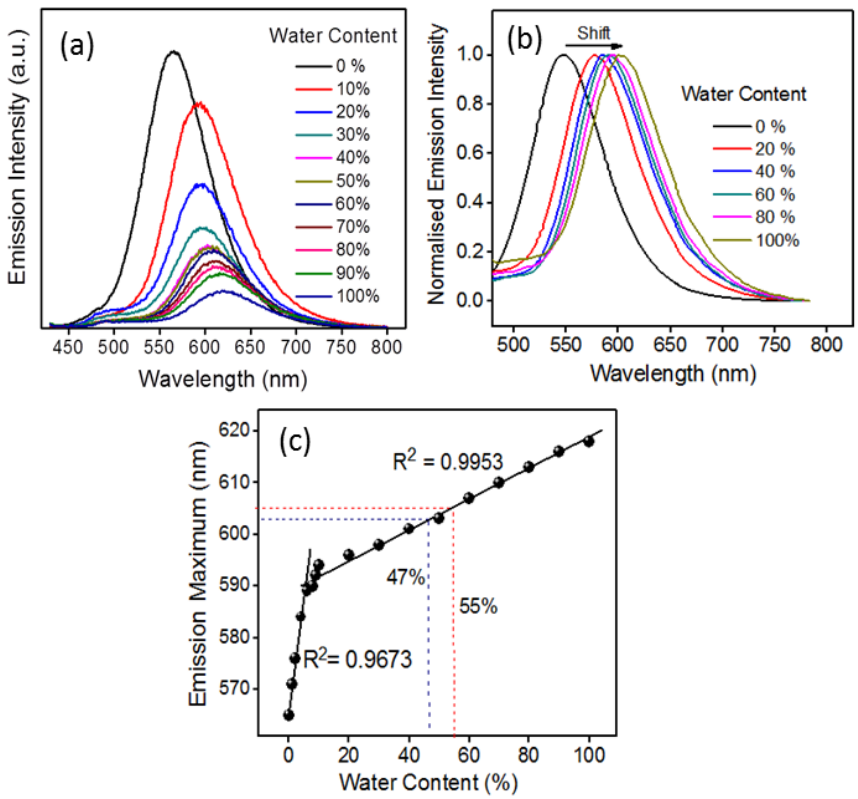

Figure 5.12 (a) Fluorescence emission spectra of PD-CNDs in 1, 4-Dioxane–water composition (0.05 to 100% with 10% increment) and **(b)** normalized emission spectra of PD-CNDs in selected 1, 4-dioxane–water compositions (0.05, 20, 40, 60, 80 and 100%, v/v) (λ_{exc} = 420 nm), **(c)** Plot showing relationship of emission peak maximum versus water content in 1,4-dioxane.

relatively less polar 1, 4-Dioxane in the binary solvent mixtures. The observed bathochromic shift and fluorescence quenching can be attributed to general solvent effects and the hydrogen-bonding interactions between the functional groups of PD-CNDs and water molecules [17]. Validation of the experiment was conducted by performing spectral studies on two mixtures of 1, 4-dioxane and water with different compositions, containing 47% and 55% water. The results were highly reliable, with predicted compositions of 46.54% and 54.68%, respectively, indicating that error percentage is less than 1% (0.97% and 0.58%, respectively).

5.5. Conclusions

This study highlights the solvatochromic behavior of PD-CNDs, demonstrating their ability to exhibit different photoluminescence colors when dispersed in various solvents. We propose a novel method for predicting solvent polarity parameters based on this solvatochromic nature. Our findings include the accurate determination of dielectric constant of binary solvent mixtures, exemplified by the methanol-1,4-Dioxane system. Additionally, we developed a simple and effective approach for quantitatively determining moisture in organic solvent with an error percentage below one. The emission color of the solutions varied with water content, showing a red shift in emission wavelength, and experiments using 1,4-Dioxane–water binary mixtures validated the procedure commendably. Notably, moisture content could even be monitored with the naked eye

under 365 nm UV light illumination. The solvent-dependent emission features of PD-CNDs present broader opportunities for studying solvent interactions. The low toxicity, facile synthesis, and solvent-dependent fluorescence make PD-CNDs promising candidates for a wide range of future scientific and technological applications.

References

1. Sato, R., Y. Iso, and T. Isobe, *Fluorescence solvatochromism of carbon dot dispersions prepared from phenylenediamine and optimization of red emission.* Langmuir, 2019. **35**(47): p. 15257-15266.

2. Pramanik, A., S. Biswas, and P. Kumbhakar, *Solvatochromism in highly luminescent environmental friendly carbon quantum dots for sensing applications: Conversion of bio-waste into bio-asset.* Spectrochimica Acta Part A: Molecular and Biomolecular Spectroscopy, 2018. **191**: p. 498-512.

3. Kundu, A., et al., *Multicolor emissive carbon dot with solvatochromic behavior across the entire visible spectrum.* Carbon, 2020. **156**: p. 110-118.

4. Sciortino, A., et al., *Solvatochromism unravels the emission mechanism of carbon nanodots.* The journal of physical chemistry letters, 2016. **7**(17): p. 3419-3423.

5. Rauf, M.A., A.A. Soliman, and M. Khattab, *Solvent effect on the spectral properties of Neutral Red.* Chemistry Central Journal, 2008. **2**(1): p. 1-8.

6. Mohammad-Jafarieh, P., et al., *An insight into the solvatochromic and photophysical behaviours of biowaste-origin carbon nanodots.* Journal of Molecular Liquids, 2021. **336**: p. 116360.

7. Tu, Y., et al., *An intelligent AIEgen with nonmonotonic multiresponses to multistimuli.* Advanced Science, 2020. **7**(20): p. 2001845.

8. Hrdlovic, P., et al., *Influence of polarity of solvents on the spectral properties of bichromophoric coumarins.* Molecules, 2010. **15**(12): p. 8915-8932.

9. Alas, M.O. and R. Genc, *Solvatochromic surface-passivated carbon dots for fluorometric moisture sensing in organic solvents.* ACS Applied Nano Materials, 2021. **4**(8): p. 7974-7987.

10. Mukherjee, S., E. Prasad, and A. Chadha, *H-Bonding controls the emission properties of functionalized carbon nano-dots.* Physical Chemistry Chemical Physics, 2017. **19**(10): p. 7288-7296.

11. Mohammed, O.F., et al., *Charge Transfer Assisted by Collective Hydrogen-Bonding Dynamics.* Angewandte Chemie International Edition, 2009. **48**(34): p. 6251-6256.

12. Messina, F., et al., *Ultrafast Solvent-Assisted Electronic Level Crossing in 1-Naphthol.* Angewandte Chemie, 2013. **125**(27): p. 7009-7013.

13. Reichardt, C., *Solvatochromic dyes as solvent polarity indicators.* Chemical reviews, 1994. **94**(8): p. 2319-2358.

14. Papanastasiou, G.E. and I.I. Ziogas, *Physical behavior of some reaction media. 3. Density, viscosity, dielectric constant, and refractive index changes of methanol+ dioxane mixtures at several temperatures.* Journal of Chemical and Engineering Data, 1992. **37**(2): p. 167-172.

15. Liang, Y.Y., *Automation of Karl Fischer water titration by flow injection sampling.* Analytical chemistry, 1990. **62**(22): p. 2504-2506.

16. Hou, F., et al., *New benzotriazole-based D–A–D type solvatochromic dyes for water content detection in organic solvents.* Dyes and Pigments, 2021. **195**: p. 109667.

17. Wei, J., et al., *A sensitive fluorescent sensor for the detection of trace water in organic solvents based on carbon quantum dots with yellow fluorescence.* RSC advances, 2018. **8**(65): p. 37028-37034.

CHAPTER 6

SUMMARY AND FUTURE OUTLOOK

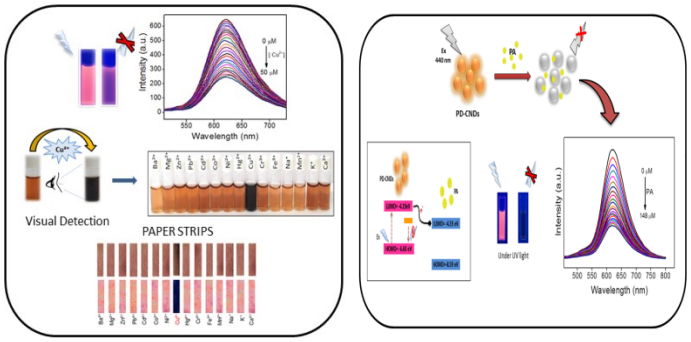

Luminescence Based Applications of PD-CNDs

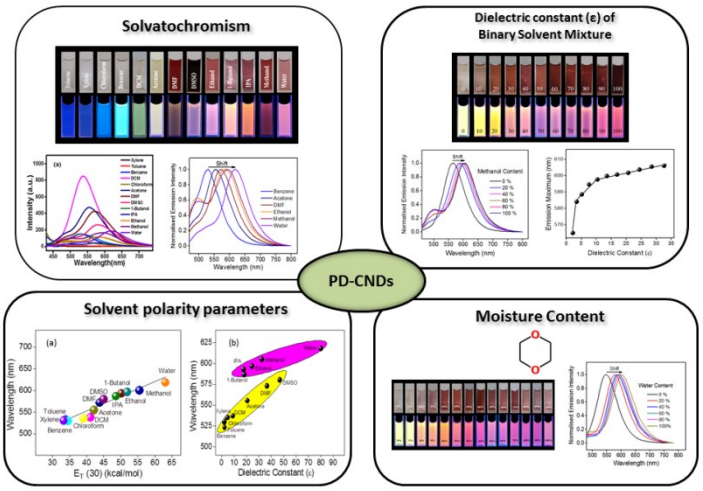

This chapter summarizes the entire thesis, offering an overview of the major highlights of the research findings and briefly discusses the future scope of the prepared system.

6.1. Summary

This work introduces highly luminescent N-doped fluorescent carbon nanodots (PD-CNDs), synthesized from p-Phenylenediamine using a straightforward one-step hydrothermal synthesis. The comprehensive characterization of PD-CNDs using spectroscopy and microscopy, reveals their structural, morphological, and optical properties. These carbon nanodots feature a carbon framework that includes pyridinic and pyrrolic nitrogen, along with amino, carboxyl, and hydroxyl groups as surface functionalities. It exhibits inherent luminescence, emitting an orange-red color. The luminescence is attributed to the participation of edge group/mid-level and surface functional groups. The study focuses entirely on the luminescence-based applications of PD-CNDs and is divided into two main sections. The first section addresses the sensing applications of PD-CNDs, while the second section explores solvent relaxation and solvatochromism-mediated applications of these nanodots.

The bright luminescence properties of the synthesized carbon nanodots were utilized for sensing applications. Carbon nanodots typically provide an excellent platform for the quantitative monitoring of various significant analytes. In this study, two sets of analytes were selected for investigation: the first part focuses on metal ions, and the second part on nitroaromatic compounds. The photoluminescence intensity of the carbon nanodots (CNDs) was found to be quenched in the presence of

Cu^{2+} ions. This property was used to develop a CND-based fluorescent sensor for the quantitative detection of Cu^{2+} ions. The mechanism behind the luminescence quenching in the presence of these ions was investigated, concluding that static quenching is responsible for these changes. This finding was further extended in to a visual detection method, achieved through the formation of a black precipitate attributed to the complex PD-CND@Cu. The optimization of PD-CND@Cu was supported by various characterization techniques. The system demonstrated high selectivity for Cu^{2+} ions, even in the presence of other metal ions. This detection capability was extended to a solid-state application using PD-CND-coated filter paper strips, enabling easy visual detection of copper ions. Therefore, the presented N-doped carbon nanodots (PD-CNDs) offer a promising platform for the rapid and selective fluorimetric and visual detection of Cu^{2+} ions. In the second part of the study, the response of the photoluminescence (PL) intensity of PD-CNDs to nitroaromatics was monitored. Interestingly, the luminescence intensity gradually decreased upon the addition of picric acid, while none of the other selected nitroaromatic compounds evoked such a response. The mechanism behind this luminescence quenching was also studied in detail. Theoretical investigations also support these findings.

The last working chapter focuses on the solvent relaxation and solvatochromism-based applications of PD-CNDs. This study delves into the solvatochromic behavior of PD-CNDs, highlighting their ability to exhibit various photoluminescence colors when

dispersed in different solvents. These investigations introduce an innovative method for predicting solvent polarity parameters based on these solvatochromic characteristics. The research accurately determines the dielectric constant of binary solvent mixtures, such as the methanol-1,4-Dioxane system. Additionally, it devises a straightforward and effective approach for quantitatively measuring moisture in organic solvents with an error margin of less than one percent. The emission color of the solutions shifted with water content, showing a red-shift in emission wavelength. Experiments with 1, 4-dioxane-water binary mixtures confirmed the reliability of this method. Remarkably, moisture content could even be detected visually under 365 nm UV light. The solvent-dependent emission properties of PD-CNDs open up new opportunities for studying solvent interactions.

6.2. Future outlook

Due to low toxicity, easy synthesis and solvent-dependent fluorescence, PD-CNDs are promising candidate for various future scientific and technological applications.

- Extending the metal ion/picric acid sensing application to real samples.
- The sensing ability of PD-CNDs can be further extended to detect pH and other significant analytes, including pesticides/insecticides, drugs, and food colorants, by

monitoring their response to variations in the PL intensity of PD-CNDs.

- The moisture sensing ability in the organic solvent 1, 4-dioxane will be extended to other commercially significant solvents such as THF and DMF in future work.
- Upcoming work will aim to confirm the results of moisture sensing in 1, 4-dioxane with the help of computational studies.
- As a long wavelength emissive carbon nanodot (orange-red emission), its application in the biological fields can also be explored.
- Its application can also be extended into the LED fabrications by mixing PD-CNDs with proper polymer matrix.

PUBLICATIONS

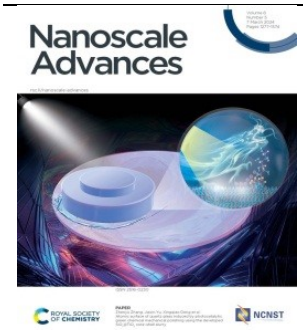

Nidhisha V, Ritu Gopal, Anjali C, Amrutha T. P, Arunima K. K.,V.K. Praveen and Renuka N. K, "p-Phenylenediamine-derived carbon nanodots for probing solvent interactions." Nanoscale Advanves., 2024, **6**(5), 1535–1547.

DOI: 10.1039/d3na00799e

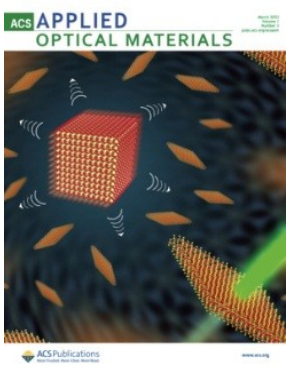

Ritu Gopal, **Nidhisha V**, Amrutha T. P, Aswathi A. A, Midhila P, Thejas K K Subrata Das and Renuka N. K, "Aggregation-Induced White Light Emission and Solvent-Induced Dual Mode Multi-Analyte Sensing by Highly Crystalline Single Component Derived N, S Co-Doped Carbon Nanodots." *ACS Appl. Opt. Mater.* 2023, 1, 3, 701–714.

DOI: 10.1021/acsaom.2c00170

Anjali, C.; **Nidhisha, V**.; Amrutha, T.; Gopal, R.; Chethan, B.; Thayyil, M. S.; Periyat, P.; Kizhakayil, R. N., Graphene oxide boosted high surface area CeO 2 for humidity sensing. Results in Engineering 2024, 21, 101752.

DOI: 10.1016/j.rineng.2024.101752

Nikhila, M.P; Anjali, C.; **Nidhisha, V**.; Devi, K. S.; Pai, M. R.; Kizhakayil, R. N., "Copper oxide modified biphasic titania for enhanced hydrogen production through photocatalytic water splitting." Results in Engineering 2023, 20, 101474.

DOI: 10.1016/j.rineng.2023.101474

PRESENTATIONS

- Oral presentation in International Seminar on Luminescence Materials (ISLM) – 2022 held at Alappuzha.
- Poster presentation in International Conference on Emerging Frontiers in Chemical Science (EFCS) – 2023 held at Farook College, Calicut.
- Oral presentation in National Seminar on Frontiers in Chemical Sciences (FCS) – 2024 held at University of Calicut.

Nanoscale Advances

ROYAL SOCIETY OF CHEMISTRY

PAPER

View Article Online
View Journal | View Issue

Open Access Article. Published on 05 February 2024. Downloaded on 3/10/2025 7:15:17 AM.
This article is licensed under a Creative Commons Attribution-NonCommercial 3.0 Unported Licence.

Check for updates

Cite this: *Nanoscale Adv.*, 2024, **6**, 1535

p-Phenylenediamine-derived carbon nanodots for probing solvent interactions†

Nidhisha V.,[a] Ritu Gopal,[a] Anjali C.,[a] Amrutha T. P.,[a] Arunima K. K.,[a] Vakayil K. Praveen [bc] and Renuka Neeroli Kizhakayil *[a]

Carbon nanodots, the luminescent nanoparticles of carbon with size restriction below 10 nm, have attracted inordinate attention in materials science due to their widespread applications in optoelectronic and biological fields. Low toxicity and facile synthesis pathways render them favourites in the above-mentioned areas in the context of green chemistry. This work presents fine applications of *p*-phenylenediamine-derived carbon nanodots (PD-CNDs) achieved *via* a facile one-pot hydrothermal method. Adequate characterization using X-ray diffraction and spectroscopic and microscopic studies confirmed spherical particles with an average particle size of 2.8 nm, functionalised with amino, carboxyl, and hydroxyl groups. The carbon framework was functionalised with pyridinic and pyrrolic nitrogens. Upon 365 nm UV light illumination, an aqueous dispersion of PD-CNDs showed red-orange fluorescence. Detailed spectral analysis using UV-visible absorption and fluorescence spectroscopy identified edge states and surface groups as luminescent centres, with a significant contribution arising from the latter. The investigation conducted using a collection of solvents, categorized into polar and nonpolar, indicated the potential of the system for applications based on its solvatochromic nature. The feature enabled the determination of different polarity parameters of the solvents, as well as dielectric constants of solvents and solvent mixtures, with considerable accuracy. The system was potent for predicting the composition of a given pair of solvents. The service of the system is also extended for moisture sensing in organic solvents within an error percentage < 1. High quantum yield values (0.61) combined with solvent composition-dependent optical features ensure broader applications of the system to probe solvent interactions.

Received 20th September 2023
Accepted 2nd February 2024

DOI: 10.1039/d3na00799e

rsc.li/nanoscale-advances

1. Introduction

Since ancient times, carbon has always been a fascinating material that has found numerous fine applications. Tailored carbon materials with excellent physicochemical properties have been designed for highly specialized applications in biological,[1] environmental,[2,3] electronic and catalytic[4,5] fields. It is well known that the applications of materials are manifolded upon reducing the dimensions to nanoframes.[6,7] Nanoconfinement and appropriate functionalization have bestowed additional luminescent features on carbon, which also extends the role of carbon into the optoelectronic field. Carbon nanotubes,[8] nanowires,[9] graphene[10,11] and fullerene[12] fall under this category. Carbon nanodots (CNDs), a comparatively new addition to this family,[13–15] are distinguished for their inherent luminescent feature, which is often excitation dependent. Low toxicity, environmental friendliness, aqueous solubility and resistance to photobleaching render them attractive alternatives to fluorescent dyes and heavy metal-based quantum dots in bioimaging, sensing, catalysis, solar cells and light-emitting diodes. Greener synthesis methods are added advantages for these particles. Herein, we present fluorescence-based fine applications of *p*-phenylenediamine-derived carbon nanodots (PD-CNDs), which are synthesised using a facile one pot hydrothermal method. The system exhibits solvent relaxation/solvatochromism,[16] by virtue of which a material exhibits different colours in different solvents, which is manifested as a change in either the absorption or emission wavelength. Autoclave-based hydrothermal procedures have been widely used to obtain luminescent carbon particles from phenylenediamine systems.[10,17] Solvothermal methods using alcohols, particularly ethanol, have also been reported. Isomer variation has led to CNDs differing in emission wavelength under solvothermal conditions, as shown by Jiang and coworkers.[18] PD-based CNDs have also been established to be fine candidates

[a]*Advanced Materials Research Centre, Department of Chemistry, University of Calicut, Kerala 673635, India. E-mail: renuka@uoc.ac.in*
[b]*Photosciences and Photonics Section, Chemical Sciences and Technology Division, CSIR-National Institute for Interdisciplinary Science and Technology (CSIR-NIIST), Thiruvananthapuram, Kerala 695019, India*
[c]*Academy of Scientific and Innovative Research (AcSIR), Ghaziabad 201002, India*

† Electronic supplementary information (ESI) available: List of selected solvents/solvent mixtures and spectral details. See DOI: https://doi.org/10.1039/d3na00799e

© 2024 The Author(s). Published by the Royal Society of Chemistry